Forschungszentrum Karlsruhe
in der Helmholtz-Gemeinschaftt

Wissenschaftliche Berichte
FZKA 7101

Analysis and Comparison of Experimental Data of Bundle Tests QUENCH-07 to QUENCH-09 about B_4C Control Rod Behaviour

C. Homann, W. Hering, G. Schanz

Institut für Reaktorsicherheit
Institut für Materialforschung
Programm Nukleare Sicherheitsforschung

Juli 2006

Forschungszentrum Karlsruhe

in der Helmholtz-Gemeinschaft

Wissenschaftliche Berichte

FZKA 7101

Analysis and Comparison of Experimental Data of Bundle Tests QUENCH-07 to QUENCH-09 about B_4C Control Rod Behaviour

Ch. Homann, W. Hering,
G. Schanz

Institut für Reaktorsicherheit
Institut für Materialforschung
Programm Nukleare Sicherheitsforschung

Forschungszentrum Karlsruhe GmbH, Karlsruhe

2006

Forschungszentrum Karlsruhe GmbH
Postfach 3640, 76021 Karlsruhe

Mitglied der Hermann von Helmholtz-Gemeinschaft
Deutscher Forschungszentren (HGF)

ISSN 0947-8620

urn:nbn:de:0005-071015

ABSTRACT

The three out-of-pile bundle tests QUENCH-07 to -09, performed at Forschungszentrum Karlsruhe, are dedicated to investigate B_4C control rod behaviour and its influence on the fuel rods during a wide range of severe accident conditions under low system pressure in a Western type light water reactor. The experimental data, mainly those that are recorded during the tests, are analysed in detail for a deeper understanding of the tests with respect to control rod degradation and other aspects, but also for a basis to improve modelling in severe accident codes. Computational analyses are left out intentionally to demonstrate the value of the experimental data alone. Important findings are listed below.

A general comparison of the test conducts shows that the experimental conditions of the early test phases were reproduced to a high degree. However, the high temperature regime before cool-down initiation was about 80 s longer in QUENCH-07 than in QUENCH-08, so that a direct comparison of experimental data of these two tests that includes the whole second transient of both tests or the subsequent cool-down phase is unreasonable and may lead to wrong conclusions.

In both B_4C tests QUENCH-07 and -09, the control rod failed near the upper end of the heated zone during the first transient and in two steps; both steps are due to the formation of eutectic melts. In both tests, the steel clad failed at a temperature of about 1550 K. 114 s (QUENCH-07) and 310 s (QUENCH-09) later, the metallic parts, if still existing, as well as the oxide scale of the guide tube failed. B_4C oxidation can only occur after the second event, if enough steam is available in the bundle, as it is the case in QUENCH-07.

In both tests QUENCH-07 and -09, the contribution of B_4C oxidation to total hydrogen production is assessed to keep generally below 10 % for hydrogen generation rate, total hydrogen production, as well as total chemical energy release. Uncertainties are quite large in the late phase of the tests because of the complex processes at that time. Comparison of QUENCH-07 and -08 shows that also indirect contributions of B_4C oxidation, e.g. by local temperature increase, are rather limited, at least up to cool-down initiation in QUENCH-08. For the subsequent time, no conclusion can be drawn, because the conduct of the two tests was too different.

During cool-down, the steam mass flow rate is not well known and hydrogen generation rate and cumulated hydrogen production are overestimated, at least in QUENCH-07. For computational analyses and model development, these experimental restrictions should be kept in mind. The consequences of insufficient synchronisation of computers in QUENCH-07 could largely be corrected.

The analysis of the experimental data confirms that material behaviour is not the result of an isolated process, but of an interaction with thermal-hydraulic environment. It also confirms that the whole system must be considered and the whole amount of data must be used for reliable test interpretations.

Analyse und Vergleich der experimentellen Daten der Bündelversuche QUENCH-07 bis QUENCH-09 über B_4C-Kontrollstabverhalten

ZUSAMMENFASSUNG

In den drei out-of-pile Bündel-Versuchen QUENCH-07 bis -09, die im Forschungszentrum Karlsruhe durchgeführt wurden, soll das Verhalten von B_4C-Kontrollstäben und ihr Einfluss auf Brennstäbe in einem weiten Bereich von Unfallbedingungen bei niedrigem Systemdruck in einem Leichtwasserreaktor westlicher Bauart untersucht werden. Die experimentellen Daten, vor allem die, die während der Versuche aufgenommen wurden, werden im Detail analysiert, um zu einem tieferen Verständnis der Versuche sowohl zum Verhalten der Kontrollstäbe als auch zu anderen Fragen zu kommen und um eine Grundlage für die Modellierung in Rechenprogrammen zur Beschreibung schwerer Unfälle zu schaffen. Rechnungen werden absichtlich nicht behandelt, um den eigenständigen Wert der experimentellen Daten zu zeigen. Im Folgenden werden wichtige Ergebnisse aufgeführt.

Ein allgemeiner Vergleich der Versuchsabläufe zeigt, dass die frühen Testphasen in großem Umfang reproduziert wurden. Jedoch dauerte in QUENCH-07 die Hochtemperaturphase vor der Abkühlung mit Dampf etwa 80 s länger als in QUENCH-08, so dass ein direkter Vergleich der experimentellen Ergebnisse dieser beiden Versuche nicht sinnvoll ist und zu falschen Schlussfolgerungen führen kann, wenn er die gesamte zweite Transiente oder die folgende Abkühlung enthält.

Der Kontrollstab versagte in beiden B_4C Versuchen in zwei Stufen während der ersten Transiente nahe dem oberen Ende der beheizten Zone durch die Bildung eutektischer Schmelzen. Zunächst versagte das Hüllrohr bei etwa 1550 K. 114 s (QUENCH-07) und 310 s (QUENCH-09) später versagte das Führungsrohr mit seinem metallischen Teil, falls noch vorhanden, und seiner Oxidschicht. Oxidation von B_4C kann erst nach dem zweiten Ereignis stattfinden, falls genügend Dampf im Bündel vorhanden ist wie bei QUENCH-07.

In QUENCH-07 als auch in QUENCH-09 wurde abgeschätzt, dass der Beitrag der Oxidation von B_4C zur gesamten Wasserstoffproduktionsrate, der gesamten Wasserstoffmenge und der damit verbundenen Energiefreisetzung im Wesentlichen unter 10 % liegt. Wegen der komplexen Vorgänge in der Abkühlphase ist die Unsicherheit in dieser Phase recht groß. Ein Vergleich von QUENCH-07 und QUENCH-08 zeigt, dass auch der indirekte Einfluss, z.B. durch lokale Temperaturerhöhung, bis zum Beginn der Abkühlung in QUENCH-08 recht begrenzt ist. Für die Abkühlungsphase können keine Schlüsse gezogen werden, weil die Versuchsführungen zu unterschiedlich waren.

Während der Abkühlung – vor allem in QUENCH-07 – ist der Dampfmassenstrom durch Kondensation und Verdampfung nicht genau bekannt und die Wasserstoffproduktionsrate und -menge sind überschätzt. Für Rechnungen und Modellentwicklungen sollten diese experimentellen Einschränkungen berücksichtigt werden. Die Folgen einer ungenügenden Synchronisation der Rechner im Versuch QUENCH-07 wurden weitgehend berichtigt.

Die Analyse der experimentellen Daten bestätigt, dass das Materialverhalten nicht isoliert von der Wechselwirkung mit dem thermohydraulischen Umfeld gesehen werden kann. Sie bestätigt auch, dass für verlässliche Interpretationen der Versuche das gesamte System und der gesamte Umfang der Daten betrachtet werden müssen.

TABLE OF CONTENTS

LIST OF FIGURES

LIST OF TABLES

ABBREVIATIONS

AEKI	Atomenergia Kutatóintézet (Atomic Energy Research Institute), formerly part of KFKI, Hungary
BWR	Boiling Water Reactor
CATHARE	Code Avancé de THermohydraulique Appliqué aux Réacteurs à Eau sous pression (advanced thermal-hydraulic code for pressurized water reactors)
CORA	Complex Out-of-pile Rod bundle Assembly
CR	Control Rod
EDX	Energy-Dispersive X-ray analysis
FRS	Fuel Rod Simulator
GDA	General Data Acquisition
GFTC	General Facility and Test Control
HR	Heated Rod (= FRS)
ICARE	Interprétation des Coeurs Accidentés pour les Réacteurs à Eau (interpretation of water reactor cores during an accident)
KFKI	Központi Fizikai Kutató Intézet (Central Research Institute for Physics [of the Hungarian Academy of Sciences, Hungary])
LOCA	Loss of Coolant Accident
LOOP	Loss Of Off-site Power
MS	Mass Spectrometer
MSDA	Mass Spectrometer Data Acquisition
PTE	Post-Test Examination
PWR	Pressurized Water Reactor
SEM	Scanning Electron Microscopy
SET	Separate Effects Tests
t	Time
t’	Time into the first transient
t_2	Time into the second transient
t”	As t_2, but with a time shift of -200 s for QUENCH-08
TC	Thermocouple
TSD	Test Sequence Diagram
z	Axial coordinate

INSTRUMENTATION AND RELATED INFORMATION

F 204	steam mass flow rate during cool-down
F 205	steam mass flow rate before cool-down
Fm 601	mass flow rate in off-gas pipe (orifice)
H_2 Zr	hydrogen release due to Zr oxidation alone
L 701	condensate measurement
MS	mass spectrometer in off-gas pipe
ox loss	steam loss due to oxidation, calculated as 9 times hydrogen generation rate
P 406	pressure in annulus between shroud and inner cooling jacket
P 411	pressure in fuel rod simulator
P 511	pressure at bundle inlet
P 512	pressure at bundle outlet
P 901	pressure near downstream end of condenser
P_{el}	total electrical power supply
T 204	fluid temperature in steam feed pipe
T 301A	fluid temperature downstream of superheater
T 303	fluid temperature at orifice in inlet pipe
T 511	fluid temperature at bundle inlet
T 512	fluid temperature at bundle outlet
T 601	fluid temperature in off-gas pipe
T 901	temperature near downstream end of condenser
TCI	temperature in inner cooling jacket
TIT	central temperature in corner rod
TSH	outer surface shroud temperature
TCRI	CR clad temperature
TFS	temperature on outer clad surface
TFS 2/1	bundle fluid temperature at level 1 (–250 mm)

TCRI are labelled “TCRI ax”, TFS and TIT as “TFS rod/ax” and “TIT rod/ax”, respectively, TSH and TCI as “TSH ax/azi” and “TCI ax/azi”, respectively, where “ax” is the number of the axial level, rod the rod type, and “azi” the azimuthal position. TCs, used for TFS, are mounted on the outer clad surface. Normally, they indicate a temperature between clad outer surface and fluid temperature, but probably close to clad outer surface temperature. In extreme conditions as during water quenching, the situation is more complicated.

GRAPHS

Legends in the right half of a graph refer to the right scale. Legends also refer to graphs, where the legend is suppressed. An additional mark “m”, referring to instrumentation in a plot legend, refers to some modification of the original data, e.g. smoothing to reduce noise. Chemical species are designated by standard nomenclature.

1 Introduction

In pressurized water reactors (PWR), the power release in the core is controlled by the boron concentration in the water and the insertion depth of control rods. In some licensing procedures, two independent diverse shut down systems are required such as control rod banks and injection of borated water. In case of an accident, all control rod banks are used to shut down the reactor. In boiling water reactors (BWR), evaporation of water inhibits the use of boron. Therefore, different drive systems are used to inject the control rods in emergency shut down cases. If during severe core degradation the absorber material is relocated relative to the fuel, the use of unborated water may cause local re-criticality for some time.

Control rods, one of the most complicated elements in a reactor core, are composed of several subcomponents with different materials. Generally, they consist of the absorber material, typically a silver-indium-cadmium alloy in PWRs, or boron carbide B_4C, mostly in BWRs, sheathed with a stainless steel cladding. In PWRs, these rods hang loosely in the guide tubes, made of Zircaloy. In BWRs, the absorber material is in horizontal stainless steel tubelets, assembled in blades that are combined to crosses. They are injected from the bottom; the adjacent Zircaloy fuel element canisters act as lateral guidance. Due to the different construction of both types, the mass ratio between absorber and cladding material differs strongly.

Though in a nuclear power reactor the number of control elements is small, only about 4 % of the number of fuel rods in a PWR and still less in a BWR, the effects of the degradation of control elements in an accident cannot be neglected because of their relatively low melting temperature and the formation of eutectic melts. When the control rod is damaged and absorber material is oxidised, the reaction products may not only have an impact on the surrounding fuel rods but also influence the radioactive source term that may be released into the containment or the environment during a severe accident. Consequently, behaviour and influence of control rods during severe accidents have to be investigated to get reliable information for basic understanding, code development, and validation. Apart from these more general objectives, the behaviour of the control rods has to be investigated particularly under delayed reflood conditions, because the core state prior to reflood initiation strongly affects the release of energy and thus hydrogen, as well as the further damage progression.

For B_4C absorber material, the formation of gaseous oxidation products of B_4C, especially of CH_4, is of interest for the source term for still another reason. When the steam mass flow in the core is small, CH_4 may be formed mainly in colder parts of the primary circuit and in the containment. When fuel rods also fail and fission products are released, CH_4 may be transformed into volatile organic iodine compounds. These compounds cannot be retained appropriately by filters, and hence are a safety concern when released into the environment.

Investigation of control rod behaviour started with separate effect test (SET) programs and the CORA bundle experiments in the eighties of the last century. Mechanistic and kinetic information was gained in the SET programs on the interactions between the components. CORA tests allowed studying interaction and relocation behaviour in realistic geometry. Unfortunately, only two reflood tests were performed in the CORA program, one for PWR and

one for BWR conditions. This database is too scarce to develop realistic damage models of the control rod behaviour, especially concerning reflood and the different mass ratio with respect to B_4C systems in BWRs and PWRs.

Because of this importance for reactor safety considerations, the impact of B_4C control rod degradation during a postulated accident in a nuclear power reactor is also dealt in the COLOSS project as a part of the Euratom Fifth Framework Programme on Nuclear Fission Safety, launched by the European Community. Among others, three integral experiments and related pre- and post-test calculations with large severe accident code systems, currently used for safety analyses in nuclear power reactors, were supported and co-financed by the European Community. This item is addressed in the CODEX-B4C experiment [1] at AEKI (formerly part of KFKI) for VVER-1000 reactor conditions and in tests QUENCH-07 [2] and QUENCH-09 [3] at Forschungszentrum Karlsruhe for Western type reactors.

The involved COLOSS partners agreed that the mass ratio of steel and B_4C in the control rod should be 3.5 in these QUENCH tests as a compromise to approach both Western type BWR and PWR conditions as much as possible so that the QUENCH tests could give a maximum benefit for both reactor types. They also agreed that a control rod, instead of a blade geometry as used in BWRs, was preferable to study radial fault propagation in the bundle. In contrast, a blade would divide the bundle into two halves and restrict their interactions substantially. This was considered a complication that should be avoided in the first tests with absorber material. For reactor applications, it should be kept in mind that interactions between absorber material and fuel rods occur later in an accident in a BWR than in a PWR. In a BWR, the fuel assemblies are enclosed in channel boxes, and the construction of the control elements is different in these two reactor types. These differences result in far less thermal coupling between the control elements and the fuel rods in a BWR.

The QUENCH tests should be as representative as possible for Western type commercial 1300 MW PWRs and BWRs and should fulfil two aims. Firstly they should provide experimental data on degradation of B_4C control rods, its impact on bundle damage progression, and the production of gaseous reaction products, in particular H_2 and CH_4, before and during reflood. Secondly, they should provide a useful database for the preparation of the PHEBUS FPT3 in-pile experiment. For the last reason, test QUENCH-07 was intended to be run as similar as possible to the PHEBUS test FPT3, planned at that time and performed on 18 November 2004 [4]. The conduct of test QUENCH-09 was similar to that of QUENCH-07, but included a test phase with a low steam mass flow rate to obtain steam starvation at bundle exit. Apart from the support of the PHEBUS test, these two QUENCH tests shed light on a large range of important reactor accident scenarios due to the different steam mass flow rates. Steam starved conditions may occur in a large break LOCA (Loss of Coolant Accident), while steam excess is likely in a LOOP (Loss Of Off-site Power) scenario or after a small break. In addition to these two tests, QUENCH-08 [5] was performed outside the COLOSS project as a reference to QUENCH-07, but without B_4C absorber.

Comparison of QUENCH-07 and -09 test data showed that B_4C control rod behaviour and its influence on the bundle are quite different. Similarly, in QUENCH-07 and -08 total hydrogen release differs by more than a factor of two, though the test conducts were intended to be the same. The reasons for such differences are not yet sufficiently clarified [5]. It is therefore

necessary to use and to compare all available data to come to a sound and detailed understanding of the processes, involved in these tests. It would be a gross error to attribute all differences between the test results to direct or indirect influences of the control rod behaviour.

A profound understanding is also indispensable as a basis for the development of any mechanistic model on the behaviour of control rods in severe accident codes. Such methods have to complement an oxidation model for B_4C, as was also aimed in the COLOSS project. In addition, much information is contained in the test data; they should be analyzed in detail for an adequate benefit of the tests. Furthermore, application of the test results to reactor conditions by mere extrapolation is not appropriate, because the conditions in such integral experiments are too complex so that such a procedure can lead to large errors and wrong conclusions.

In this report, the data, recorded during the tests (on-line data) are evaluated in much detail to understand the control rod behaviour in severe accident conditions, addressed in the tests. They are complemented by a summary of results of post-test examination (PTE), as documented in [2], [3], and [5] for the respective tests and updated in this report. Implicitly in PTE, much information like material property data and general material behaviour is taken from SET. The present work aimed at understanding the various processes, their local and temporal interactions, as well as the effect of control rods on neighbouring fuel rods and allowed to identify the damage sequence of the B_4C control rods. This outcome can be considered as a guideline to develop a damage model for Western type B_4C control rods. Consideration of BWR specific conditions for control blades requires further experiments and is beyond the scope of this report.

For the first time, test sequence diagrams (TSD) for both B_4C tests were established to give a condensed (one-page) overview of the whole test. It contains two-dimensional (axial elevation versus time) presentation of temperature development and other important information like the axial extension of bundle damage or hydrogen generation rate as a function of time. This tool can be very helpful for global analyses and comparison of two tests, but also allows identifying local conditions in the bundle e.g. to derive limits for material reactions.

Initially, this report was intended to give an overview of B_4C control rod behaviour in QUENCH-07 and -09, but the progress of the work showed that analysis of QUENCH-08 should be included to the same extent. Analysis of the data also raised a number of new questions, and it answered some questions to other subjects. These additional items are also discussed in the present report. In this context, inherent uncertainties of such integral tests and particular ones of the present tests were investigated; some work is dedicated to the reliability of the hydrogen measurement. Before this work can be presented, basic features of the QUENCH tests and synchronisation of the various data sources are discussed, and a comparison of the test conducts is performed to identify differences that are important to understand the test results.

Usually, a report addresses the experimental results, their interpretation, and related discussion in different sections. Because of the variety of results, outlined here, such work is collected under the same headings to keep information on the respective phenomena together.

Since some aspects, dealt in this report, are linked logically, a number of cross references is given.

Computational work, related to these QUENCH tests, is documented in [6] and [7]. This and other computational work is only mentioned marginally in this report, if at all. This is done intentionally: It is also a purpose of this report to demonstrate the value and power of the experimental data alone. For this reason, it is not necessary to rely on any computational results for the present work.

2 QUENCH Tests

2.1 QUENCH Facility

In the following a short description of various aspects of the QUENCH facility is given. More details are documented in reports [2] and [3] for tests QUENCH-07 and -09, respectively, with a B_4C control rod (CR) and in [5] for QUENCH-08, meant as a reference test for QUENCH-07, with an unheated fuel rod simulator instead of the control rod. The QUENCH facility (Fig. 2.1) consists of the test section as its main part and a number of external devices (Fig. 2.2).

The test section consists of a bundle with 21 rods (Fig. 2.3). Their arrangement and their cladding (Zircaloy-4) are typical for commercial Western type PWRs. In B_4C tests QUENCH-07 and -09, the central rod is a control rod with B_4C pellets in the heated zone up to axial elevation 1008 m; helium at some overpressure is used as a filling gas to detect rod failure. In all other QUENCH tests, performed up to now, the central rod is an unheated fuel rod simulator. The other 20 rods are fuel rod simulators with annular ZrO_2 pellets and with a mixture of argon and krypton as a filling gas to detect rod failure. These 20 rods are heated electrically over a length of 1024 mm; the tungsten heaters are connected to a combination of molybdenum and copper electrodes at both ends. Electrical power supply is independent for the eight inner and the twelve outer fuel rod simulators. The four Zry corner rods are intended to give a flat lateral temperature profile in the bundle; in addition, they are used for instrumentation. One of them may be removed during the test to analyze the axial profile of the oxide layer thickness, formed up to that time. The bundle is held in its position by five grid spacers; the lowermost grid spacer is made of Inconel, the others of Zry. Their lower edge is at axial positions -200 mm, at 50, 550, 1050, and 1450 mm, respectively, where axial elevation 0 mm is set to the lower end of heated length.

A mixture of steam and argon enters the bundle from the bottom; the fluid, i.e. steam, argon, hydrogen and other products that may be formed or released in the bundle, leaves the bundle at its top to enter the off-gas pipe. System pressure is set during the starting procedure for a test to about 2 bar by adjusting a spring at a valve near the downstream end of the condenser and upstream of the Caldos instrument for hydrogen detection (Fig. 2.1). There is no control to maintain that value during the test so that the system pressure changes during cool-down by 0.35 bar in QUENCH-07. In QUENCH-09, about 1.8 bar may be expected from pressure at bundle outlet; instrument P 901 was not available in that test.

The bundle is contained in a Zry shroud and insulated by ZrO_2 fibre material, filling the annulus between shroud and the inner cooling jacket. This configuration is cooled by countercurrent water (upper electrode zone) and argon (heated zone and lower electrode zone) flows within the cooling jackets. The whole set-up is enclosed in a steel containment for safety reasons.

The test section up to and including the outer cooling jacket is equipped with nearly 90 thermocouples at 17 axial locations in the heated and in both electrode zones. They begin at -250 mm (level 1) and are 100 mm apart from one another. Therefore, levels 4 to 13 refer to

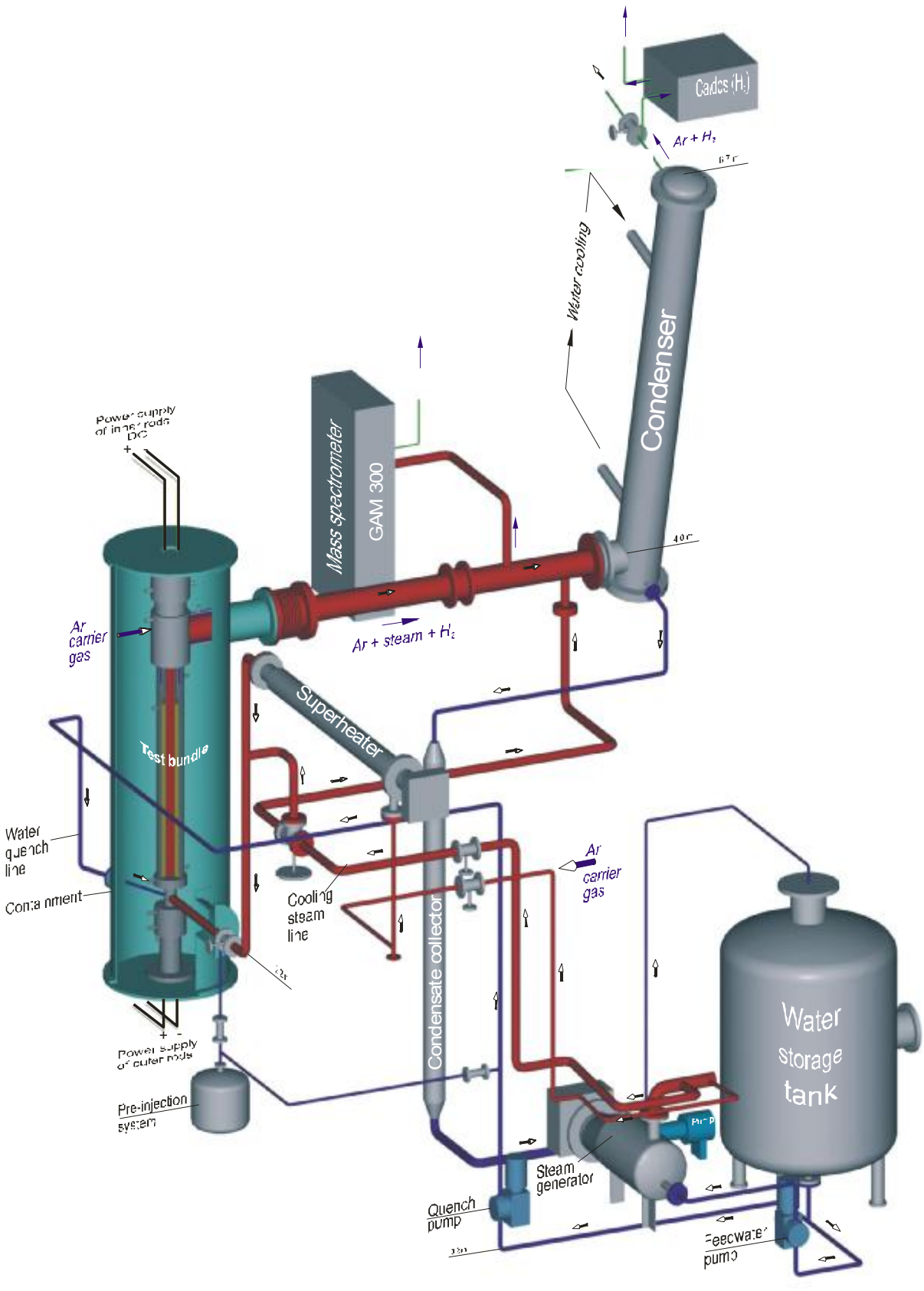

Fig. 2.1: Main components of QUENCH facility

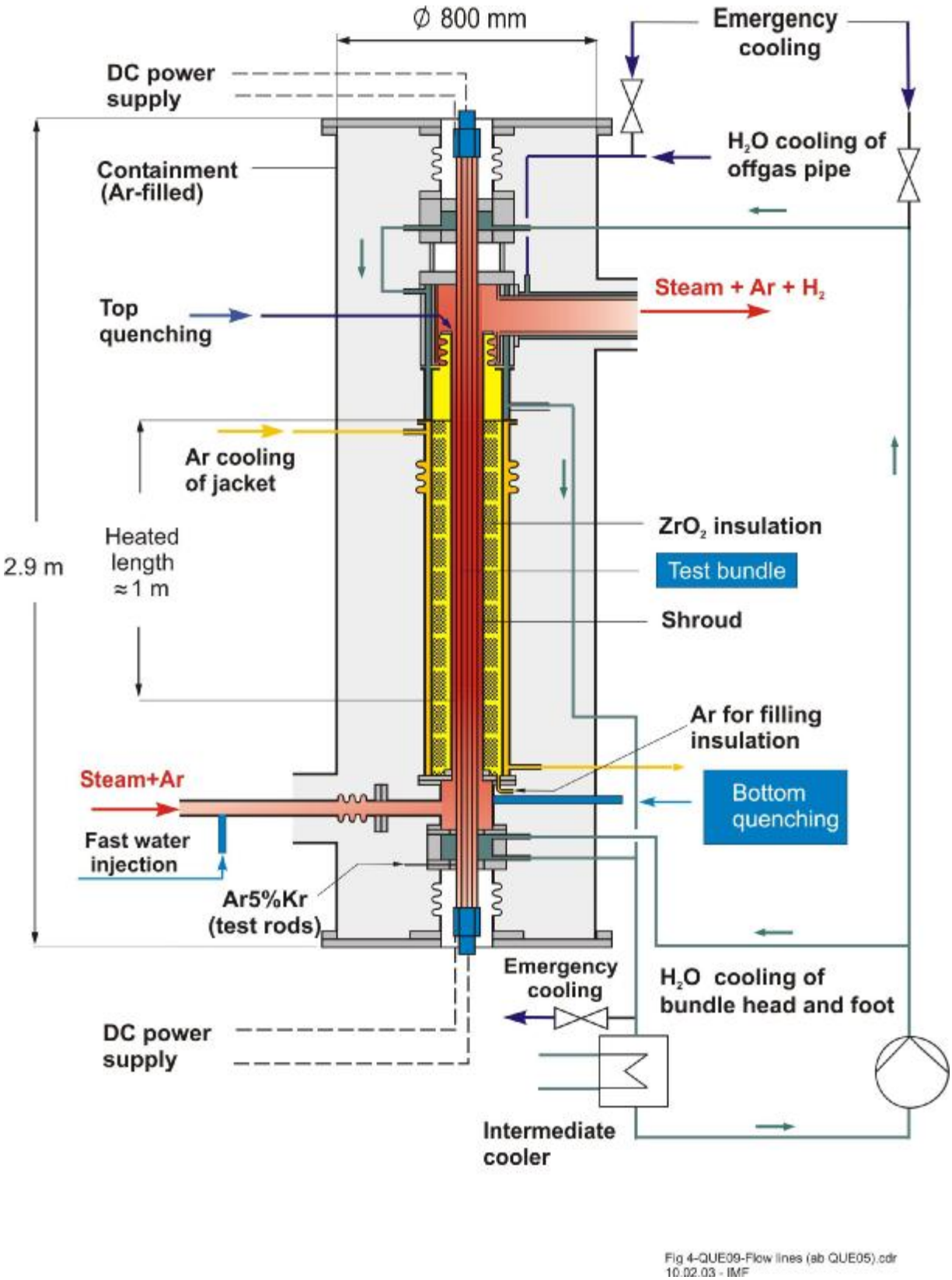

Fig. 2.2: Main flow paths in the QUENCH facility

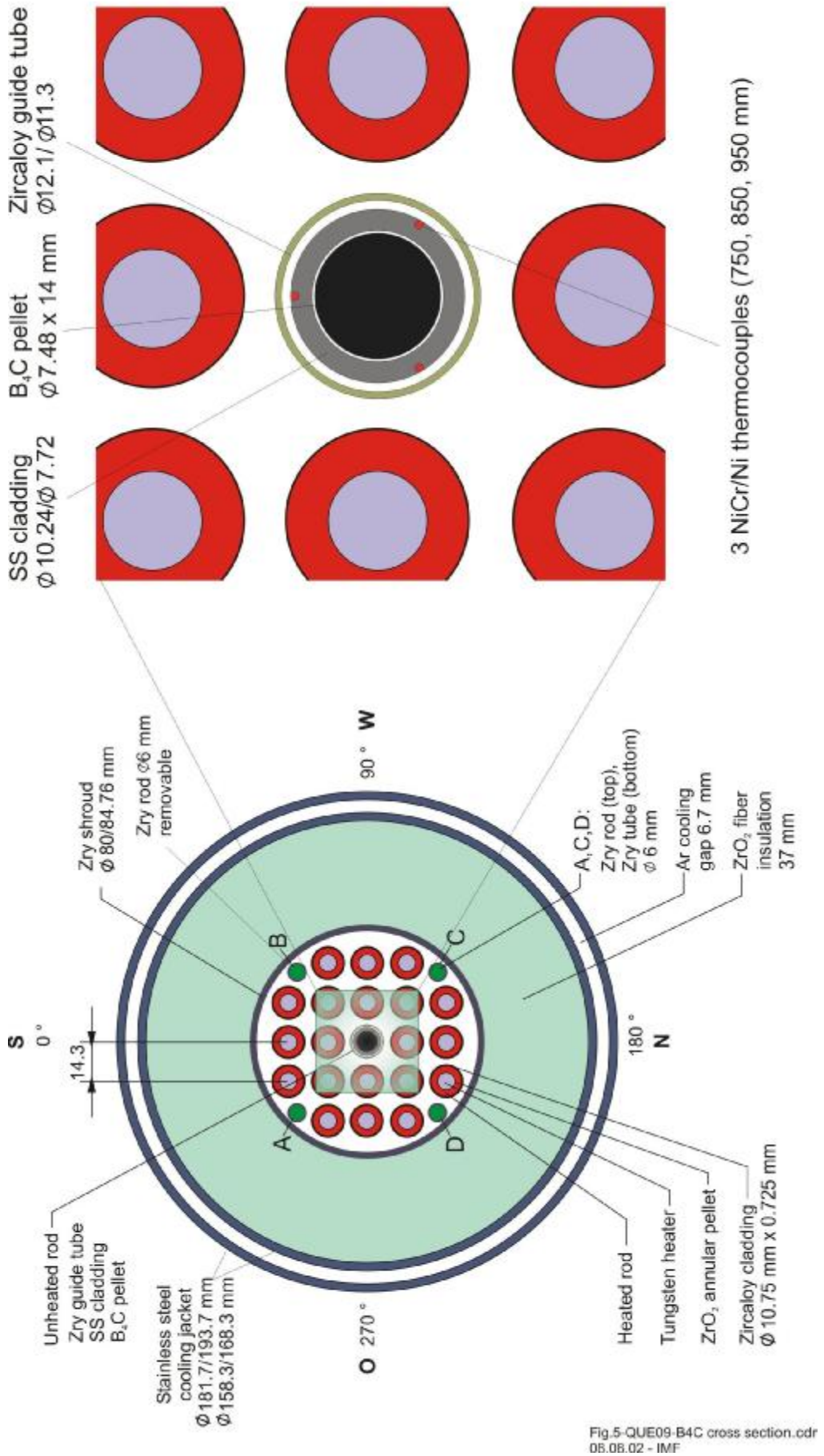

Fig. 2.3: Bundle cross section with B_4C rod instead of unheated fuel rod simulator

instrumentation of the heated zone. TCs, labelled TCRI, are imbedded in a groove of the outer clad surface of the CR; they are hence situated within the guide tube. Their outer diameter is 0.5 mm. TFS and TIT are TCs on the outer clad surface of fuel rod simulators, and in the centreline of corner rods, respectively. TSH are TCs, mounted on the outer shroud surface and TCI are imbedded in the inner cooling jacket. Details are given in the respective reports like [2]. When temperature is high, it may happen that a TFS or TSH looses its contact with the adjacent surface or that a new junction forms. In such cases, readings become unreliable, and only qualitative conclusions can be drawn, if at all.

Total electrical power P_{el} is calculated as the product of measured current and voltage and summed over the two electrical circuits. Since voltage measurements are outside the heated rods, they contain voltage drops e.g. in wires and the sliding contacts at the ends of the heated rods. Therefore, electrical power, released into the bundle, is smaller than P_{el}, but for simplicity, only P_{el} is considered throughout this report.

Downstream of the bundle, three sorts of instrumentation are important. About 2 m into the off-gas pipe, an orifice is installed with pressure, temperature, and mass flow detection, labelled P 601, T 601, and F 601, respectively. These data are used to derive the mass flow rate Fm 601, based on the well-known formula for orifices for steady state conditions. For this reason, the results are wrong for transient conditions. Besides, the mixture density can only be assessed, and even for steady state, a minimum mass flow rate is required. In sum, this instrumentation can only be used for qualitative considerations about mass flow rates. Fluid composition is mainly analyzed by a quadrupole mass spectrometer “GAM 300” at about 2.7 m into the off-gas pipe, in the text simply called “mass spectrometer” or “MS”. Downstream of the condenser, a hydrogen detection system “Caldos 7 G”, based on measuring thermal conductivity of the fluid, and a mass spectrometer “Prisma”, simpler than “GAM 300”, are installed close to one another, the latter only in QUENCH-07 and -09. Since mass spectrometers analyse species according to their mass number, different chemical species with the same mass number cannot be distinguished. In this way, CO and N_2 cannot be distinguished. The same is true for CO_2 and HBO_2. Analysis is, however, unique for hydrogen.

For the MS, several improvements have been made since the start of the QUENCH program [8]. Among others, measurement of steam mass flow is calibrated with an external source for the QUENCH tests, discussed in this report, so that the results should be reliable. A pump to decouple the driving pressure drop for the MS from pressure in the off-gas pipe was not yet installed in the tests, discussed in this report. When a large portion of steam is consumed in the bundle, less steam can be condensed in the condenser, and the pressure drop in the condenser should decrease. Due to the argon flow, there is, however, always a residual pressure drop. Since the system pressure is not kept constant at that level during the whole test in one or another way, the original set-up may give unsatisfactory results in some cases.

Since evaluation of all MS data relies on argon, large uncertainties occur, when argon concentration is small or otherwise unreliable [8] as in the cool-down phase of QUENCH-09. Though it is claimed by the experimentalists that MS data only rely on concentrations and the inlet argon mass flow and are hence independent of hydrodynamic conditions, some doubt arises sometimes that at least during fast transients MS readings are questionable. In this

report, however, the data are assumed reliable. At the foot of the condenser, condensate is measured (L 701).

2.2 Test Conduct

Since QUENCH-08 with an unheated rod instead of a B_4C control rod was intended as a reference test for QUENCH-07, the test conduct was planned to be the same for both tests. In fact, there were small, but important differences, as will be demonstrated in section 4. In all three QUENCH tests, the bundle is heated from room temperature to nearly 900 K (heat-up phase), and the various systems are checked (Fig. 2.4). The fluid is a mixture of about 3 g/s of steam and argon each up to cool-down initiation. Shortly before the end of this stabilisation phase, data acquisition systems are switched on. In QUENCH-07, -08, and -09, the bundle is then heated to more than 1700 K by increasing electrical power (first transient). The subsequent temperature plateau phase is intended to oxidize the absorber material with large chemical reaction rates; in QUENCH-08, this phase is normal pre-oxidation as in other QUENCH tests. In QUENCH-07 and -08, a second power transient by increasing electrical power linearly follows, and finally the bundle is cooled down with 15 g/s steam. About 20 s after cool-down initiation, electrical power is reduced to 4 kW to simulate decay heat level and shut down when the bundle temperature have reached rather low levels. Main events are given in Tab. 2.1. Since decisions about time may depend on personal interpretation, slight differences with respect to existing reports may happen.

The test protocol for QUENCH-09 differed from that for QUENCH-08 for several aspects. The target temperature at the end of the first transient was 50 K higher than in QUENCH-07, i.e. 1773 K instead of 1723 K to extend the temperature range, investigated in these two tests. Besides, it was planned that the power transient should be replaced by a reduction of steam mass flow rate so that steam starvation occurs in the bundle. The mass flow reduction also leads to substantial temperature increase due to the reduction of convective heat transport. Finally, cool-down was performed, with 50 g/s steam instead of 15 g/s as in QUENCH-07 and -08.

In QUENCH-09, an undesired temperature escalation had started, when electrical power was reduced (Fig. 2.4). To stop it, steam mass flow rate was reduced to the predefined value. After some time, electrical power was increased stepwise to maintain the given maximum temperature in the bundle, but there was no second transient as planned. Comparison of inlet steam mass flow rate and hydrogen generation rate shows that indeed steam starvation occurs in the bundle after steam mass flow reduction, as it was predicted in the pre-test calculations [7] for such conditions. In spite of the unforeseen temperature escalation, the planned test conduct was performed as foreseen, as far as it was possible under such circumstances.

QUENCH-07 Date: 25.07.2001 Start of data acquisition: 09:56:56		**QUENCH-08** Date: 24.07.2003 Start of data acquisition: 10:15:12		**QUENCH-09** Date: 03.07.2002 Start of data acquisition: 09:33:04	
0	Start of data acquisition	0	Start of data acquisition	0	Start of data acquisition
240	Start of first transient	135	Start of first transient	465	Start of first transient
2022	CR failure (He)			2280	CR failure (TCRI 13 + He)
2136	CR failure (CO)			2590	CR failure (CO)
				2600	First failure of FRS (P 411, Kr)
2200	Start of temperature plateau	2277	Start of temperature plateau	2602	Power reduction
3090	Withdrawal of corner rod B (start)	3181	Withdrawal of corner rod B		
3140	Start of second transient	3240	Start of second transient		
3467	First failure of FRS (Kr, P 411)				
3484	Shroud failure (P 406)	3764	Shroud failure (P 406)	2623	Shroud failure (P 406)
				2633	Start of steam reduction
				2837	Stepwise power increase
3557	Start of cool-down	3775	Start of cool-down	3315	Start of cool-down
3568	Start of temperature decrease	3776	Start of temperature decrease	3317	Start of temperature decrease
		3785	First failure of FRS (P 411)		
3585	Start of power decrease	3814	Start of power decrease	3340	Start of power decrease
				3344	Inner cooling jacket failure
3601	Decay power level reached	3830	Decay power level reached	3356	Decay power level reached
3749	Start of power switch off	4018	Start of power switch off	3424	Start of power switch off
5107	Start of steam switch off			4491	Start of steam switch off
5527	End of data acquisition	4648	End of data acquisition	4551	End of data acquisition

Tab. 2.1: Main events in QUENCH-07, -08, and -09

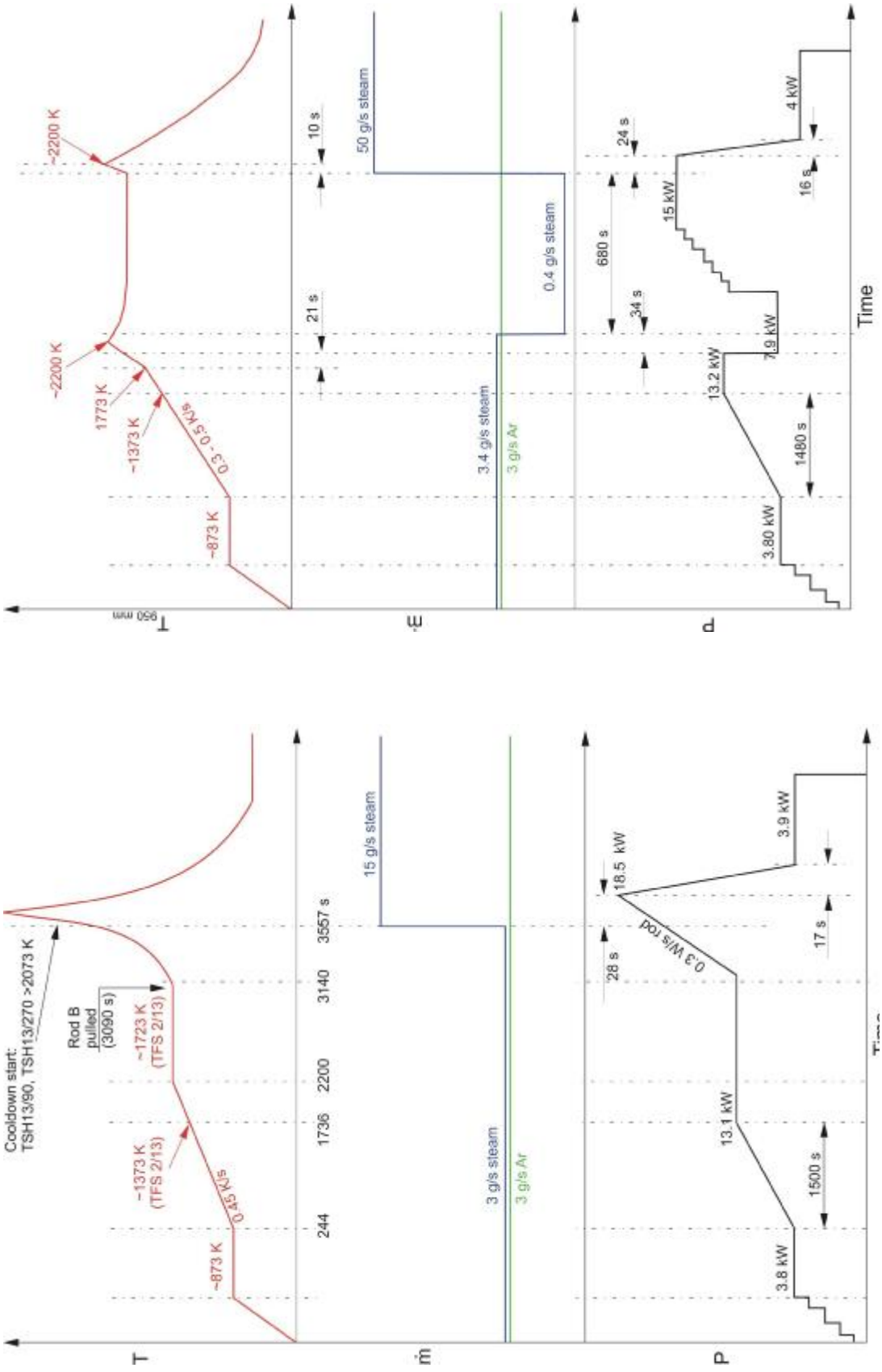

Fig. 2.4: Conduct of tests QUENCH-07 (left) and QUENCH-09 (right)

3 Data Synchronisation

3.1 Problem

Data evaluation for the cool-down phase showed that in QUENCH-07 production of H_2, CO, CO_2, and CH_4 increase simultaneously, as one may expect. In contrast to all experience of previous tests, however, production does not increase at the start of cool-down initiation, but more than 20 s afterwards. For a better understanding of the work to find an explanation, some more details about QUENCH tests are given in the following.

In QUENCH tests, several computers are involved. There is one main computer for general facility and test control (GFTC), e.g. triggering the various actions at the start of the cool-down phase and the decrease of electrical power some ten seconds later. Important events like the start of data acquisition or the start of the cool-down phase are stored in a data log file. Most experimental data like temperatures, pressure, and mass flow rates are stored in the computer for general data acquisition (GDA), where the start of data acquisition is also stored. Mass spectrometer (MS) data are stored in a third computer, namely that for acquisition of mass spectrometer data (MSDA). Unfortunately, there is no data log file, related to MSDA; only the internal clock is stored. Up to now, the various computers are synchronised automatically after booting and should be synchronised just before the start of data acquisition. Since problems occurred during the preparation of previous tests, no continuous synchronisation is made during the test.

The results, given in the following discussion, refer to the local clock of the respective computer. Statements like “clock A advances clock B” and “signal A’ is delayed with respect to signal B’” are used as synonyms, where A and A’ refer to one computer, and B and B’ to the other.

Since in QUENCH-07 and -09 more chemical species are investigated with MS, the frequency of data acquisition is not about 1 Hz as in other QUENCH tests, but somewhat below 0.2 Hz, and it is only in post-test data evaluation that original data are interpolated to a frequency of 1 Hz. Therefore, the accuracy of post-test data synchronisation, presented below, will in any case be limited. For the data evaluation, given in this section, the original MS data are used without interpolation.

A further, general, source of uncertainty of MS data concerns the transportation time from the place of the chemical reaction to the MS. It depends on the mass flow rate, fluid composition, and temperature. For the standard fluid composition of 3 g/s of steam and argon each, 4 s may be a characteristic time at high bundle temperature, according to assessments of the experimental team and to velocities, calculated with SCDAP/RELAP5; for the cool-down phase it should be not more than 1 s according to similar SCDAP/RELAP5 calculations, probably less. Because of its larger cross section and length, the delay is mainly caused in the 2.7 m long flow path of the off-gas pipe.

For QUENCH-07, it was found from the data log that GDA clock is delayed by 8 s with respect to GFTC clock, according to the respective data log entries. In other tests, the time

difference at the start of data acquisition is much smaller. Assuming that hydrogen production increases immediately after cool-down initiation, they also found from the GFTC log file and the MS clock and hydrogen data that MSDA clock advances GDA clock by about 16 to 21 s. As it will be explained in section 3.3, increase of hydrogen production in the cool-down phase is delayed because of condensation of steam in parts of the steam feed pipe that were not used before cool-down initiation. As a result, all involved persons agreed that the best estimate for dominant condensation is 7 s and that the best estimate for time difference of GDA and MSDA is 15 s. In the following, our contributions are presented.

3.2 Synchronisation

The essential aim of our work was a direct synchronisation of GDA and MSDA, GFTC information normally being of minor interest. Such a synchronisation can be made for events, when respective information is available in both data sources. For MSDA, the relative time since the start of data acquisition is used in the following, because it is stored with two decimal digits and hence more accurate than storage of MSDA clock (1 s interval).

In principle, failure of heated fuel rod simulators can be used. This choice has the advantage that there is no complication because of condensation. Rod failure may be detected by release of Kr that is part of the filling gas in QUENCH-07 and that is stored in MSDA and by decrease of rod pressure P 411, available as GDA information (Fig. 3.1). In the top of the figure, an overview is given, starting shortly before the first failure. The various Kr peaks may be interpreted as subsequent failure of various rods. Rod pressure is seen to drop at about the same time of the peaks of Kr concentration.

Detailed inspection of the various fuel rod failures, given in Fig. 3.1, reveals difficulties for interpretation: For the failure of the first fuel rod simulator, a time shift of 15 s is appropriate. For the other Kr peaks this choice cannot easily be confirmed, and for the Kr peak at about 3660 s the decrease of rod pressure becomes even lower after about 3630 s, though the flow cross section for filling gas escape increases with every rod failure. There are two possibilities to interpret these facts: either the two signals are not appropriate for the synchronisation or further effects play a role that hinder reliable interpretation.

As a second possibility, the start of the cool-down phase can be used for synchronisation. Fig. 3.2 shows that steam mass flow rate (GDA information F 205 and F 204) changes at 3557 s, whereas steam mass flow rate remains constant up to 3579 s according to MS. The next data point is at 3585 s. It cannot be decided whether the increase of steam mass flow rate between 3579 s and 3585 s really occurred during the test or whether it is a numerical effect due to the sampling frequency. Assuming the second possibility, an extrapolation of the steep increase after 3585 s down to the pre-cool-down value of 2.2 g/s suggests that increase of steam mass flow rate should have been detected at 3584 s at the latest. Therefore, the delay of increased steam mass flow rate according to MSDA is between 22 s and 28 s with respect to GDA. The effect of condensation, included in this delay, will be treated in the next section.

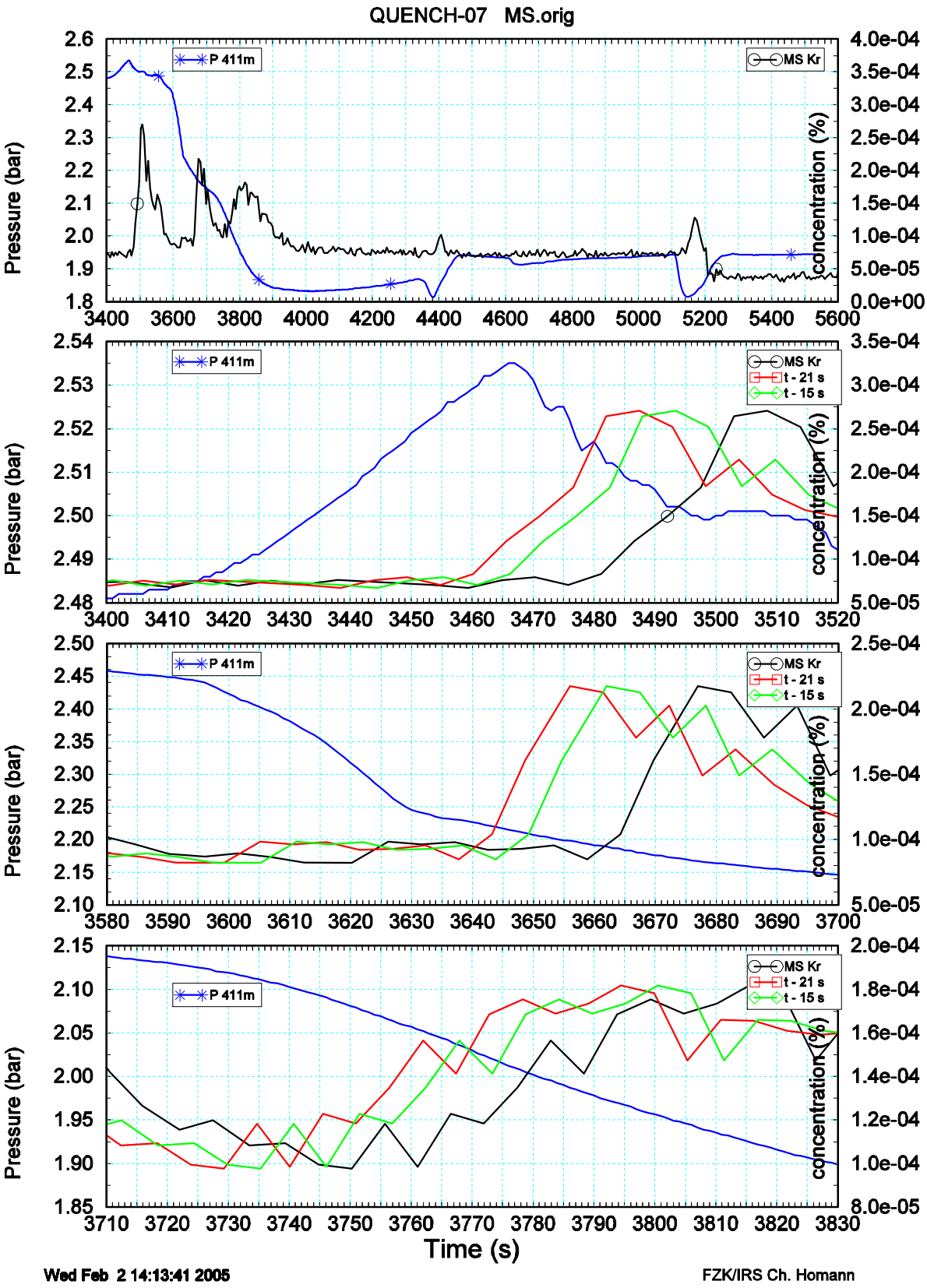

Fig. 3.1: Rod pressure and Kr concentration for various time intervals in QUENCH-07

To reduce noise, rod pressure signals P 411 (left) are given for a frequency of 1 Hz. For the krypton signal (right), the original sampling frequency is used. In all but the top plot, the Kr signal, shifted by 21 and by 15 s, is added.

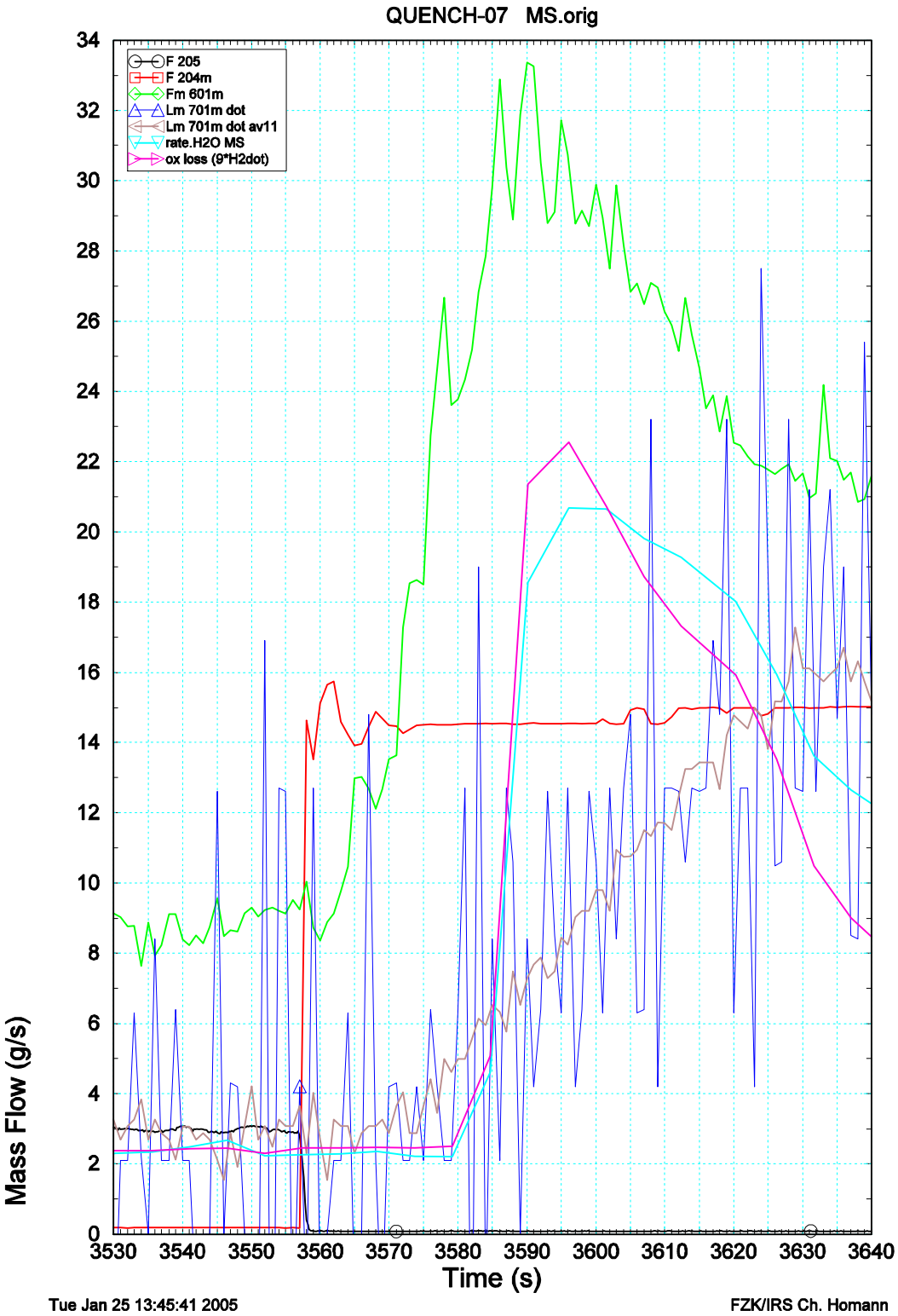

Fig. 3.2: Information about steam mass flow rate during cool-down in QUENCH-07

The figure shows steam inlet mass flow rate before (F 205) and during (F 204) cool-down, orifice measurement Fm 601 in the off-gas pipe, time derivative of condensate mass Lm 701, and MS data for steam mass flow rate in the off-gas pipe. “ox loss” is consumption of steam due to oxidation, based on hydrogen generation rate. To reduce noise, some data are shown with a frequency of 1 Hz. For MS signals, the original sampling frequency is presented.

3.3 Condensation in the Steam Feed Pipe

Further work revealed that this synchronisation, based on the start of the cool-down phase is even more complicated. Steam, used for the cool-down phase, bypasses the superheater by the steam feed pipe and joins the inlet pipe, used for argon and for steam before cool-down initiation, in its last vertical part (Fig. 2.1). This bypass is not used before cool-down initiation, and the steam condenses in that pipe. Since such condensation has already been remarked in the first test with steam cool-down, QUENCH-04, an appropriate electrical heating has been installed to avoid this effect. This has been done in the upper horizontal part of the bypass and, in a second electrical circuit, in the adjacent part between the valve and the point where the bypass joins the vertical pipe from the superheater. In QUENCH-07, the latter was switched off intentionally during the test, probably to perform cool-down at a temperature as low as possible. However, the effect was by far larger than desired.

A number of TCs in the facility that has direct fluid contact proved appropriate for this purpose. They are listed in Tab. 3.1; temperature histories for these and some bundle TCs in both electrode zones and the lower end of the heated zone are given in Fig. 3.3. After cool-down initiation, they continue like in the previous transient for some seconds, before they show behaviour as known from other cool-down tests, i.e. normally a decrease up to and including the lower part of the bundle and an increase up to escalation in the upper part. T 303 eventually falls to saturation value (at 3576 s) and stays at that value up to 3666 s, i.e. for 90 s. As outlined in [9] for QUENCH-06 (ISP-45), this may be due to droplet deposition on the TC tip and is not necessarily a sign of global single-phase liquid flow. Even T 301A in the hot part of the inlet pipe near the point, where the steam feed pipe joins it, shows a decrease. The very small temperature change in the first seconds after cool-down initiation as monitored by T 511 and TFS 2/1 suggests, however, that the vapour portion is quite small and hence condensation substantial, maybe complete. Delays after cool-down initiation are given in Tab. 3.1.

Further indications are listed in Tab. 3.2. Fig. 3.2 demonstrates the difficulties to interpret signals like Fm 601 and Lm 701. The reading of Fm 601 is wrong even before cool-down initiation, namely too high; the time derivative of Lm 701 is rather noisy, and a running average is included in the figure for an easier interpretation. Therefore, only the change is interpreted in these signals. A detailed evaluation of the various instruments with their advantages and drawbacks is given in [9]. Mass flow signals, exceeding bundle inlet values, are discussed in section 7.2.

Further inspection of TC readings shows that T 511 and TFS 2/1 increase somewhat about 60 s after cool-down initiation. This demonstrates that long-term behaviour of inlet temperature is governed by heat transfer from rather hot structures. Consequently, a reduction of inlet temperature as forced in test QUENCH-07 might only be useful during the start of cool-down. The duration of the low temperature phase depends on the duration of the test phases before, including the stabilisation phase. Since experimental data for this part of the piping system are not available and heat losses can only be guessed, respective modelling in computational analyses is difficult or even impossible as in pre-test calculations.

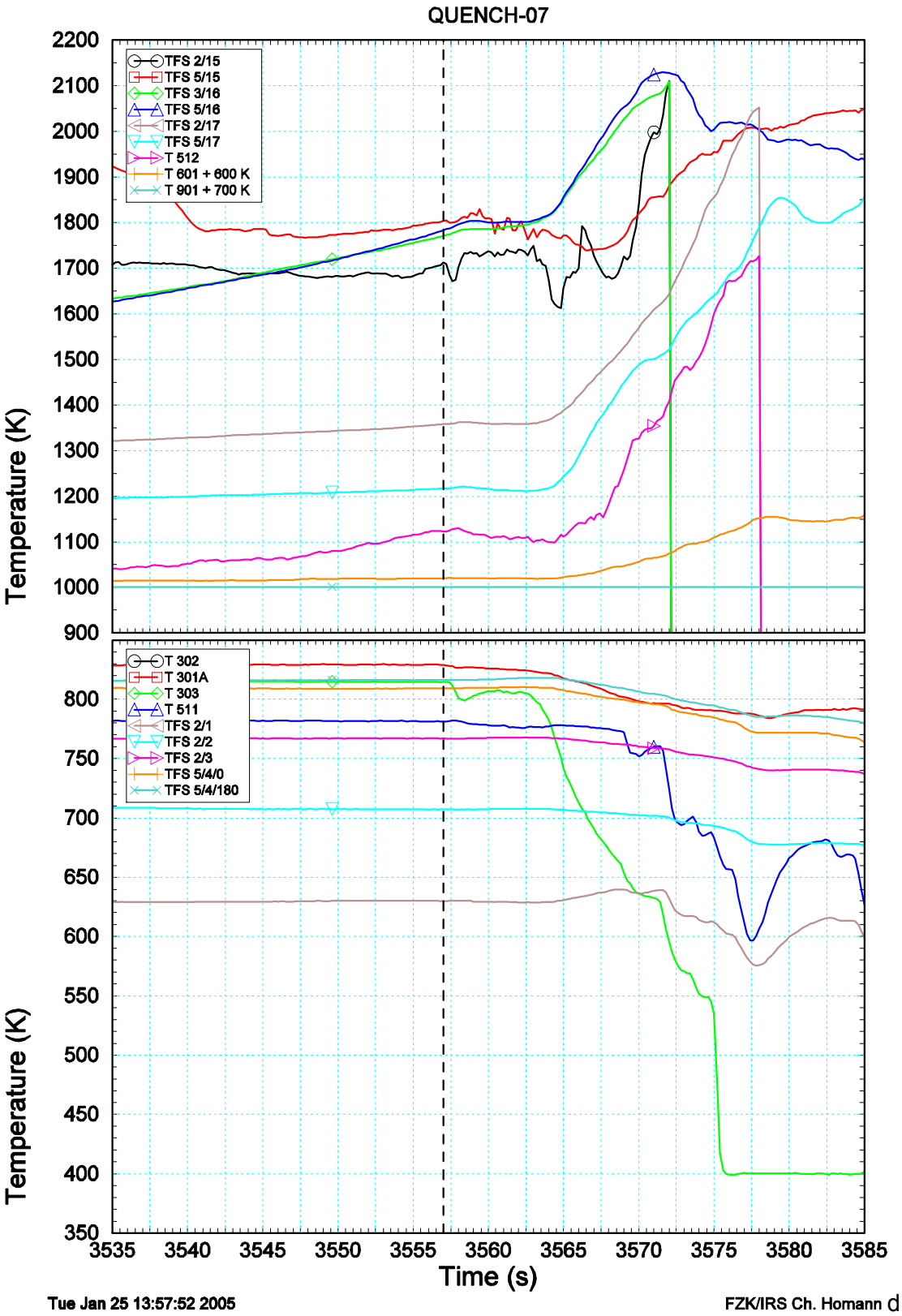

Fig. 3.3: Temperatures at various locations in the test facility for QUENCH-07

The figure shows temperatures in the upper electrode zone and the off-gas pipe (top) and in the inlet pipe and the lower part of the bundle. TCs with direct fluid contact in levels 11 to 13 failed before cool-down initiation. The dashed vertical line refers to cool-down initiation.

Tab. 3.1: Start of sensible temperature change during cool-down in QUENCH-07

TC	Location	Time [s]	Delay [s]
T 301A	behind superheater	3564	7
T 303	orifice, inlet pipe	3563	6
T 511	near bundle inlet	3569	7?
TFS 2/1	bundle	3572	7
T 512	near bundle outlet	3564	7
T 601	off-gas pipe	3564	7

Tab. 3.2: Further indications for condensation in QUENCH-07

Sensing instrument	Kind / Location	Time [s]	Delay [s]
P 511	pressure / bundle inlet	3562	5
P 512	pressure / bundle outlet	3562	5
TFS	escalation / upper electrode zone	3634	7
Fm 601	orifice / off-gas pipe	3560 … 3563	3 … 6
MS	mass spectrometer / off-gas pipe	3579 … 3584	22 … 28

Values refer to original sources. Therefore, MS data include synchronisation error.

3.4 Recommendations

Taking in mind the difficulties to interpret the various signals reliably and comparing the various results in Tab. 3.1 and Tab. 3.2, the minimum value for Fm 601 seems to be too small. A delay of 5 to 7 s due to heavy condensation seems to be appropriate, 7 s to be preferred from the experience that TCs are easier to interpret; after that time, steam mass flow rate can be assumed to increase substantially as it was foreseen to occur exactly at the start of the cool-down phase. Therefore, the delay of MSDA signals with respect to GDA should be between 15 s and 21 s, the first value being chosen as a final decision of all involved persons.

Data evaluation, outlined in this section, shows further that the experimental procedure to lower fluid inlet temperature during cool-down, as performed in QUENCH-07, is not desirable for both experimental and analytical reasons.

3.5 Further Remarks

When no steam is supplied into the bundle, oxygen diffuses from the ZrO_2 layer into the adjacent α-Zr(O) layer and so dissolves the ZrO_2 layer. When afterwards enough steam is available, oxidation may be very strong, because the α-Zr(O) layer behaves like pure metal. Experience from SET [10] shows, however, that this effect may be neglected within the first minutes of steam unavailability. Therefore, it need not be considered with respect to hydrogen generation rate during cool-down in QUENCH-07.

Because of the steam condensation in the steam feed pipe, it is likely that no steam is available for oxidation in the hot zone and after the delay, the steam mass flow rate in the bundle is uncertain, at least for some time that is relevant for hydrogen production. During that same time, electrical power input and hence bundle temperature increase. Consequently, the oxidation rate is higher than just before cool-down initiation, when sufficient steam is available for noteworthy oxidation, and part of the hydrogen production is due to this effect. However, the surface mounted TCs in the hot zone of bundle, where most of the hydrogen is produced, have already failed so that this increase of hydrogen production cannot be assessed.

4 Comparison of Test Conducts

4.1 First Transient and Temperature Plateau Phase

Fig. 4.1 shows measured axial temperature profiles of QUENCH-07, -08, and -09 at the start of the first transient. The bundle and shroud temperatures are mostly the same within about 30 K. Experimental scatter is largest in the hot zone. The cooling jacket temperatures agree within 15 K so that the initial conditions for the first transient are very close together for all three tests, and so is the fluid inlet temperature. The differences between shroud and cooling jacket temperatures are nearly identical so that the radial heat loss is practically the same in all three tests at that time.

For an inspection of time dependant results, time has been shifted appropriately so that t' = 0 s corresponds to the start of the first transient of the respective test (e.g. in Fig. 4.2). This time into the first transient is used in this section. A similar time shift will also be used for subsequent test phases. By doing so, the differences due to previous test phases only play the role of initial conditions for the new test phase. Especially, when test conditions are quite close together up to the start of the new phase, these initial conditions are similar, and interpretation of the new test phase is facilitated.

As a representative temperature for comparison of the tests, outer clad TC TFS 2/13, located near temperature maximum in the bundle, is chosen. Electrical power input is the same up to power reduction in QUENCH-07. For this reason, temperature increases (Tdot) are essentially the same in the three tests. Hydrogen generation rates and hence cumulated hydrogen mass are nearly identical in QUENCH-07 and -09 up to the start of the escalation in that test and somewhat smaller in QUENCH-08. In contrast to measured temperatures, it is a global value, but experience shows that it is more sensible than temperature and for this reason a valuable tool for test conduct and interpretation. In sum, the results demonstrate the high quality of work of the operators.

Whereas the argon mass flow rate is practically the same in all three tests, the steam mass flow rates are 3, 3.15, and 3.4 g/s in QUENCH-07, -08, and -09, respectively. However, temperatures in QUENCH-07 and -09 are closer together than in QUENCH-07 and -08, demonstrating that the slight differences that can be expected from the slightly different convective cooling may even be more than balanced by other effects. Temperatures in the shroud and the inner cooling jacket at a given axial level have been averaged over the respective azimuthal position. Their difference is only a rough measure for radial heat loss, because the thermal conductivity varies by about a factor of three in the temperature range in question. For all axial levels (Fig. 4.3), the temperature differences agree so well for the three tests that the radial heat losses are nearly the same, too. Up to axial level 9, the values for QUENCH-07 and -08 are closer together than for QUENCH-09, at higher elevations those for QUENCH-07 and -09 agree better. This demonstrates that there are small differences between the tests, and that these differences may vary locally. Perhaps, the somewhat different initial and boundary conditions or slight geometrical differences of the bundle configuration add to these differences. In any case, it is not a single reason that causes the slight differences of the test results in the first transient.

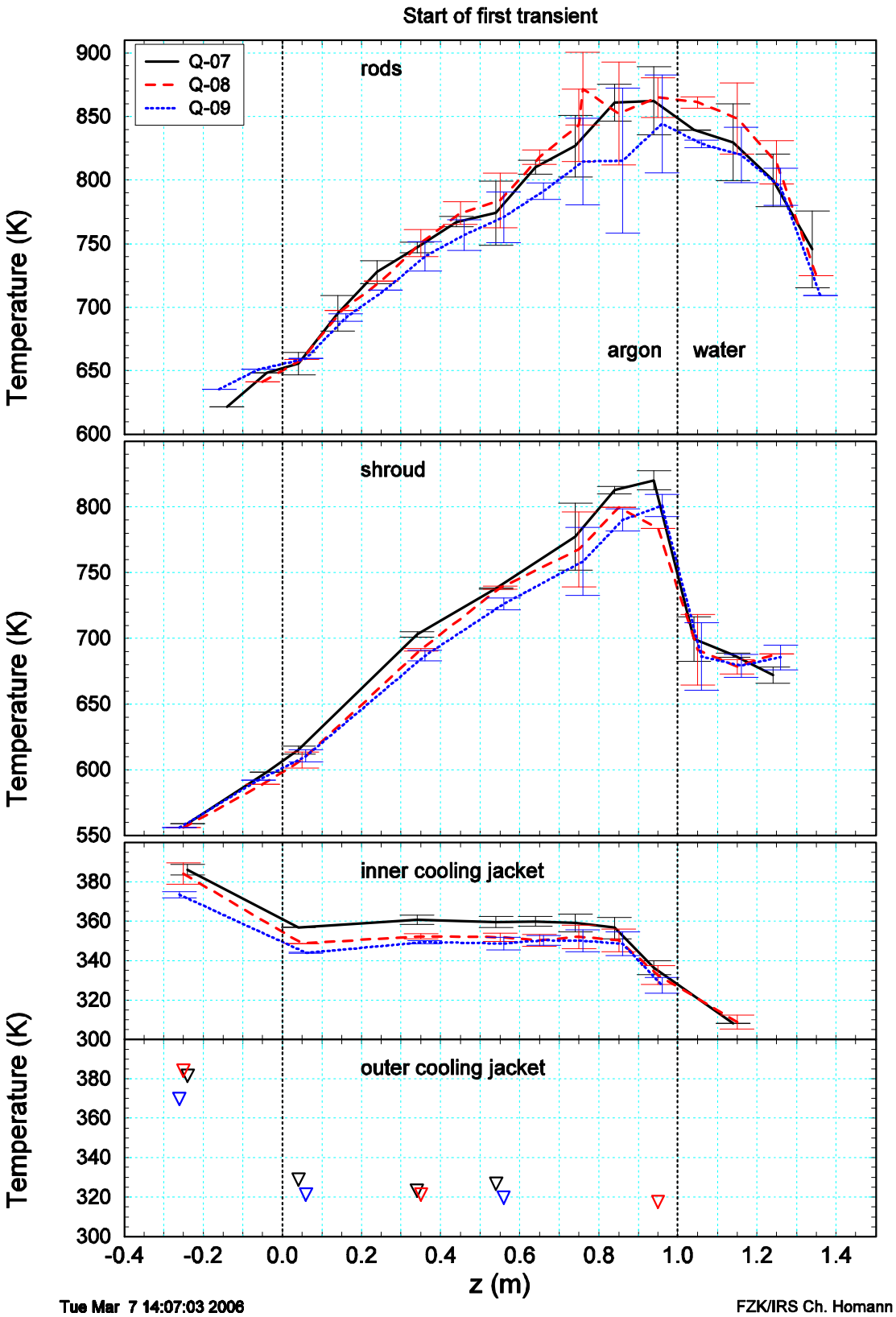

Fig. 4.1: Axial temperature profiles at the start of the first transient

The figure shows from top to bottom a comparison of temperatures of the clad outer surface, the shroud, and the inner and outer cooling jacket for QUENCH-07, -08, and -09. Error bars indicate the experimental scatter. The axial positions of measuring planes are slightly shifted for a better readability of the error bars.

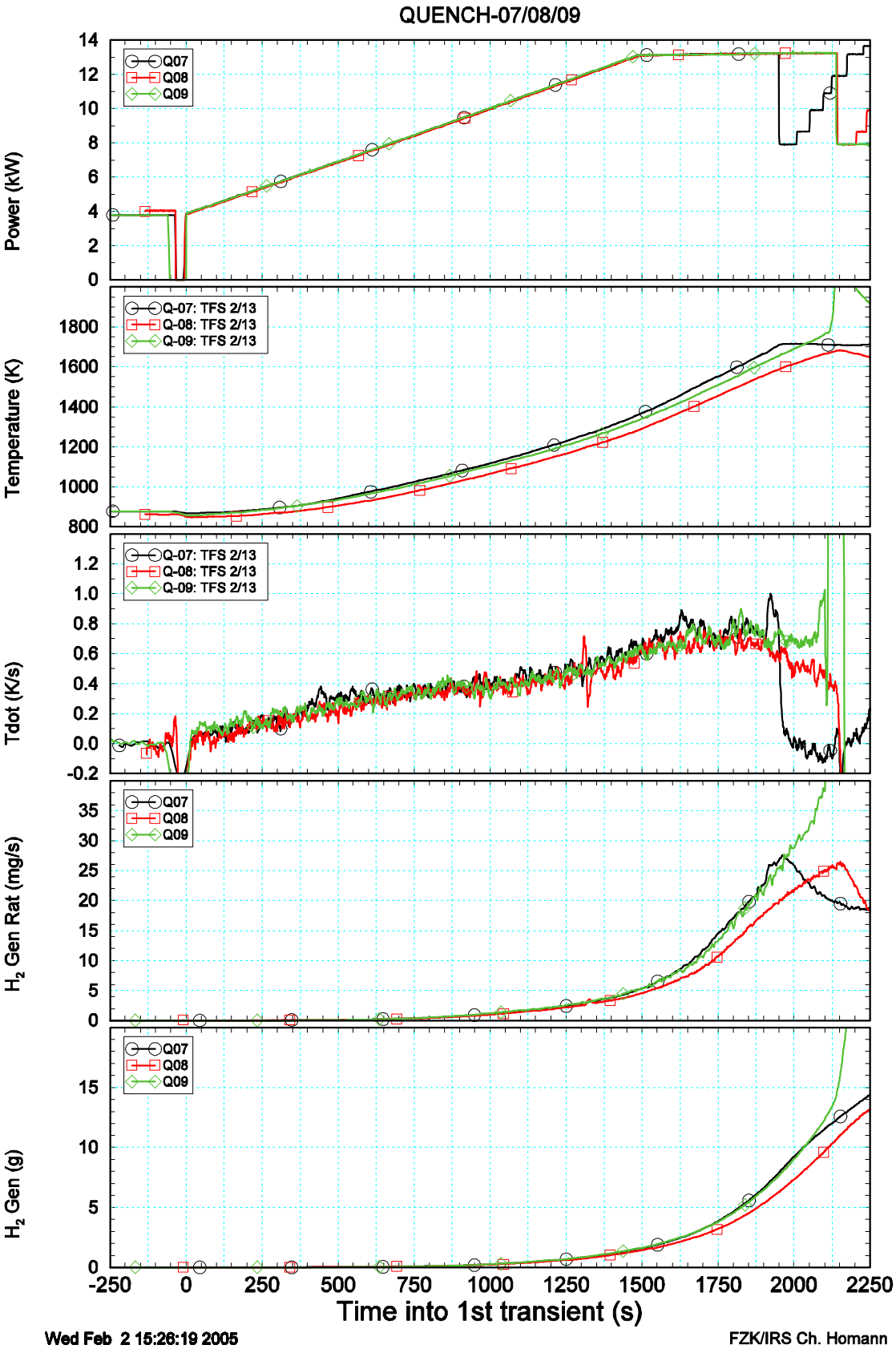

Fig. 4.2: Main variables for QUENCH-07, -08, and -09 during the first transient

The figure shows from top to bottom electrical power, temperatures at level 13 (950 mm) and their time derivative, hydrogen generation rate and cumulated hydrogen mass for QUENCH-07, -08, and -09.

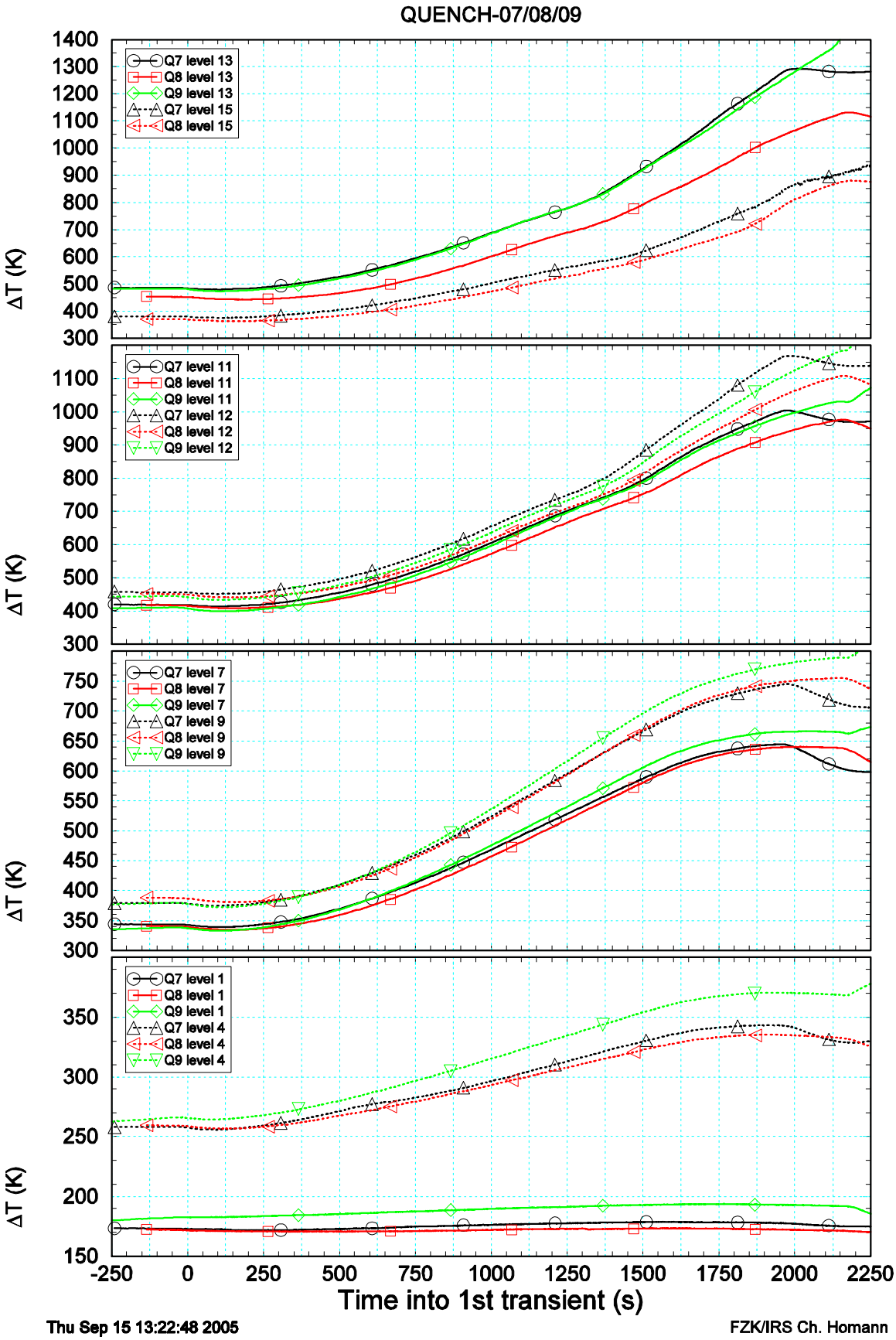

Fig. 4.3: Radial temperature differences during the first transient

The figure shows the mean temperature difference between shroud and inner cooling jacket at various axial levels for QUENCH-07, -08, and -09.

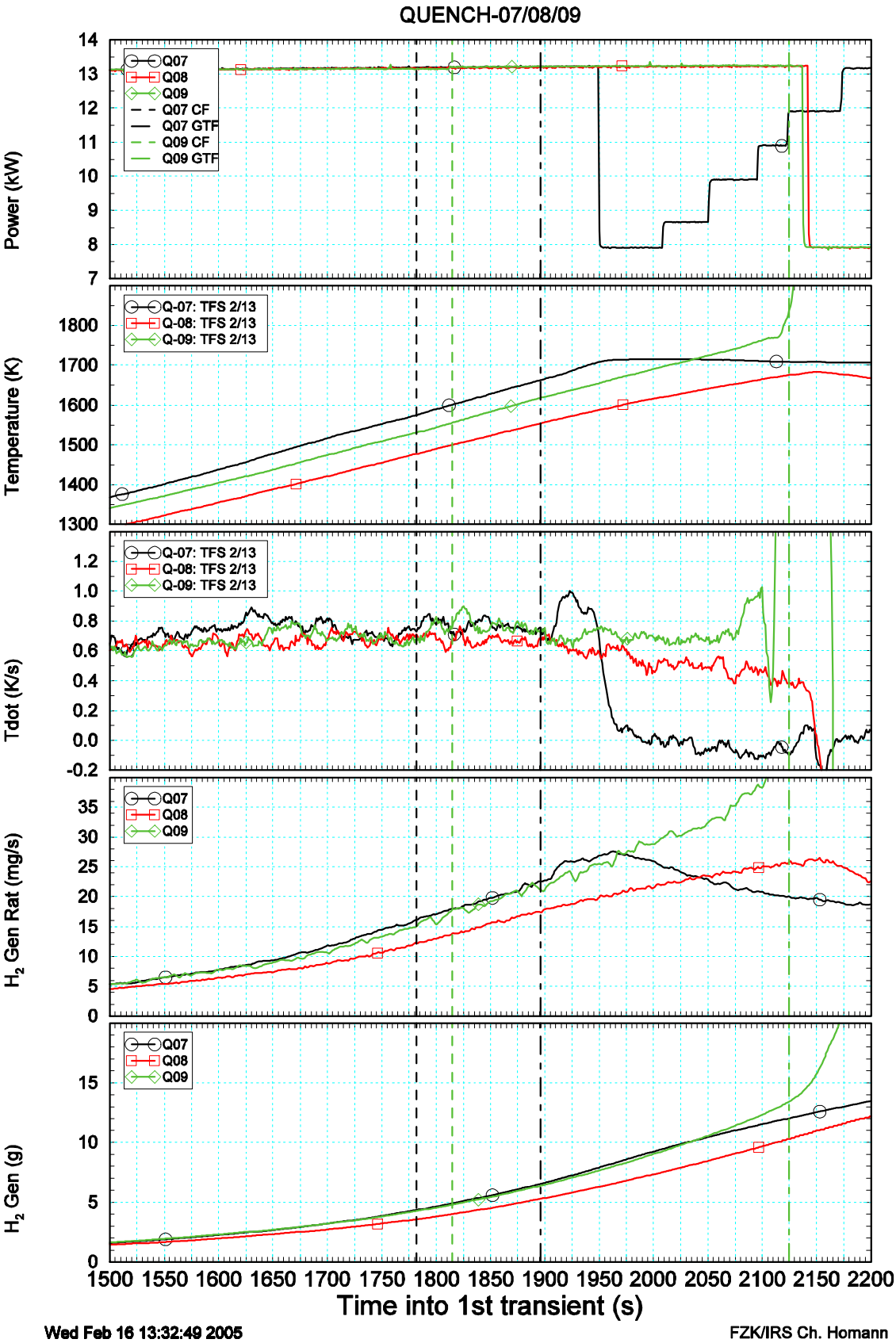

Fig. 4.4: Detail of Fig. 4.2

The figure also contains CR clad (CF) and guide tube (GTF) failure for QUENCH-07 and -09. For a better readability of the figure, these events are only included in the topmost legend.

The differences entail, however, a slower heat-up in QUENCH-08 (Fig. 4.2) with respect to QUENCH-07 so that electrical power is reduced 193 s later. On an average for the three tests, a temperature of 1680 K is reached at 2030 s ± 110 s after the start of the first transient, corresponding to a deviation of about ±5 %. The differences in hydrogen generation rate continue during the temperature plateau phase. It was somewhat difficult to stabilize maximum bundle temperature, and shortly after t' = 2400 s, electrical power had to be reduced to avoid too high bundle temperatures. For such reasons, the real test conduct differs from the envisaged test protocol, and the original plans cannot be resumed. This leads to higher hydrogen generation rates in the second part of that phase in QUENCH-07 and to differences with QUENCH-08 in the subsequent test phases that cannot be avoided.

Taking into account 1.6 g of hydrogen production (details of the related model will be given in section 5.4) that is due to oxidation of B_4C up to the end of the temperature plateau phase, the cumulated hydrogen masses, due to oxidation of Zr alone, differ by 0.4 g only at that time. The status of oxidation should therefore be similar in both tests.

Whereas in QUENCH-07 a stable temperature at about the target value of 1723 K could be maintained for about 15 minutes in the plateau phase, a temperature escalation occurred in QUENCH-09 near the end of the first transient, when the bundle was heated up to reach the plateau phase at the target temperature of 1773 K. To study this difference in more detail and to learn about the limits of stable operation of the QUENCH facility, i.e. an operation without temperature escalation, the two tests are compared for that test phase, as explained in the following. A temperature escalation is caused by a sharp increase of oxidation rate with temperature and enhanced by positive feedback of local electrical power in metallic heaters (local electrical power input increases with temperature).

A temperature of 1700 K is reached at t' = 1940 s in QUENCH-07 and at t' = 2014 s in QUENCH-09. This slight difference has nearly no consequence on hydrogen production. In contrast to QUENCH-07, where electrical power input was reduced shortly after 1940 s, it was kept constant in QUENCH-09 (Fig. 4.4). Temperature continued to increase with a constant rate of about 0.7 K/s up to 1740 K at 2073 s and at a rate of up to 1 K/s until a temperature of nearly 1770 K was reached. Temperature remained constant for about 10 s and then increased drastically. Hydrogen generation rate remained constant up to 2075 s, demonstrating that there is no remarkable temperature increase in the bundle. The temperature escalation in QUENCH-09 is entirely due to the continued heating of the bundle after reaching 1700 K.

These findings suggest that a stable operation under conditions as in QUENCH-07 and -09 is possible up to a maximum temperature of about 1740 K. The ultimate limit is about 1770 K, but it cannot be advised to take credit of this very last safety margin. One should keep in mind that the margin to reduce power, when a temperature of 1700 K is reached, is only one minute for such tests. Consequently, an alternative test conduct, prepared in advance, is indispensable, to react on a temperature excursion, if it occurs. For QUENCH-08, this work has been done [11].

4.2 Second Transient

Only QUENCH-07 and -08 can be considered in this section, because a second transient was planned in QUENCH-09, but not performed (see section 2.2). Fig. 4.5 shows axial temperature profiles in the test section at selected times: The bottom graphs refer to the end of the first transient, the other graphs refer to the same times into the second transient, t_2. The meaning of the symbols, as far as it is not given here, is explained in Fig. 7.2. For a long time of the tests, the differences in bundle behaviour, remarked earlier, can hardly be seen, even in the hot zone. It is only for later times, that these differences become large. Analysis is, however, more difficult than in previous test phases, because the number of TCs in the hot zone that can be considered becomes more and more restricted. Besides to "normal" failure, bundle TCs at levels 11 and 12 (750 mm and 850 mm) and shroud TCs in the upper electrode zone become unreliable at high temperatures in all tests including QUENCH-09. In [3] this problem is called "hot zone effect", and quantitative information about such TCs, called questionable TCs, is given in a table. These TCs are not included in the figures of the present report. The problem refers to QUENCH-07 and -09 and has been avoided in QUENCH-08 and subsequent tests by experimental changes.

Because of the small differences in the test conduct, summing up with time, we found useful for comparison to shift QUENCH-08 results by -200 s so that temperature histories in the hot zone agree during escalation as well as possible (Fig. 4.6). In spite of the differences of local temperature histories, the hydrogen generation rate, a more sensitive variable than temperature, agrees very well with that of QUENCH-07 up to the end of the second transient in QUENCH-08. It was also found that a shift of 198 s or 202 s still gives satisfactory results for the hydrogen generation rates, but a shift outside this range does not. Inspection of this figure shows that the main difference between the two tests in the first part of the second transient is this time shift. In the following, t" will be used for the time into the second transient for QUENCH-07 and for the time into the transient after the time shift of -200 s for QUENCH-08.

After this time shift, bundle temperature at level 13 (950 mm), hydrogen generation rates and their time derivatives agree well, the latter up to about t" = 310 s, i.e. nearly up to the (time shifted) start of cool-down in QUENCH-08 (t" = 335 s). Up to that time, hydrogen productions agree also well (Fig. 4.6 and Tab. 4.1). For QUENCH-07, the first value for hydrogen gives the total amount, the second one the production for oxidation of Zr alone, calculated as described in section 5.4. The last column refers to QUENCH-08 results after the time shift of 200 s, discussed in the text, i.e. time in the first column is t" instead of t_2 as for the other results of this table. Taking in mind that the cumulated masses refer to accumulation since the start of MS data acquisition, this is a sign that globally the two tests are very similar in spite of differences in detail.

Fig. 4.6 also shows that after t" = 335 s the test conduct was very different: In QUENCH-07, the time from significant increase of hydrogen production to the start of the cool-down phase was longer by about 82 s, and much of the hydrogen production in the second transient of QUENCH-07 occurs in this time interval. It is not only in the upper part of the heated zone but also in the upper electrode zone that temperatures are seen to increase so that the region, where most of the hydrogen is produced, is quite large. It has been remarked early in

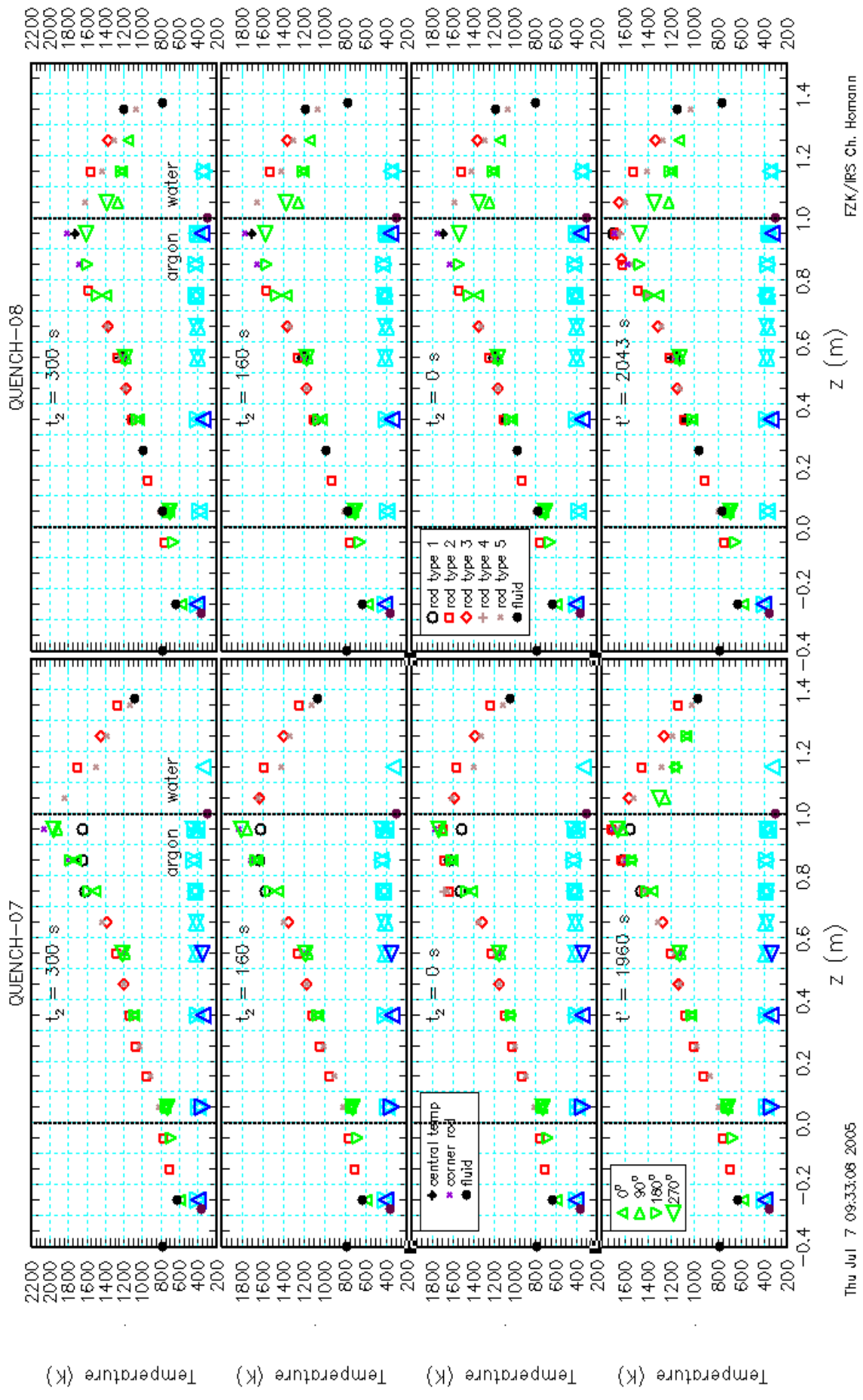

Fig. 4.5: Axial temperature profiles for QUENCH-07 and -08 at selected times

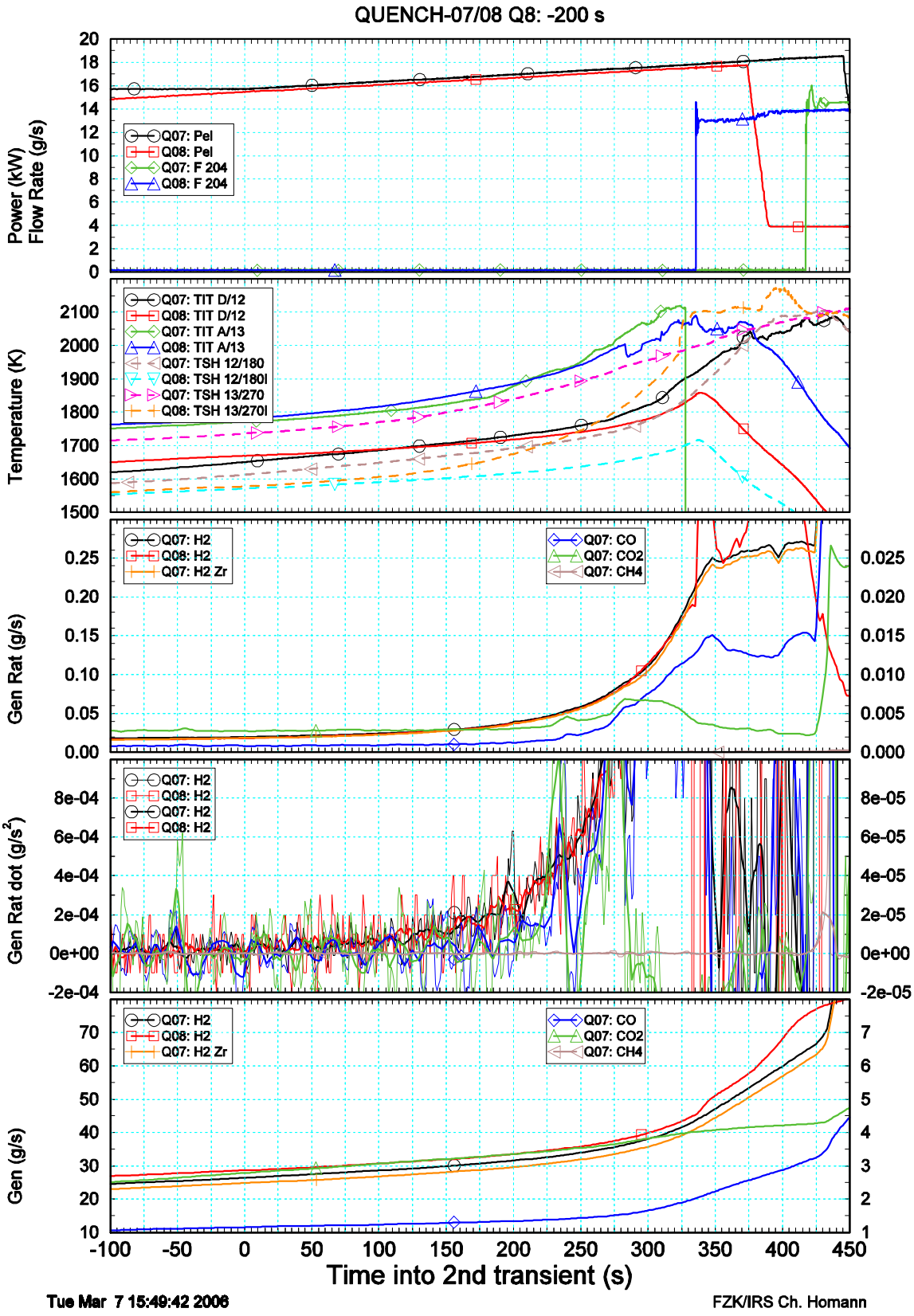

Fig. 4.6: Main variables for QUENCH-07 and -08 during the second transient

The figure shows from top to bottom steam mass flow rate and electrical power, temperatures at levels 12 and 13, generation rates, their time derivatives, averaged over 11 subsequent time steps, and cumulated masses for H_2, CO, CO_2, and CH_4.
In this figure and in this figure only, QUENCH-08 time scale is shifted by -200 s.

Tab. 4.1: Cumulated hydrogen mass at selected times into the second transient

t" [s]	Hydrogen production [g]		
	QUENCH-07	QUENCH-08	Q-08 mod
0	26.3/24.8	25.2	28.6
315	40.0/37.6	31.0	41.9
335	43.5/41.0	31.5	45.2
417	64.5/61.3	45.2	

post-test data evaluation [12], that hydrogen mass, produced in the two tests, is very different in the second transient, but the reason was not understood at that time.

Three conclusions can be drawn from this work. Firstly, tests QUENCH-07 and -08 cannot be compared directly for any other purpose, if the second transient of QUENCH-07 or the cool-down phase is included in the comparison. In particular, a comparison of hydrogen release of the various test phases, as done e.g. in [5], is not adequate for the second transient and the subsequent cool-down phase and may lead to wrong conclusions. Secondly, it is very difficult or even impossible to gain local information about the bundle status in the hot zone for two reasons. In QUENCH-07 surface mounted TCs, TFS, in the heated zone above 550 mm have failed long before the last 80 s of the second transient, and protected TCs have a sensible thermal capacity. The third conclusion refers to future tests: if two tests should be performed as similar as possible under high temperature conditions, special attention must be paid to the duration of that phase. Decisions should probably best be based on hydrogen generation rate and hydrogen production during that time. A given amount of hydrogen production, after hydrogen generation rate exceeds a given threshold might be used. Perhaps, time derivative of hydrogen generation rate should also be monitored to determine the start of enhanced hydrogen production. Such a procedure cannot give perfect results, but the similarity of the tests in question might be improved. It is emphasised that the time interval for operator reactions is rather small.

4.3 Cool-down

Reduction of electrical power was somewhat different in the three tests: It started 28 s, 39 s, and 25 s, respectively, after cool-down initiation. Steam mass flow rate is about 0.5 to 1.3 g/s lower in QUENCH-08 than in QUENCH-07. Electrical power stayed at decay heat level for 148 s, 188 s, and 68 s, respectively. Because of the decisive differences of QUENCH-07 and -08 in the second transient, it cannot be found out from experimental data, to which extent the differences of the test conduct in the cool-down phase affect the results. Due to the different conduct of tests QUENCH-07 and -08, especially during temperature escalation in the second transient, a direct comparison of the cool-down phases seems impossible though QUENCH-08 was intended as a reference test for QUENCH-07. The unreliable MS data, discussed in section 7.2, add to this problem.

5 Control Rod Damage

The three QUENCH tests are investigated in detail to extract as much information about B_4C behaviour as possible, relying mainly on on-line data. This analysis was performed to understand the tests and to achieve a sound basis for modelling, not available up to now. This strategy gives the possibility to shed light on the time sequence of control rod degradation and its relation to other events occurring during the tests. As a by-product, some insight is also gained about other topics. Following the second rule in the second section of [13], where it is recommended to split a given problem into as much smaller ones as possible and necessary for a better solution, the different test phases are investigated separately.

5.1 First Transient and Temperature Plateau Phase

Tests QUENCH-07 and -09 show very different behaviour with respect to B_4C oxidation (Fig. 5.1, and Fig. 5.2). This occurs even during the first transient, when the experimental conditions are still quite similar. To clarify this item, some detailed work on on-line data was performed.

From the start of data acquisition, a small signal is detected by MS in both tests, suggesting release of CO and CO_2, though the control rod should be intact. The signals are interpreted to come from impurities in the bundle. Some N_2 from impurities of the argon supply may add to the CO signal, both species having the same mass number of 28, but this contribution is neglected in this report.

CO and CO_2 signals together correspond to the consumption of about 2 mg/s of steam. The basis for this assessment is outlined in section 5.4. Assuming laminar flow, the steam mass flow rate in the gap between the CR clad and guide tube is assessed to be about 5.0E-5 or even less of the steam mass flow rate in the bundle, hence no more than 0.15 mg/s for nominal steam mass flow rate. The CO_2 signal alone corresponds to the consumption of about 1 mg/s of steam. Therefore, B_4C reactions within the control rod are negligible. CH_4 signal is much smaller than CO_2 signal and therefore not considered further.

Until the end of the temperature plateau phase of QUENCH-07, the generation rate for CO_2 is higher than that for CO. The same is true for QUENCH-09 for the time between 2135 s and 2195 s. The reasons for this finding are not investigated further. In any case, the Boudouard equilibrium for the reaction

$$C + CO_2 \leftrightarrow 2\ CO$$

alone cannot be used for an explanation, because chemical reactions of CO and CO_2 with steam like

$$C + H_2O \leftrightarrow CO + H_2$$
$$CO + H_2O \leftrightarrow CO_2 + H_2$$

may contribute to the overall results.

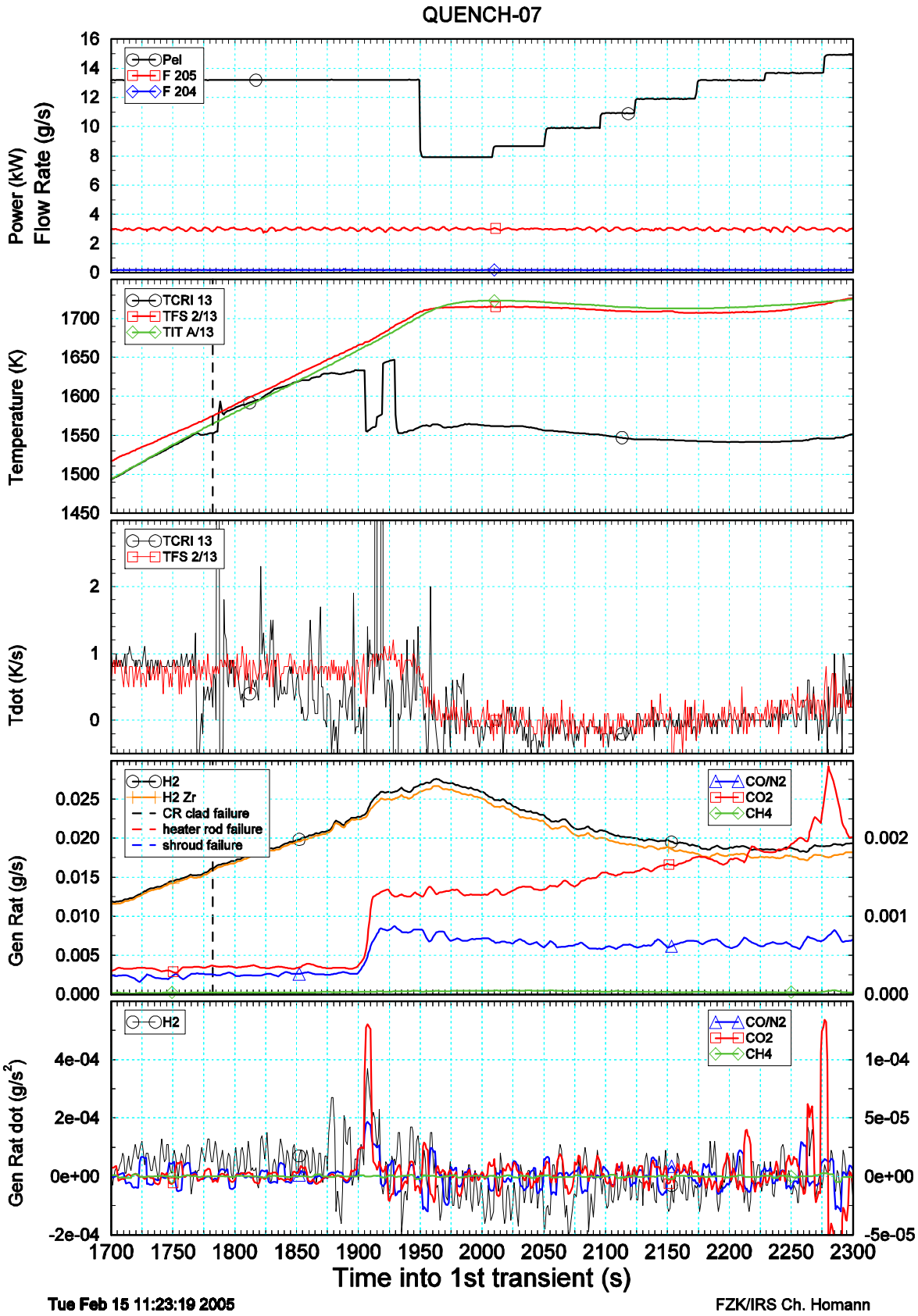

Fig. 5.1: CR failure in QUENCH-07

The figure shows from top to bottom electrical power and steam mass flow rate, temperatures at level 13, its time derivative, generation rates for H_2, CO, CO_2, and CH_4 and their time derivatives.

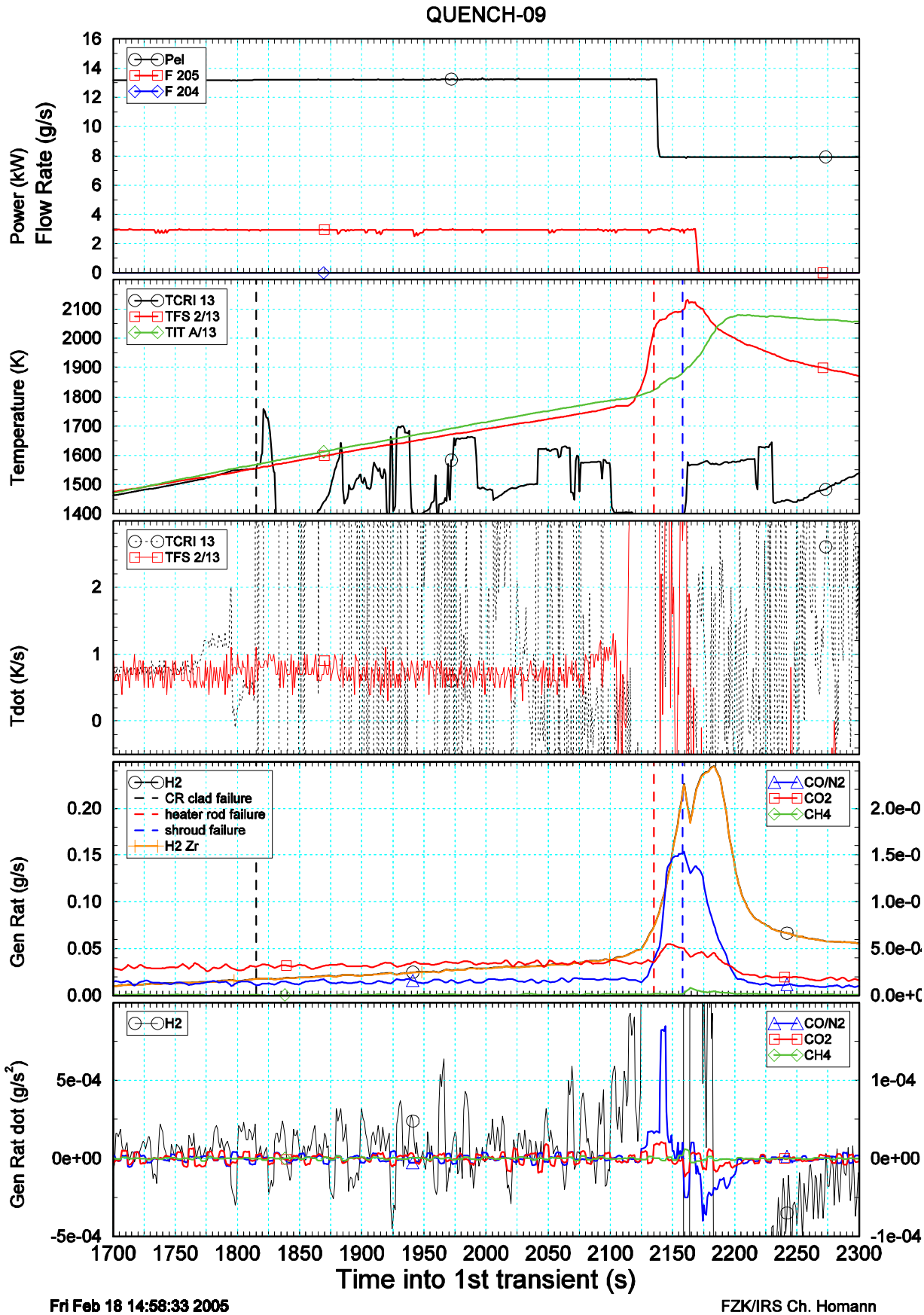

Fig. 5.2: CR failure in QUENCH-09

The layout of this figure is the same as for Fig. 5.1.

Before the end of the first transient, at about t' = 1770 s in QUENCH-07 and about 1790 s in QUENCH-09, TCRI 13 changes signal behaviour, as can be seen directly from temperature or from its time derivative (Fig. 5.1 and Fig. 5.2). Shortly afterwards, helium release, detected by the MS at t' = 1782 s for QUENCH-07 and 1815 s for QUENCH-09, indicates control rod clad failure. In [2] and [3], this event is termed as control rod failure.

To understand control rod degradation, however, it is necessary to be more precise. For both tests, maximum temperatures at the time of helium release are close together, 1575 K and 1555 K (see also Fig. 4.4). Since reaction rates increase with temperature, it is assumed that the axial failure position is at the location of maximum temperature. Maximum temperature is reached near the upper end of the heated zone, as predicted in the calculations and measured in the test, and as will be confirmed in section 8.

As can be expected, CO and CO_2 release do not increase immediately after control rod clad failure, because at that time, only the very small steam mass flow rate in the small gap between CR clad and guide tube is available for oxidation. In addition, eutectic melt of control rod material ("absorber melt") relocates and closes that gap because of its small viscosity and good wetting, thus ceasing steam flow and hence B_4C oxidation in this gap. PTE shows that such blockages exist down to elevations of 650 mm and 503 mm, respectively in both tests. The absorber melt freezes at about those elevations, as will be discussed in section 8.

The similarities between the two tests end with control rod clad failure. In QUENCH-07, CO and CO_2 generation rates increase significantly 114 s after control rod clad failure (Fig. 5.1). Since the steam mass flow in the gap within the control rod is too small for such signal levels, they can only be caused by steam in the bundle fluid channel, coming into contact with absorber melt. We deduce therefore that at the time, when CO and CO_2 production increase, not only the metallic material of the guide tube fails, if it is not already completely dissolved, but also its oxide scale fails. In the following, the failure of both materials is meant, when guide tube failure is addressed. In principle, an outer as well as an inner oxide scale should form during early test phases, but due to the small steam mass flow rate in the gap, the latter can be neglected. As for CR clad failure, the failure position should be near the upper end of the heated zone.

For a better understanding of the phenomena, some results of SET are summarized in the following. It is commonly known (see. e.g. [14]) that melt formation is initiated in a CR assembly by interactions between stainless steel and B_4C and between stainless steel and Zry, if solid state contact is provided, eutectic temperatures are exceeded, and existing scale barriers are dissolved. During subsequent temperature increase, the gap in the CR is filled and steel melts, resulting in internal accumulation and relocation of absorber melt of variable local composition. Melt release or possibly ejection under constraint through perforated, breached, or dissolved guide tube scale takes place into the surrounding bundle.

H_2 generation rate is somewhat larger than before guide tube failure, but the slope is unchanged after the step. CO release essentially remains constant after guide tube failure, whereas release of CO_2 and CH_4 even increase during the subsequent temperature plateau phase. It is supposed that this effect is caused by melt relocation outside the control rod, such increasing the surface that is available for oxidation.

In QUENCH-09, release of CO and CO_2 increases 310 s after control rod clad failure (Fig. 5.2). As in QUENCH-07, this observation is interpreted as failure of the CR guide tube near the upper end of the heated zone. The time interval between CR clad and guide tube failure is nearly 200 s longer than in QUENCH-07 (Fig. 5.1 and Tab. 5.1). The maximum bundle temperature at this time is much higher, namely 1830 K instead of 1663 K as in QUENCH-07, and the generation rate for CO is higher than that for CO_2. In spite of the well-confirmed basic knowledge, given above, it is unfortunately not possible to analyze the reasons for the rather large time difference of about 200 s between the two B_4C tests into details of component interactions and test conditions.

The guide tube failure occurs during the temperature escalation, and happens after a sensible increase of hydrogen production (see time derivatives in Fig. 5.2), suggesting that up to this time control rod degradation is only a consequence of general bundle behaviour and not its cause. The peak values of CO and CO_2 generation rates, 1.6 mg/s and 0.6 mg/s, respectively, are in the same range as the generation rates after guide tube failure in QUENCH-07 of about 0.7 mg/s and 1.3 mg/s. The ratio of CO and CO_2 generation rates is quite different from that in QUENCH-07, perhaps due to the higher temperature, but as stated earlier, this cannot be analyzed in more detail.

Also in contrast to QUENCH-07, CO and CO_2 generation rates decrease quickly after guide tube failure, the final values being even below those before control rod clad failure. A closer inspection of the test conduct shows that at this time the steam mass flow rate in the bundle is reduced from 3.4 to 0.4 g/s. The supposed failure position near the upper end of the heated zone suggests that after steam mass flow reduction far less steam is available for oxidation of absorber melt at that axial level than before. This idea is supported by pre-test calculations [7]. Some absorber melt may have been released directly after guide tube failure and may even have relocated, but the MS signals suggest that its oxidation cannot be large. In sum, the experimental data suggest strongly that in QUENCH-09 control rod degradation with failure of both clad and guide tube occur during the first transient. Therefore, the previous assumption that the oxide scale of the guide tube might keep intact until cool-down initiation [3] must be corrected.

In contrast to noteworthy oxidation of absorber melt, formation of absorber melt continued without restriction during the phase of reduced steam mass flow rate and increased the extent of control rod degradation. Unfortunately, the progress of bundle degradation and the influences of released and relocated absorber melt cannot be deduced from PTE of the final bundle state. PTE shows that no residual B_4C is left in the hot zone, but it is impossible to identify the time when the B_4C disappeared and to correlate it with MS data.

Based on the chemical reactions, considered relevant for hydrogen production due to B_4C oxidation (see section 5.4), about 7 mg/s of steam are consumed in QUENCH-07, and 9 mg/s in QUENCH-09 just after guide tube failure. A further increase in QUENCH-09 may be inhibited by the reduction of electrical power. After decrease of steam mass flow rate, the CO and CO_2 signals together correspond to a consumption of about 1 mg/s of steam. The ratio of this value to steam consumption before guide tube failure is roughly the same as the ratio of steam mass flow rates before and after steam mass flow reduction. This is a further indication that the decrease of CO and CO_2 generation rates is caused by steam flow reduc-

tion. Impurities in the bundle may have been burnt nearly completely during the temperature escalation. The slow decrease of H_2, CO, and CO_2 signals just after reduction of the steam mass flow rate may be due to the longer transit time from the bundle to MS. The differences in decrease may be caused by the different extent and level of the regions, where the gases are produced.

In QUENCH-09, TCRI 12 failed at about the time of power reduction at the end of the first transient. In both tests, the various TCRI may show signals after contact with absorber melt or guide tube failure and suggest physical effects, at least qualitatively, but interpretation is dubious so that no more information can be obtained.

5.2 Cool-down

Whereas in the second transient of QUENCH-07 and -08 not much new insight can be gained, some remarks should be made for the cool-down phase. In QUENCH-07, H_2, CO, CO_2, and CH_4 production increase simultaneously after a certain delay, due to condensation in cold parts of the steam feed pipe for cool-down steam, as explained in section 3.3. They show approximately the same trends up to about 85 s into cool-down (Fig. 5.3). The peak value of hydrogen production is higher than the maximum possible value, i.e. 1/9 of the inlet steam mass flow rate. As will be discussed in section 7.2, this is probably due to a measuring error, its reasons still being unknown.

Further inspection reveals that the slopes change sometimes quite sharply, e.g. at 40 s into cool-down for CO and CO_2 production and at about 48 s and 87 s for H_2 production. At about 80 s, a second peak of CO and CO_2 generation rates occurs, but it is not paralleled by hydrogen release. TCs do not contribute much to understand these observations; some shroud TCs (TSH) show some change starting about 40 to 50 s into cool-down that might be taken as an indication for material relocation and oxidation, but this interpretation is not sure.

In QUENCH-09, highly porous absorber melt has been found in PTE. Its external and internal surfaces have probably substantially increased until cool-down initiation. The amount of molten or re-solidified masses should have substantially increased due to dissolution of rod cladding under formation of diluted mixtures. Their partial oxidation can be a reason for formation of gaseous products like CO and CO_2 and thus foaming, realized within the blocked hot bundle zone during PTE. Closed porosity has to be distinguished from open pores and channels, where exposure to a large supply of steam takes place now. The large surface may explain the high generation rates of CO and CO_2 in the cool-down phase (Fig. 5.4), as well as the simultaneous increase of the H_2 signal.

Differences later in the cool-down phase may also be due to the various differences in the three test conducts. Therefore, in QUENCH-09 CO_2 generation rate increases later than CO generation rate and keeps below CO values. As in QUENCH-07, hydrogen generation rate decreases later in the cool-down phase, whereas CO_2 production increases. For an overall comparison of control rod degradation, the main events are listed in Tab. 5.1, for QUENCH-07 in the left and for QUENCH-09 in the right part.

Tab. 5.1: Sequence of CR degradation

QUENCH-07	QUENCH-09
First transient	
CO/N_2 + CO_2 signal due to impurities	
CR clad failure	
Detected by helium release	
1575 K / 1782 s	1555 K / 1815 s
Interaction B_4C/steam not detectible	
Guide tube failure	
Detected by CO + CO_2	
Begins at level 13	
1663 K / 1896 s	1830 K / 2125 s
into the 1st transient, hence	
114 s	310 s
after CR clad failure	
Simultaneous with increased H_2 production	Begins after
Temperature plateau phase	
Ratio CO/CO_2 typical for	
low temperatures	high temperatures
CO/CO_2	
increases with time	ends by steam flow reduction
Second transient	**Steam starvation**
increase of CO/CO_2 begins after enhanced temperature increase	CO/CO_2 signals decrease below initial values
	Continuing interaction between B_4C, steel, and Zr within CR
	Release of CR melt into bundle, interaction and relocation, but no significant oxidation
Cool-down phase	
H_2, CO/CO_2 signals increase simultaneously	H_2, CO signals
	CO_2 signal delayed

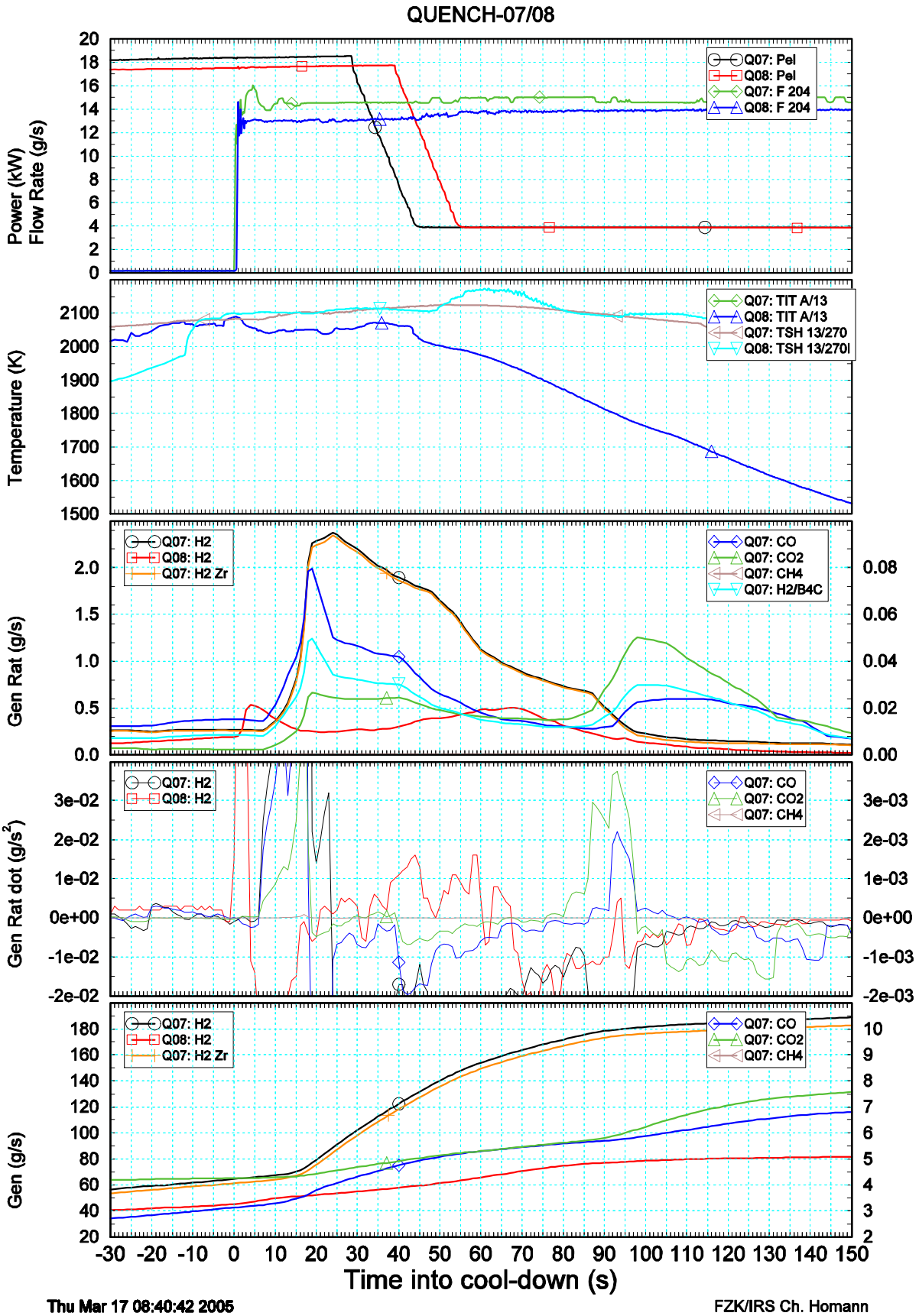

Fig. 5.3: Main variables for QUENCH-07 and -08 during cool-down

The layout of this figure is the same as for Fig. 4.6.

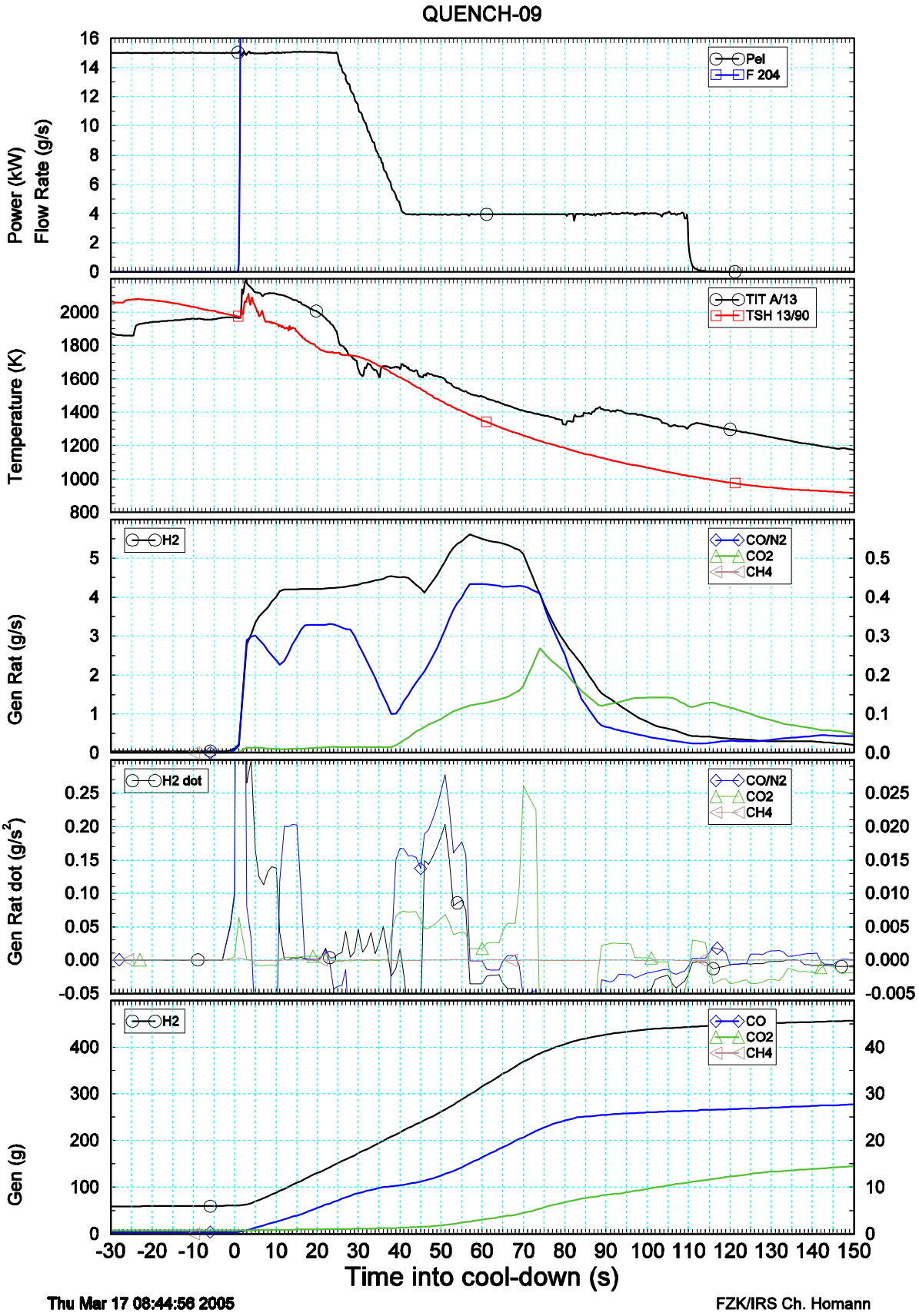

Fig. 5.4: Main variables for QUENCH-09 during cool-down

The layout of this figure is the same as for Fig. 4.6.

5.3 Relation to Failure of Heated Rods and Shroud

In QUENCH-07, guide tube failure occurred long before failures of heated rods and shroud (Tab. 2.1), namely 1331 s and 1348 s earlier. In QUENCH-09, first failure of heated rods and shroud were detected 10 s and 33 s after increase of CO generation rate, hence much earlier than in QUENCH-07, where failure of heated rods and shroud occurred during the second transient. In both tests, heated rods and shroud fail before cool-down initiation. This is in contrast to QUENCH-08 and most other QUENCH tests and suggests that CR degradation has an impact on fuel rod degradation. We cannot deduce definitely from experimental data in either of the two tests, to which extent failure of heated rods is influenced by control rod degradation. However, we can argue from a long experience with SET that a direct contact of the fuel rod cladding with ejected absorber melt may well do much harm to the cladding. The oxide scale can only delay but not prevent in principle the complex physico-chemical interactions and may have mechanical consequences as well. Detailed investigations are difficult, because the interactions depend strongly on the boundary conditions.

5.4 B_4C Contribution to Oxidation

5.4.1 Basic considerations

In this section, we try to assess the direct influence of control rod degradation on the bundle with respect to both hydrogen generation and release of chemical power by determining the ratio of B_4C contributions to those of Zry. The work is therefore exclusively based on MS test data. Relying on [15], the chemical reactions between B_4C and steam, given below, are considered the essential ones under the given conditions and therefore used in our assessment. In addition, oxidation of Zr is considered.

$$B_4C + 7\ H_2O \rightarrow 2\ B_2O_3 + CO + 7\ H_2 - 760 \quad (1)$$

$$B_4C + 8\ H_2O \rightarrow 2\ B_2O_3 + CO_2 + 8\ H_2 - 792 \quad (2)$$

$$B_4C + 6\ H_2O \rightarrow 2\ B_2O_3 + CH_4 + 4\ H_2 - 987 \quad (3)$$

$$Zr + 2\ H_2O \rightarrow ZrO_2 + 2\ H_2 - 595 \quad (4)$$

The last numbers in these exothermal chemical reaction equations are enthalpy changes in kJ per mol of the leftmost specie on the respective left hand side, i.e. of B_4C or Zr. They do not include enthalpy changes due to B_2O_3 evaporation. Surplus steam reacts with liquid boron oxide to form volatile boric acids [15]:

$$B_2O_3 + H_2O \rightarrow 2\ HBO_2 \quad (5)$$

$$B_2O_3 + 3\ H_2O \rightarrow 2\ H_3BO_3 \quad (6)$$

Tab. 5.2: Hydrogen and chemical power release related to B_4C and Zr oxidation

	Hydrogen Release	**Power Release**
CO	0.5 * co	54.29 * co
CO_2	0.37 * co_2	49.5 * co_2
CH_4	0.5 * ch_4	123.38 * ch_4
Zr	$h_{2\,tot}$ - 0.5 * co - 0.37 * co_2 -0.5 * ch_4	148.75 * h_{2zr}

$h_{2\,tot}$, co_2, co, and ch_4: measured generation rates in g/s of H_2, CO, CO_2, and CH_4, respectively. Hydrogen and power release are in g/s and kW, respectively.

The hydrogen generation rates due to oxidation of B_4C and zirconium, expressed as mass per time, and the related chemical power release are calculated from chemical reactions (1) to (4) from measured generation rates for H_2, CO, CO_2, and CH_4. The factors for transforming measured generation rates into related hydrogen generation rates and release of chemical power are given in Tab. 5.2. The factors, related to hydrogen generation rates, are the product of the number of moles of H_2 in the respective chemical reaction and the ratio of the molecular weight of H_2 and the other gaseous reaction product in question. The factors, related to chemical power release, are given by the specific power release divided by the product of the number of moles of hydrogen and its molecular weight.

It is clear that the results, presented in this section, rely on a number of assumptions that are probably quite well met in the respective tests, but they are listed for the sake of completeness, firstly about B_4C oxidation. Boric acids are measured to be negligible and are consequently not taken into account. Above all, in later test phases, the bundle status becomes more complicated than just after CR guide tube failure, and a number of other reactions is possible, e.g. oxidation of atomic carbon in the absorber melt, resulting in far less CO and CO_2 production and heat release. Other chemical reactions are even endothermic instead of exothermic as those taken into account. As stated above, it is assumed in [15] that their contributions are small enough so that they can be neglected. For the same reason, experimental information is not available in the respective QUENCH tests, and their registration would have further decreased the sampling frequency.

The B_4C pellets are surrounded by a steel cladding that contributes to oxidation. Its contribution to hydrogen production should be about 3 g and 7 g, respectively, in the two tests. This contribution is not taken into account. Another contribution to hydrogen production is the oxidation of the tungsten heater, giving additional 23 g of hydrogen in QUENCH-09. In both tests, the molybdenum electrodes are partly oxidized, contributing with 22 g and 100 g, respectively. Both contributions cannot be taken into account, because the respective time histories are not known. Tantalum oxidation (TC component), corresponding to 1 g and 3 g hydrogen production, can be neglected. All these values are taken from [8]; they are based on the amount of CR degradation, as seen in PTE, and cited at the end of section 6 of the present report.

The contribution of nitrogen from impurities in argon mass flow, having the same molecular weight as CO, is negligible and therefore not taken into account. The amount of transformation of CO into CO_2 on the way of the fluid from the hot bundle to the colder off-gas pipe and

MS (Boudouard reaction), leading to the formation of elementary C, is not measured and hence not taken into account neither.

Apart from these chemical considerations, some further remarks are necessary for understanding the results of this work. It should be kept in mind that the generation rates depend on global information, i.e. MS data from samples downstream of the bundle exit. Consequently, the ratios are global values for the whole bundle, too. In the tests, it cannot be taken for granted that the region that gives the main contribution for B_4C oxidation is the same as that for Zr oxidation. This is important, e.g. when the claddings in the upper electrode zone contribute significantly to Zr oxidation, because the B_4C stack is restricted to the heated zone. Therefore, the local contribution of B_4C oxidation may be relatively high, leading locally to enhanced oxidation of Zr. On the other hand, the region, where B_4C oxidation has an influence on the surrounding fuel rod simulators is restricted for the same reason, letting aside energy transport.

In addition, hydrogen measurement is unreliable, at least, when a high generation rate is measured during the cool-down phase in QUENCH-07 (see section 7.2). Assessment of B_4C contribution to hydrogen production relies therefore on the assumption that at least relative MS results are credible during the whole test.

5.4.2 Results

Fig. 5.5 shows the contributions of B_4C to overall oxidation for QUENCH-07 up to the start of the second transient. In this and the subsequent figures, all y-axis labels are given on the left-hand side, but it is reminded that variables, listed in the right-hand legends, refer to the right-hand scale. At the time of guide tube failure (2136 s), there is a slight increase of hydrogen production due to Zr oxidation, but the time derivative of total hydrogen generation rate then decreases to about the same value as before guide tube failure (Fig. 5.1), demonstrating that the impact does not increase much during the first transient. Just after guide tube failure, about 0.9 mg/s of hydrogen generation rate is due to B_4C oxidation, contributing to about 3 % to hydrogen generation rate and chemical power release. Until the end of the first transient, the influence of B_4C reaction on hydrogen production and hence on bundle degradation does not change significantly and consequently keeps limited. TCs in the bundle do not show any change that might be attributed to guide tube failure; as shown in Fig. 5.1 for the end of the heated zone, temperature increase in the hot zone is given predominantly or even exclusively by power history.

During the temperature plateau phase, the amount of hydrogen generation rate, due to B_4C oxidation, increases somewhat, and so do the B_4C contribution to overall oxidation with respect to hydrogen generation rate, hydrogen production, and release of chemical power, reaching about 7 to 8 % at the end of that phase. 1.2 g of hydrogen production is assessed to be due to B_4C oxidation from guide tube failure up to that time.

During the second transient, all three ratios decrease to about 3 % at its end (Fig. 5.6). Temperatures suggest (see Fig. 7.1 and section 8) that the upper electrode zone becomes more and more important for Zr oxidation. Since in that region no absorber material is available, if not by transport after guide tube failure, the decrease of the ratios is evidently due to the ex-

tension of Zr oxidation zone, at least partially. Hydrogen generation rate due to B_4C stays below 2 mg/s for a long time and increases markedly only when temperature escalation starts. Though the respective histories differ, the contributions of B_4C to hydrogen generation rate and cumulated hydrogen mass are similar up to the start of cool-down.

At cool-down initiation, the contributions of B_4C to hydrogen generation rate and chemical power release decrease to somewhat more than 1 % (Fig. 5.7). In later times of cool-down, data evaluation becomes more difficult, as it has been stated in section 5.2, because further physical and chemical processes may be involved. As an obvious example, CO and CO_2 generation rates increase at about 3645 s, but this effect is not paralleled by an increase due to Zr oxidation, as can well be seen from chemical power release, so that the relative contribution of B_4C oxidation to hydrogen generation rate and chemical power release increases substantially. On the other hand, the absolute contribution is quite small so that such effects do not need much consideration.

In QUENCH-09, data evaluation after the steam flow reduction shortly after guide tube failure is dubious because of the uncertainty of data, especially the amount of nitrogen. Therefore, only cool-down phase is important for consideration. Because of the long time, where steam mass flow rate was reduced and control rod degradation by absorber material interaction could continue, more material is probably accessible for oxidation. Peak values are higher by a factor of two than for QUENCH-07 (Fig. 5.8), and it is plausible to attribute this effect to the above-mentioned phenomena. Increases and decreases in the curves and changing slopes are more pronounced. As for QUENCH-07, interpretation is difficult, but again, details should not be important for general understanding.

Evaluation of MS data indicates that in total 40 % and 100 %, respectively, of B_4C are oxidized in the two tests [17], [18]. Evaluation of the post-test bundle status gave an amount of 20 % and 50 %, respectively. Because of this bandwidth, the data evaluation in this section should be considered with some caution.

From the procedure to evaluate experimental data, as outlined in section 5.4.1, it is clear that only direct contributions of B_4C oxidation to hydrogen production and power release can be assessed. However, B_4C oxidation has also indirect effects on the bundle. Due to B_4C oxidation, local temperature is increased locally, and Zr oxidation rate is also increased. Such effects cannot be derived in the way, outlined in section 5.4.1.

Indirect effects can, however, be assessed from a comparison of hydrogen release in QUENCH-07 and -08. Results (Fig. 4.6 and Tab. 4.1) suggest that indirect contributions are limited up to cool-down initiation in QUENCH-08; afterwards, the differences between the test conducts are too large to draw any conclusion. If B_4C oxidation had a remarkable indirect impact on Zr oxidation, hydrogen production for Zr oxidation alone in QUENCH-07 should be larger than in QUENCH-08 after the time shift of -200 s (last column in Tab. 4.1). In fact, measured hydrogen production in QUENCH-07, including B_4C contributions, is even below QUENCH-08 values after the time shift. In contrast to the experimental finding, calculations for these two tests with ICARE/CATHARE suggest [16] that indirect contributions to hydrogen production exceed direct ones appreciably, but calculated temperatures, especially for QUENCH-07, are so far overestimated that such a conclusion is not reliable.

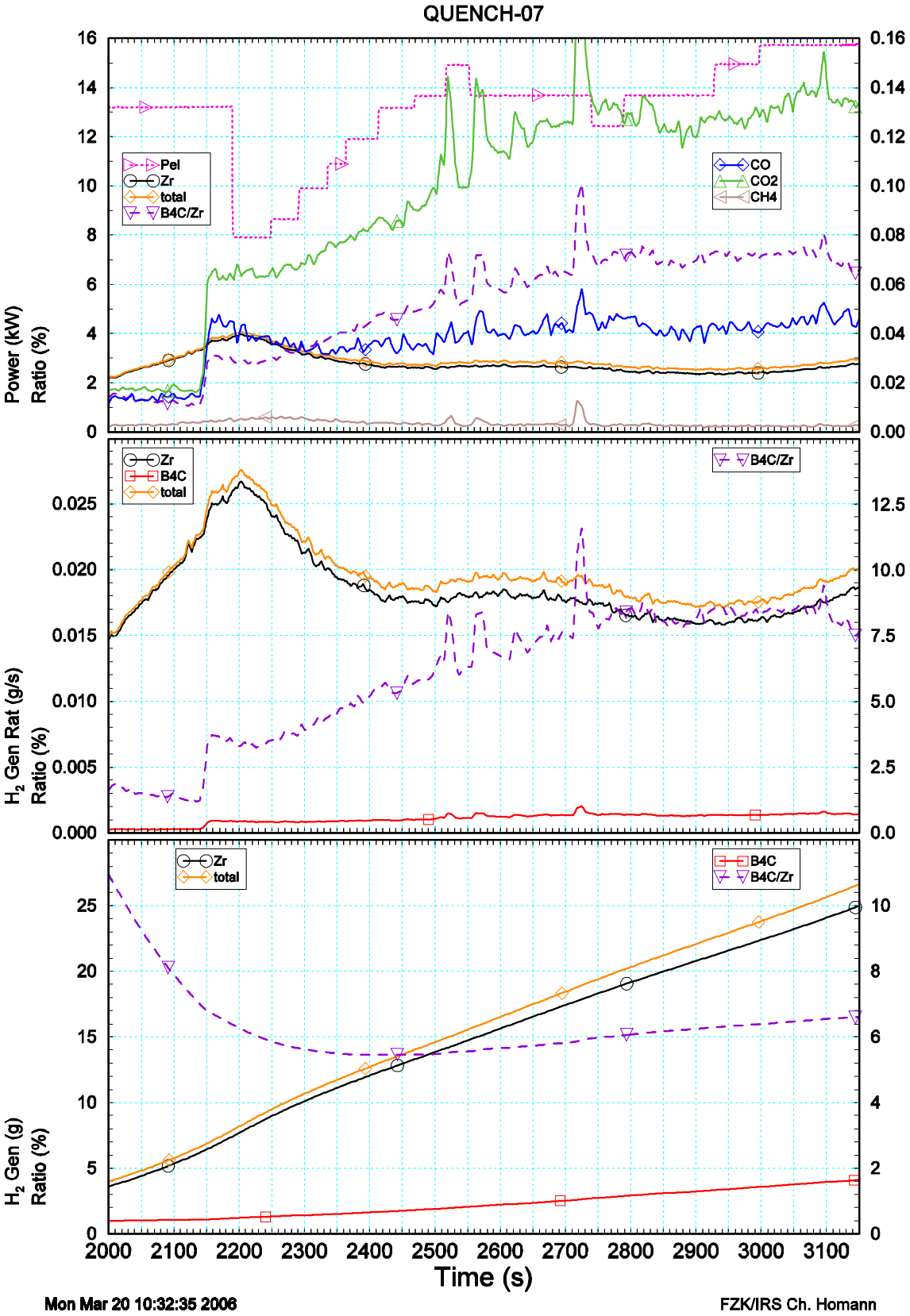

Fig. 5.5: Impact of CR oxidation during temperature plateau phase in QUENCH-07

The figure shows from top to bottom chemical power release, hydrogen generation rates and cumulated hydrogen masses due to B_4C and Zr oxidation by steam. B4C/Zr is the ratio of the respective values for B_4C and Zr oxidation in percent (dashed lines).

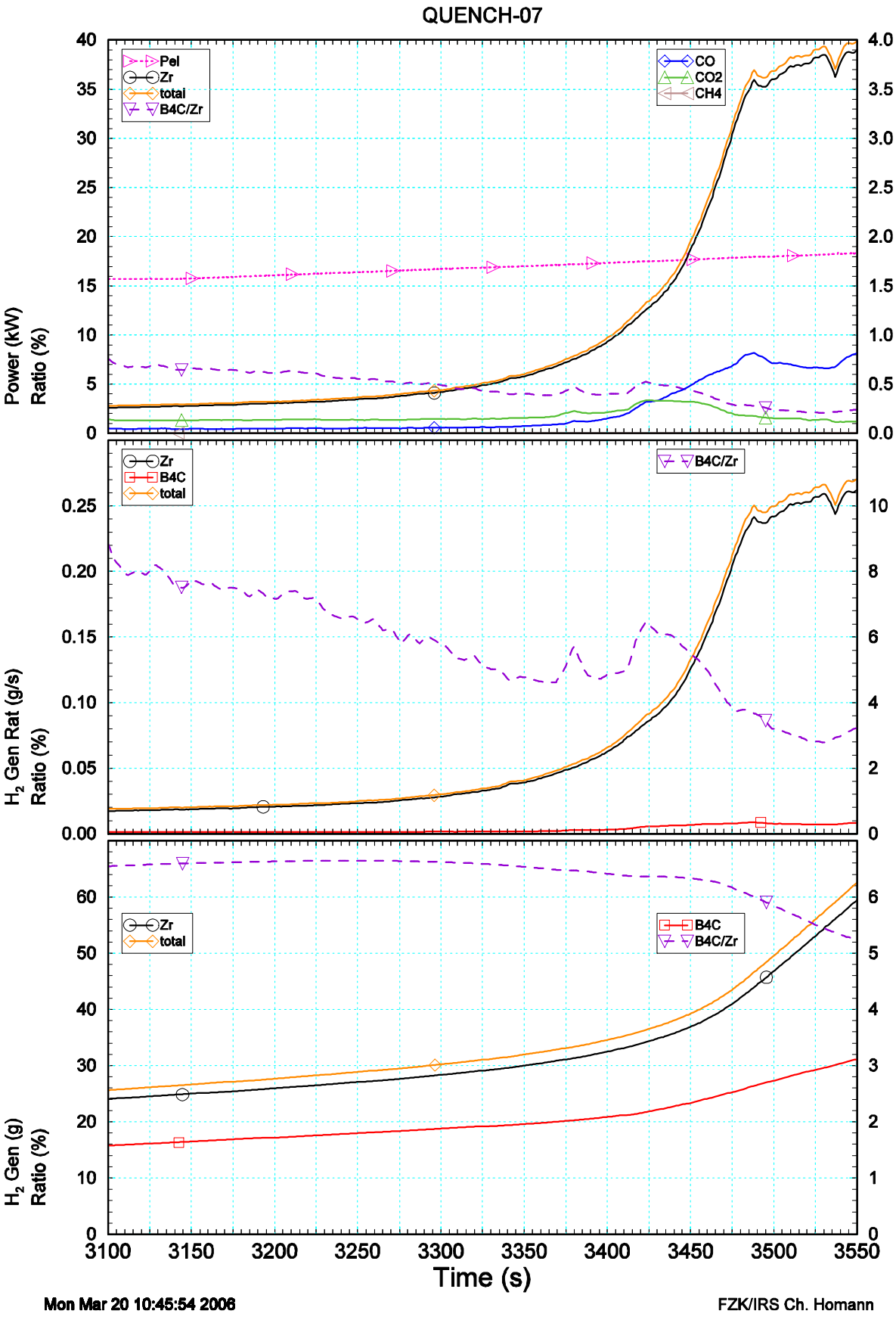

Fig. 5.6: Impact of CR oxidation during the second transient in QUENCH-07

The layout of this figure is the same as for Fig. 5.5.

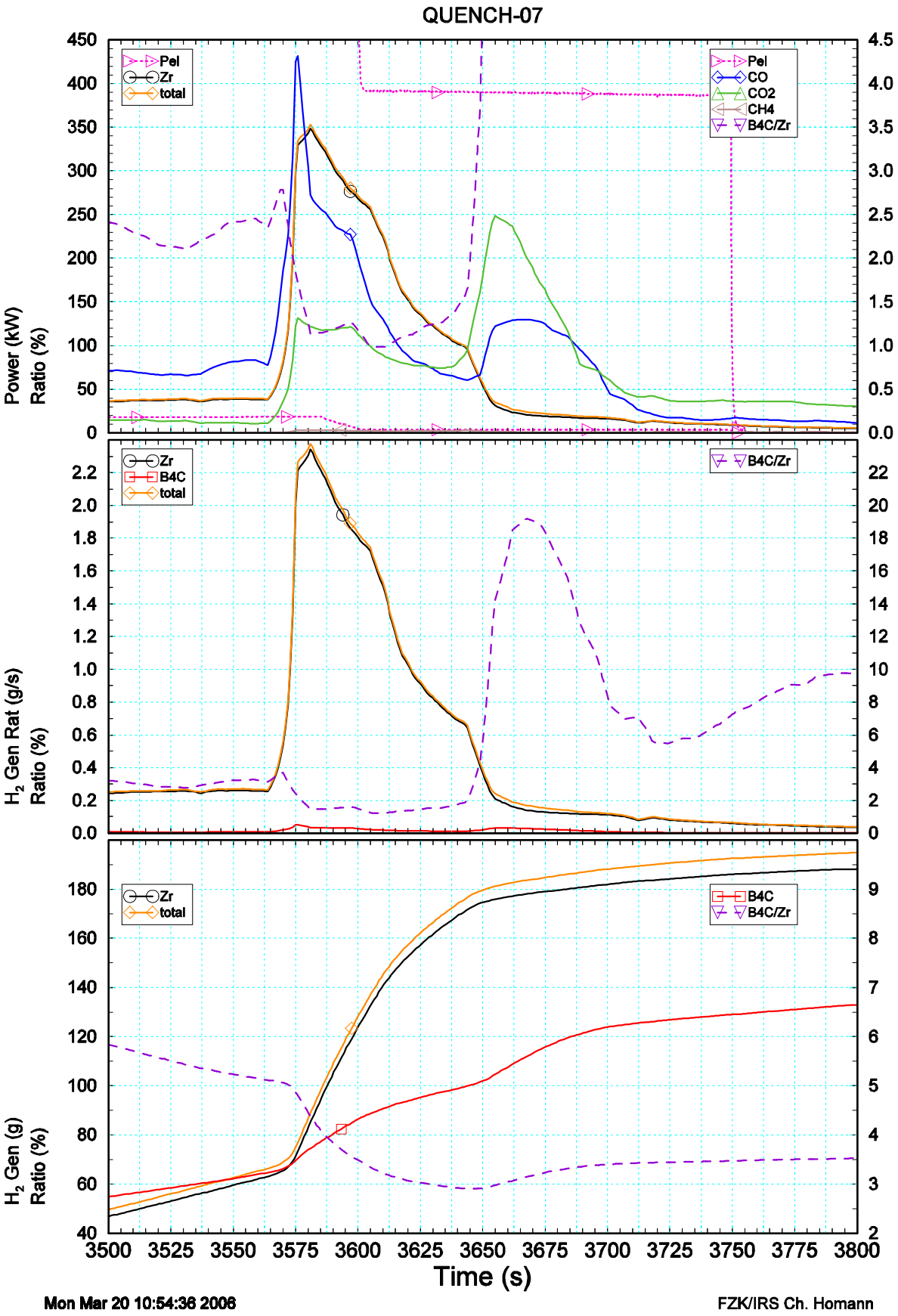

Fig. 5.7: Impact of CR oxidation during cool-down in QUENCH-07

The layout of this figure is the same as for Fig. 5.5.

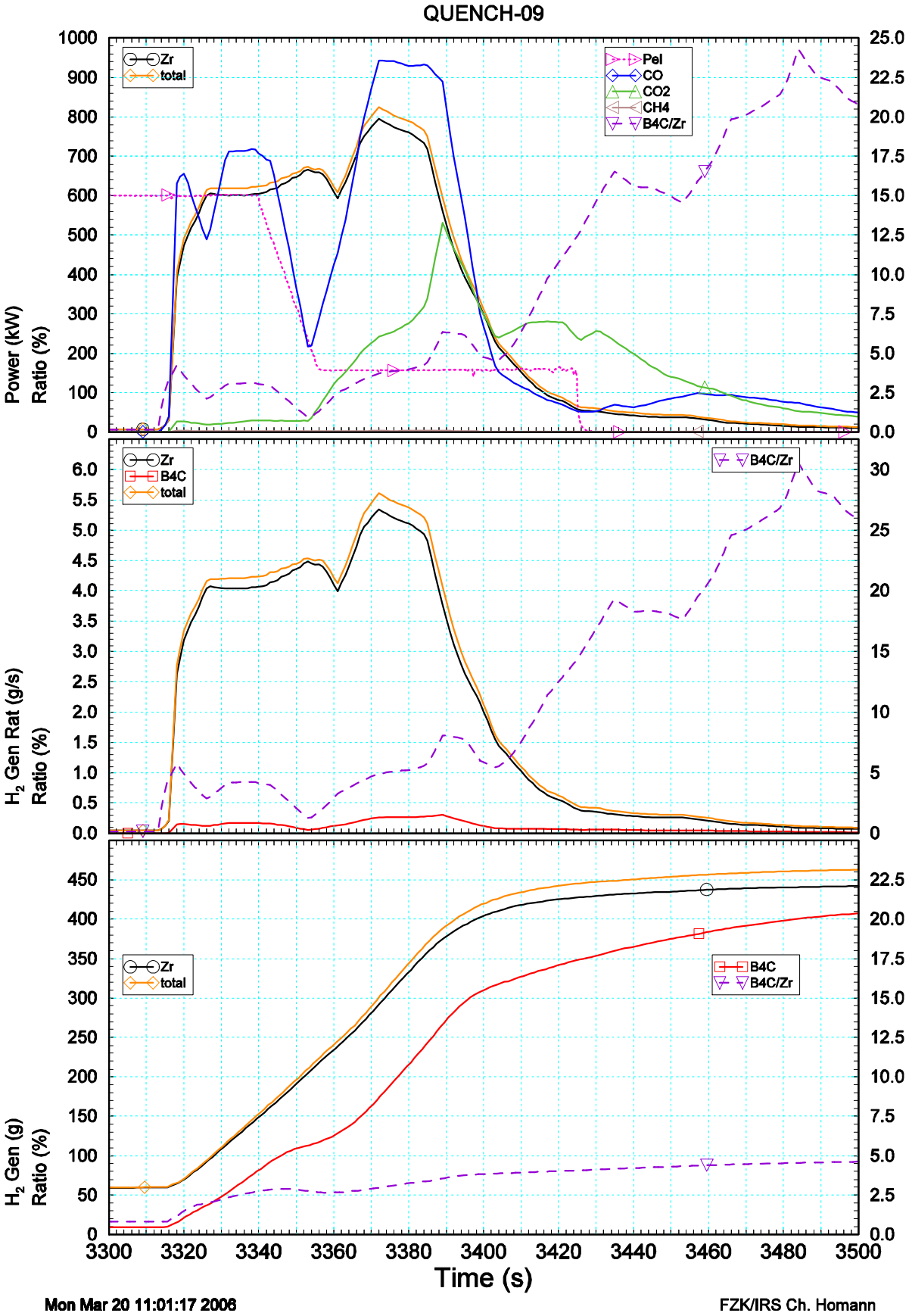

Fig. 5.8: Impact of CR oxidation during cool-down in QUENCH-09

The layout of this figure is the same as for Fig. 5.5.

6 Knowledge from Post Test Examination

Apart from the on-line data, analyzed in previous sections, PTE, mainly based on interpretation of the bundle cuts for high temperature information, helps understanding the experiment. In contrast to evaluation of on-line data, PTE reveals the final status; this makes attribution of observed phenomena to times or events during the test difficult or even impossible. For this reason, conclusions from the post-test status to bundle conditions prior to the cool-down phase may be questionable, especially, when violent processes during water reflood occur, resulting in strong material reactions and interactions between the fluid and structures. Therefore, a comparison of PTE findings and on-line data is necessary, though not always successful, for further insight.

In this section, PTE results of the three considered bundles, documented in [2], [3], and [5] for the respective tests, are summarized and updated, mainly, but not entirely focused on CR behaviour. They are based on the metallographic inspection of a series of cross sections and supporting SEM/EDX analyses. Basic information on material behaviour and property data, mostly available from SET, is implicitly applied. This holds especially for the interactions between the components of the B_4C CR, which are in the focus of interest.

For the reference test, QUENCH-08, PTE of the bundle gives results as summarized in the following: The axial profiles of external cladding oxidation and damage follow the axial distribution of peak temperatures. In parallel, the observed internal oxidative pellet interaction proceeds at positions of contact. Up to the level of ca. 850 mm, the rod arrangement remains quite regular. The lower limit of melt relocation within the bundle was found at 860 mm, that of external shroud melt relocation at 900 mm elevation. At peak temperature level 950 mm local cladding matrix melting and melt re-distribution within rods took place (e.g. within the instrumented central rod), but the influence in total can be neglected. Finally, full cladding conversion to the ceramic state is observed here.

An important source and sequence of long-range melt relocation within the peak temperature zone is identified as external shroud melting, neck formation between shroud and corner rods, melt transfer into the surrounding bundle, and continuing meltdown in form of “candling” events; those are distinguished by growth of ZrO_2 scale, dissolution of embedded scale, and empty scale remnants. This contribution to bundle degradation is not fully typical for the bundle state itself, since the more massive metallic shroud and corner rod structures are involved. Another type of relocation, that of superheated (Zr,O) melt from the near upper vicinity, has formed thin partial covers on a few rods, characterized by the inclusion of bubbles, and the completed oxidation. Finally, the candling of some almost non-oxidized melt is detected; this relocation is deduced to have taken place during the cool-down phase.

The bundle inspection at 1000 mm elevation and the electrode zone levels above, performed to analyze the strong interim superheating during the cool-down phase, supports the given interpretation of late long-range melt relocation. Shorter-range relocation within the considered zone took place as well. This melt redistribution was supported by neck formation between rods, and shows quite similar candling features as described for the shroud melt. Within the rods, cladding melting, some attack of the zirconia coating of molybdenum elec-

trodes by melt, and some Mo exposure to steam took place, however with negligible electrode damage. The brittle fragmentation of thin ceramic structures during cool-down is mentioned.

QUENCH-07 and -09 show a more complicated test history, insofar as the B_4C CR has influenced the bundle degradation behaviour. It is known from SET that CR damage itself is initiated by the formation of two types of eutectic melt: At about 1450 K, slow solid-state interaction of B_4C pellets with the surrounding stainless steel cladding is intensified under progressive melting. At about 1570 K contact between the steel clad and the surrounding Zry guide tube leads to another melt zone after dissolution of scales, which can only delay the interaction. Both melts may merge due to further dissolution of stainless steel below its melting range (lower limit about 1620 K).

For both bundles QUENCH-07 and -09, the detection of filling gas release indicates the CR clad perforation failure, which cannot be inspected. In both tests penetration of melt through this opening has occurred, according to the observed quite similar filling of the gap and downward relocation within the guide tube until blockage formation due to melt freezing at the lowest final level. It is mentioned that such melt is known to have low viscosity and good wetting of metallic surfaces, as confirmed by the PTE.

Though boreholes near the ends of the CR allow access of steam to the gap, the large flow resistance in this channel limits the oxidation of the channel walls significantly. This is why any absorber melt can be seen as oxygen-poor and termed “primary” until escape into the bundle, where its character is quickly changed into “secondary”, which shall indicate the oxygen pick-up and scale formation. This change is accompanied by increasing viscosity and improved wetting of ceramic surfaces. Of course, the melt temperature at the release event is another important parameter. Since the delay period until guide tube scale failure and melt release (according to the detection of CO and CO_2) was different, both bundles will be discussed separately in the following.

Results of the QUENCH-07 bundle inspection besides the above-described initial phase of CR degradation are given. One part of the released CR melt has obviously fallen in form of droplets, most of them captured and re-solidified within spacer grids, as identified at levels 73 mm and 550 mm. Practically no oxidation of this melt and no interaction with the structures have taken place. Another part of the released melt has relocated laterally and axially and is found at the 750 mm level and above, kept between rods or closely attached to them. Those lumps may contain pores and larger voids. They are enclosed by scales, which often show partial spalling. At 750 mm, the CR consists of the thinned B_4C pellet column enclosed by melt, which is still confined by guide tube scale. At 850 mm only this scale structure remains, whereas no products of CR destruction are found at central position here and above. Melting of FRS cladding, neck formation between contacting rods and the shroud, and shroud melt accumulation indicate violent general bundle degradation. This is why a separation between CR and bundle damage is not possible for all the examined higher elevations. Above the heated zone, the CR has disappeared and the bundle cross sections show the distribution of mixed molten interaction products between rods, attack of rod cladding, and complete oxidation of spacer grid structures. In total, those findings are compatible with a fast damage progression during the second transient and the cool-down phase.

The variation of melt composition and the lack of information on the oxidation of mixed melts is a field of uncertainties. It is often seen that Zr-containing melts form an external ZrO_2 scale and irregular internal sub-scales with embedded metallic inclusions, so that simple parabolic kinetics cannot be assumed. The SEM/EDX analysis of interaction products at various final positions has confirmed the existing knowledge about the progress of CR degradation. To derive detailed information, however, it would be necessary to identify the components and phases to get a statistically relevant number of melt lump volumes. The dilution of “primary” CR melt, which played no major role in QUENCH-07 due to the fast oxidation, should be taken into account as well. Nevertheless, it is quite plausible to assume that CR degradation products have promoted the progression of rod degradation e.g. by local cladding interaction with CR melt, stress induced mechanical failure, and oxidation heat release, but its degree is unknown.

The PTE of the QUENCH-09 bundle, supported by SEM/EDX analysis, allows further insights into the coupled degradation and meltdown of a FRS/CR configuration, especially concerning the interim steam supply limitation and the faster cool-down in steam compared to QUENCH-07.

As described for QUENCH-07, the poor thermal stability of the CR due to chemical incompatibility of its components is responsible for relatively early CR degradation and CR melt release. The failure of the CR clad initiated the filling of the gap to the guide tube by internally relocated absorber melt. The reasons for the longer delay period from CR clad perforation (filling gas detection and pressure signals) to guide tube scale failure (CO, CO_2 signals) in QUENCH-09 are not obvious. Any one of the following factors may be decisive or may have an influence: test-to-test variations of the internal CR melt redistribution, the size of the breach, lateral deviations of the nominally concentric tubes and B_4C pellets, the melt release by pouring or possibly by ejection due to pressure build-up. The superheating of the confined melt before delayed release should have decreased its viscosity.

The lateral distribution of released melt cannot be seen as trigger mechanism for fuel rod degradation, as interpreted earlier. In the considered experiment, the fuel rods may have already been in the damage initiation phase at the time of contact with the CR melt. However, the dramatic bundle degradation, observed in the PTE can only be explained by a promotion of rod damage progression: Shortly after melt release, the steam flow rate was drastically reduced. Physico-chemical interactions between melt and contacted rods were thus favoured during the large time span until complete melt oxidation.

No free falling of CR melt droplets in the bundle was found, but cannot be excluded neither. The identification of CR components within some rods, which must have relocated downward internally, can be explained by CR melt penetration after axial rod splitting, crack growth, and split opening (“flowering”, previously not observed in QUENCH, but in CORA tests [22]). Alternatively, melt-induced rod splitting with the same consequences cannot be ruled out. The hot zone extends downward mainly because the steam mass flow rate is reduced so that nearly no more steam is available for oxidation at the upper end of the heated zone and release of chemical power and hence temperature are reduced. This is enhanced by the positive feedback of the axial electric rod power profile. A number of further phenomena may contribute more or less, namely the heat, contained in the relocated melt, the internal oxida-

tion of the breached cladding, the oxidation of accumulated melt. The downward extensions of the hot zone and of the degradation are more pronounced than observed for any previous QUENCH test.

The transition from a bundle configuration to a flow channel / blockage configuration, observed at higher levels within the hot zone, is a unique feature of this test as well; in all previous tests including QUENCH-07 no blockage of the bundle or only small partial ones have been formed. Here, the axially extended blockage configuration can be distinguished into the mostly blocked lower part, filled mainly by porous melt, and the more open upper part, the net source of melt relocation. It is plausible to attribute enclosed melt porosity to gaseous oxidation products of minor melt components from the CR degradation, compared to the observed dense form of pure (Zr,O) type melt, which forms a massive block.

The melt distribution, in the final state completely ceramic masses, allows the tentative interpretation that the incoherent CR melt release or ejection and the interaction of this melt with surrounding rods have stabilized the mainly metallic product melts against downward relocation due to the increase of melting temperatures and the support by viscous drag forces. During the phase of reduced steam supply, melt oxidation was impossible, selective, or incomplete at the given elevation. Unfortunately, the final state of the bundle does not allow deducing all essential information on the previous damage progression. E.g., residual bare B_4C that might have survived the steam starvation phase in the hot zone is not found after cool-down, so that no information about this contribution to the gas analysis signals is available. According to gas analysis and temperature measurements, the response to the cool-down phase conditions was violent. This compares well with the assumption that residual metallic fractions of the dispersed materials and more recently relocated melt from increasing elevations were oxidised quickly during the phase of high steam supply. However, it is not possible to quantify the importance of the preceding phase of reduced steam supply on the cool-down. In comparison to QUENCH-07, the higher steam supply rate in the cool-down phase of QUENCH-09 may lead to higher oxidation and damage as well. Partial steam flow into the annulus between shroud and inner cooling jacket after shroud failure may play a role in this context.

Concerning the simulation quality, it can be assumed that dissolution of zirconia pellets and fuel pellets by CR melt is quite similar. The axial and lateral distribution of interaction and oxidation products might be less prototypical due to the facility specific distribution of electric power and its positive feedback in contrast to the nuclear power profile. In addition, the tungsten heaters may stabilize the pellets in their position in contrast to the conditions in a nuclear reactor. The tungsten and molybdenum dissolution is a facility specific artefact, and the contribution of the oxidation of respective melts to the hydrogen evolution signal cannot be neglected. Based on PTE, it has been assessed in [8] that in QUENCH-07 22 g of hydrogen are due to oxidation of the molybdenum electrodes and 100 g in QUENCH-09. In the latter test, further 23 g of hydrogen are due to oxidation of the tungsten heaters.

7 Further Experimental Results

In this section, a number of results are presented that developed as by-products during evaluation of experimental data. They are supposed to be interesting or useful for those who want to understand the tests in more detail. Some cases show the limits of available experimental information, and the related interpretations may be ambiguous. They are nevertheless included in this report to demonstrate that evaluation of experimental data may give deep insight, but cannot answer ultimately all questions, even if an answer is highly desirable.

7.1 Hydrogen Generation Rate in Second Transient of QUENCH-07

After t = 3488 s, hydrogen generation rate increases far more slowly than before. In [19], it is concluded from comparison of temperatures, thought to be reliable at that time, and hydrogen generation rate (Fig. 7.1) that this effect is due to partial steam starvation, caused by high temperatures in the upper part of the bundle. Total steam consumption would correspond to a hydrogen generation rate of about 0.33 g/s, but not more than about 0.27 g/s of hydrogen are measured in the second transient. This conclusion in [19] implies that the differences between QUENCH-07 and -08 would even be higher if the steam supply in the second transient of QUENCH-07 were larger. Axial temperature profiles in the test section are given in Fig. 7.2 for more clarification. They demonstrate that temperatures in the lower part of the bundle remain rather constant.

We note, however, that in QUENCH-09, total steam starvation was observed, and it is not clear why steam starvation should remain incomplete in QUENCH-07. Furthermore, the change from unlimited oxidation to assumed partial steam starvation is rather abrupt, and there is even a slight and short decrease in H_2 and CO generation rates. Since steam diffuses through the hydrogen layer at the outer oxide surface to oxidize further metal, such a change should be smoother. We also note that at level 15 (1150 mm) bundle temperatures decrease, as it is expected, when oxidation decreases due to reduced steam supply upstream of the TC position. However, they decrease later than at the time of supposed start of partial steam starvation, and, furthermore, they decrease at considerably different times, namely at t = 3500 s (TFS 2/15) and 3527 s (TFS 5/15). At the same time, both bundle TCs at level 16 (1250 mm) continue to increase, and the rise rate is substantial. Furthermore, CO and CO_2 generation rates develop similarly to hydrogen production in that phase, suggesting partial steam starvation at lower elevations so that temperatures at higher elevations should decrease, because the heat source due to oxidation lacks. Evidently, this behaviour is in contrast to the interpretation in [19].

In addition, the temperatures decrease at level 15 is at an axial level, where a large hydrogen generation rate is expected due to high temperature and thin initial oxide scale, and it is not a single TC, but two of them at the same level, giving some confidence that this decrease is meaningful. It suggests a sensible change from usual oxidation behaviour. The figure also shows that at about 3490 s, a number of TCs at elevated temperature deviates from smooth increase or even fails, including TIT D/12. Experience shows that high temperature TCs may fail, when they are exposed to steam for rather a long time, but TIT designates a TC that is

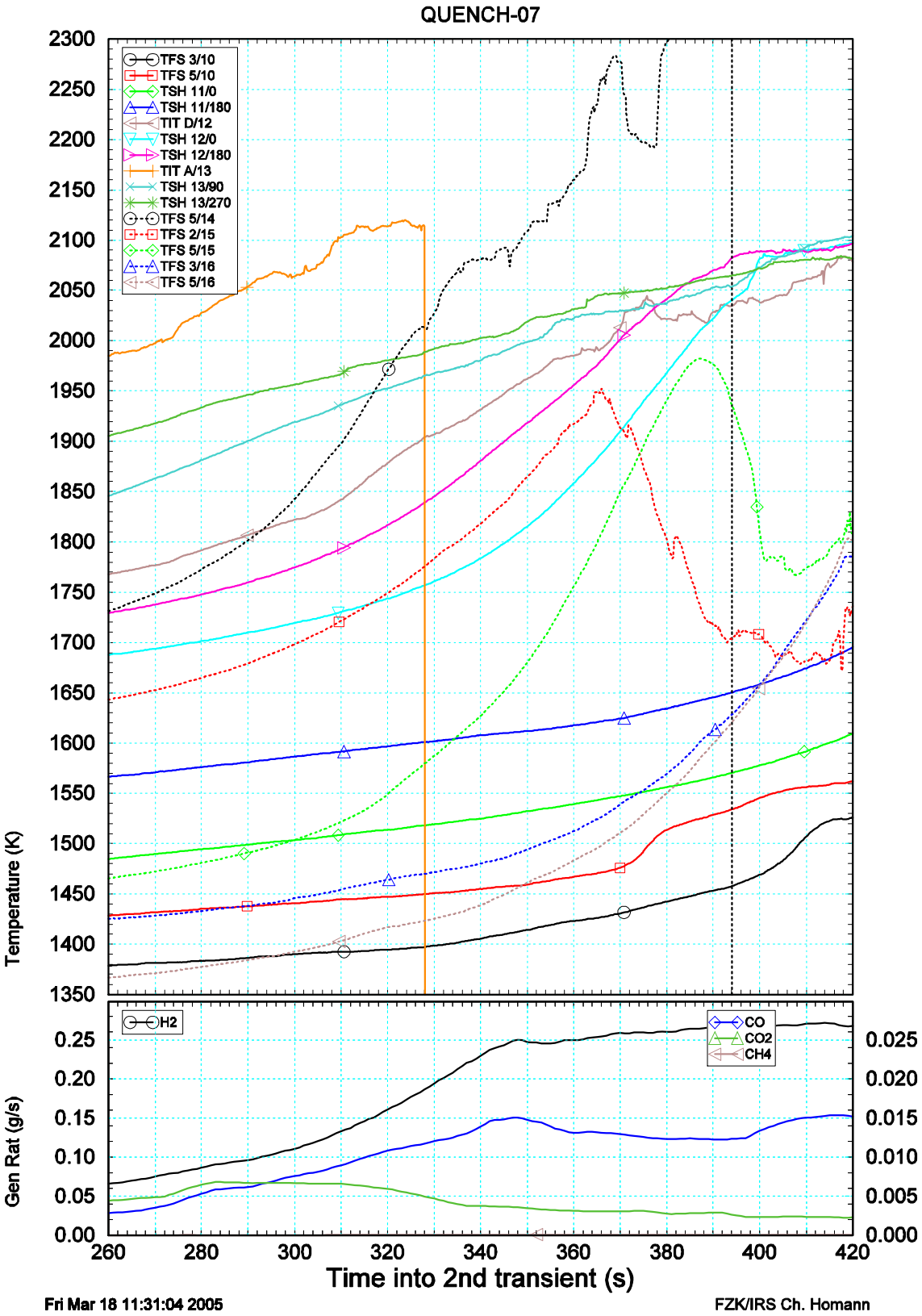

Fig. 7.1: Temperatures and generation rates in QUENCH-07

The figure shows bundle and shroud temperatures above about 1400 K (top) and generation rates for H_2, CO, CO_2, and CH_4 (bottom). Only those TCs are included that are supposed to be reliable.

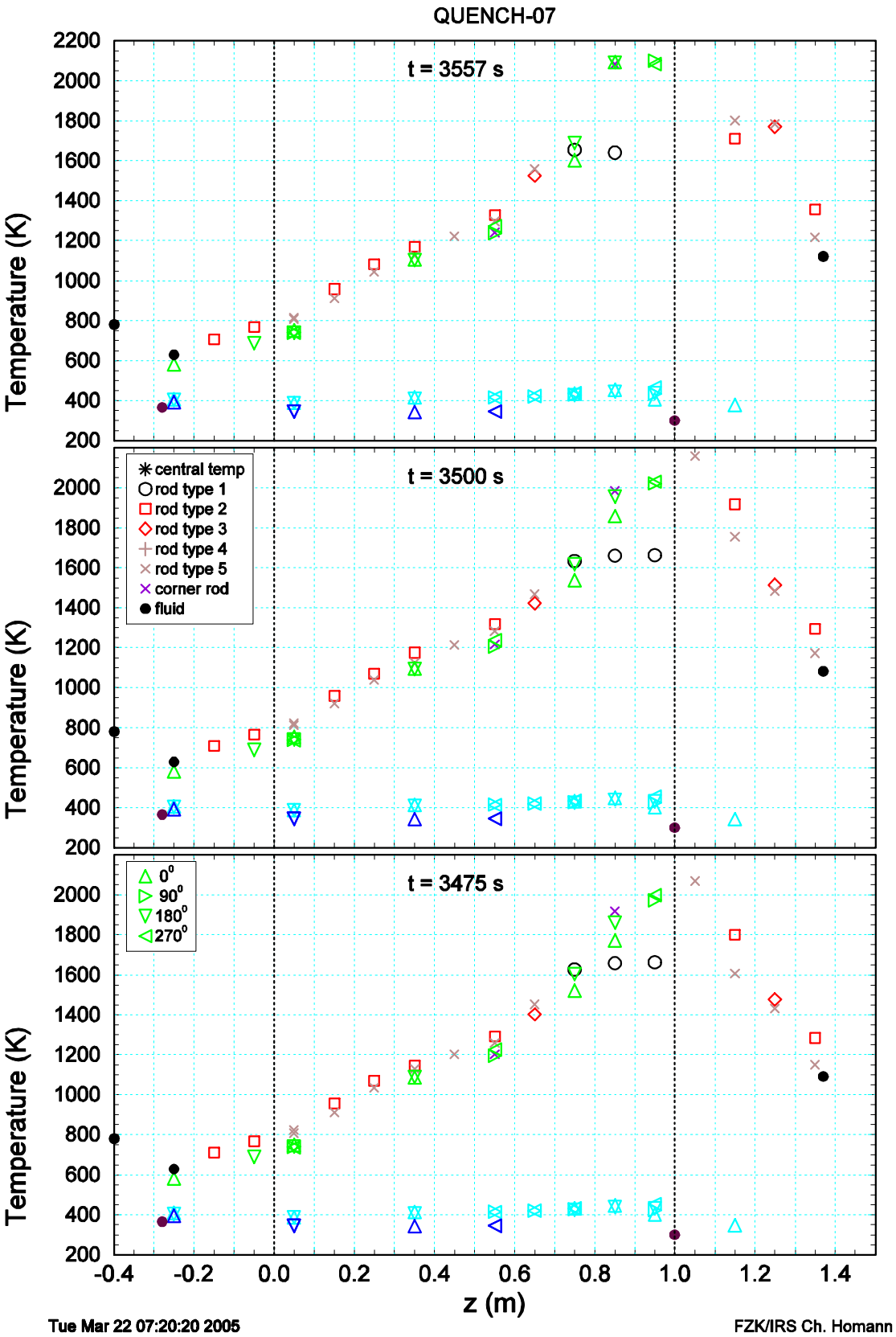

Fig. 7.2: Axial temperature profiles for QUENCH-07 during the second transient

Axial temperature profiles are given for bundle, shroud (green), inner (light blue) and outer cooling jacket (dark blue). All triangles refer to azimuthal orientations as indicated for the shroud.

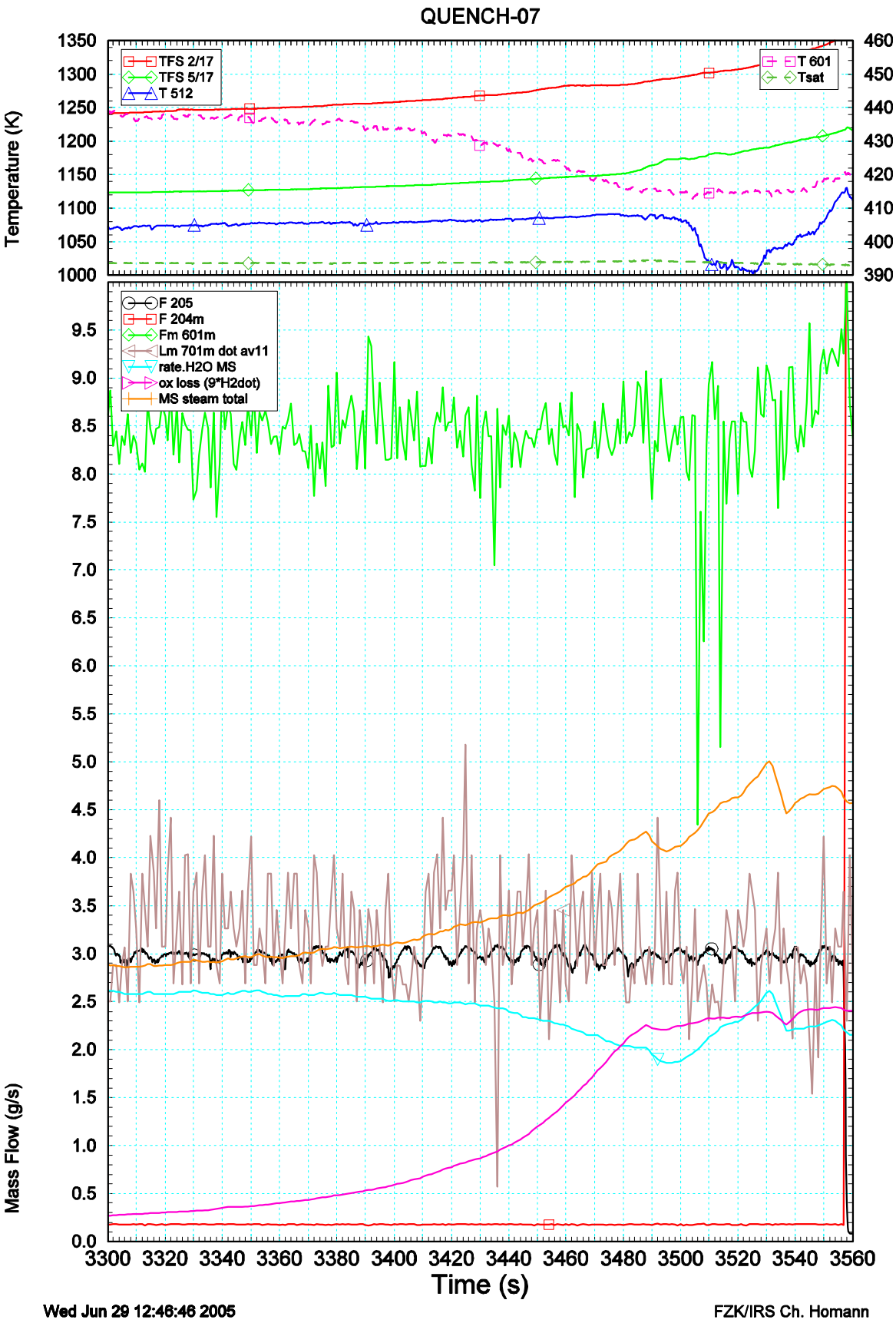

Fig. 7.3: Mass flow instrumentation in QUENCH-07 during the second transient

The figure shows temperatures (top) and steam mass flow rates similarly to Fig. 3.2.

located in the centre of a corner rod; for this reason they should be protected against oxidation. These observations together may therefore indicate an important change of the bundle status.

The rather abrupt change of hydrogen generation rate (Fig. 7.1) occurs only a few seconds after shroud failure (3484 s), and causality is possible, but interpretation of the experimental data is difficult and ambiguous. Pressure signals cannot be used for further insight, as stated above (section 7.2). Qualitatively, steam mass flow rate, deduced from condensate measurement and time averaged for better interpretation, also changes slightly with some delay that is expected for that instrumentation. Furthermore, fluid temperature at bundle outlet, T 512, decreases substantially, but clad surface temperatures at axial level 17 i.e. nearly at the same axial level as T 512, does not show a comparable decrease (Fig. 7.3). This finding suggests that something happens in the bundle that influences the fluid, but not the structures. In sum, some credit might be given to these data. Mass flow and pressure measurements of GDA are too noisy for interpretation. Orifice temperature T 601 and related saturation temperature may only give qualitative information for that mass flow rate. Material relocation, changing oxidation, would have to be rather large to explain the change of hydrogen generation rate. This is not supported by TC signals, neither in the region of its formation nor in the region of its deposition. So, the problem cannot be solved definitely.

If flow paths are changed just after shroud failure and steam penetrates into the annular space between shroud and inner cooling jacket, the effect is probably limited to the region of upper electrode zone; TCI in the heated zone do not give any indication of a contact with steam.

7.2 MS Hydrogen and Steam Measurement

Apart from “normal” data acquisition, MS steam mass flow data become interesting in the second transient and the cool-down phase. Though hydrogen generation and steam mass flow rates are calibrated before the test, the measured and consumed steam mass flow rates, “MS steam total”, do not sum up to the input value F 205 and F 204, respectively. This effect is known: a portion of the steam that leaves the bundle is condensed in the off-gas pipe, depending on temperature and the inlet steam mass flow rate, as documented in the appendix of [20]. The effect is smaller at higher temperature and higher mass flow rates. For mass flow rates as during cool-down, the asymptotic value should be reached in rather a short time, perhaps less than a minute.

Problems related to this effect are very pronounced in QUENCH-07 and discussed in the following. When temperature rises during the second transient (Fig. 7.3), this condensate may be evaporated. The decreasing temperature T 601 probably indicates this enthalpy loss of the fluid. Consequently, the measured steam mass flow rate cannot simply be interpreted as the difference of its value at bundle inlet and consumed steam, but also contains this evaporation. Therefore, the derivative of condensate mass L 701 should increase for a certain time after about 3400 s. However, this cannot be detected. (In this and the subsequent figure, this signal is averaged over 11 subsequent points to reduce noise.) There is only an increase of orifice measurement Fm 601, but far later, i.e. after 3500 s. Its value is evidently

grossly overestimated from the start of data acquisition. Other instrumentation is too noisy for a reliable data evaluation.

During cool-down, there is even steam excess. In addition, not only the total steam mass flow rate exceeds bundle inlet value, but also the measured steam mass flow rate alone and the consumed steam mass flow rate alone do so. This situation persists for a long time: more than 30 s for the measured and the consumed steam rate (the latter from 3575 s to 3607 s) and more than 70 s for the sum of both (Fig. 7.4). Subsequent oscillations of steam mass flow rate, measured with MS, have another shape and therefore do not explain the excess.

For better comprehension, some temperatures are added in the figure; comparison with Fig. 7.3 shows the difference in physical conditions. Temperatures at bundle outlet are rather high; temperatures at bundle inlet and in the off-gas pipe are above saturation so that no extraordinary effects may be expected. Since consumed steam is derived from hydrogen measurement, there is no error due to other chemical species with the same mass number. The steam mass flow meters F 204 and F 205 have been tested and found sufficiently reliable. Orifice mass flow measurement Fm 601 is not reliable, because current calculation for the mass flow rate from the measured pressure difference relies on the assumption of steady state conditions. Condensation measurement L 701 is too slow to derive a steam mass flow rate.

When the inlet steam mass flow rate is increased at cool-down initiation, the fluid inventory is expelled from the bundle. However, the excess may not be explained in this way, because the transportation time to the MS is only a few seconds, as stated in section 3.1. Further evaporation of condensate in the off-gas pipe can be supposed in accordance with the respective temperature histories and the appendix of [20]. This may help to explain the excess of measured steam mass flow rate.

With respect to the consumed steam, the situation is more difficult. Steam can only be consumed in the bundle, when it has entered the bundle. Therefore, the excess must have been created upstream of the bundle inlet. Evaporation of condensate in the steam feed pipe seems unlikely already about 10 s after cool-down initiation: Since just after cool-down initiation, a large portion of steam, perhaps all of it, condenses in the steam feed pipe (see section 3.3), partial condensation in that pipe should continue, when the MS signal starts to rise. It seems also unlikely that such an increase may be caused by entrainment of droplets, because the steam velocity is only some meters per second in that pipe. It might be possible that some condensate moves back to the hot region near the steam generator and evaporates, but this effect is supposed to give only little evaporation, if at all.

In this context, two issues should be kept in mind, rising general doubt that the MS signals are credible at the start of cool-down. Firstly, the MS signal for consumed steam shows an astonishingly sharp increase from rather low mass flow rates to excess within one measuring cycle (5 s). Secondly, the excess of consumed steam is only a lower limit for the steam mass flow rate at bundle inlet, because there may also be steam that enters the bundle but that is not consumed. Even this lower limit is about one-half of the steam mass flow rate that is created in the steam generator. On the other hand, an even higher peak is measured with the

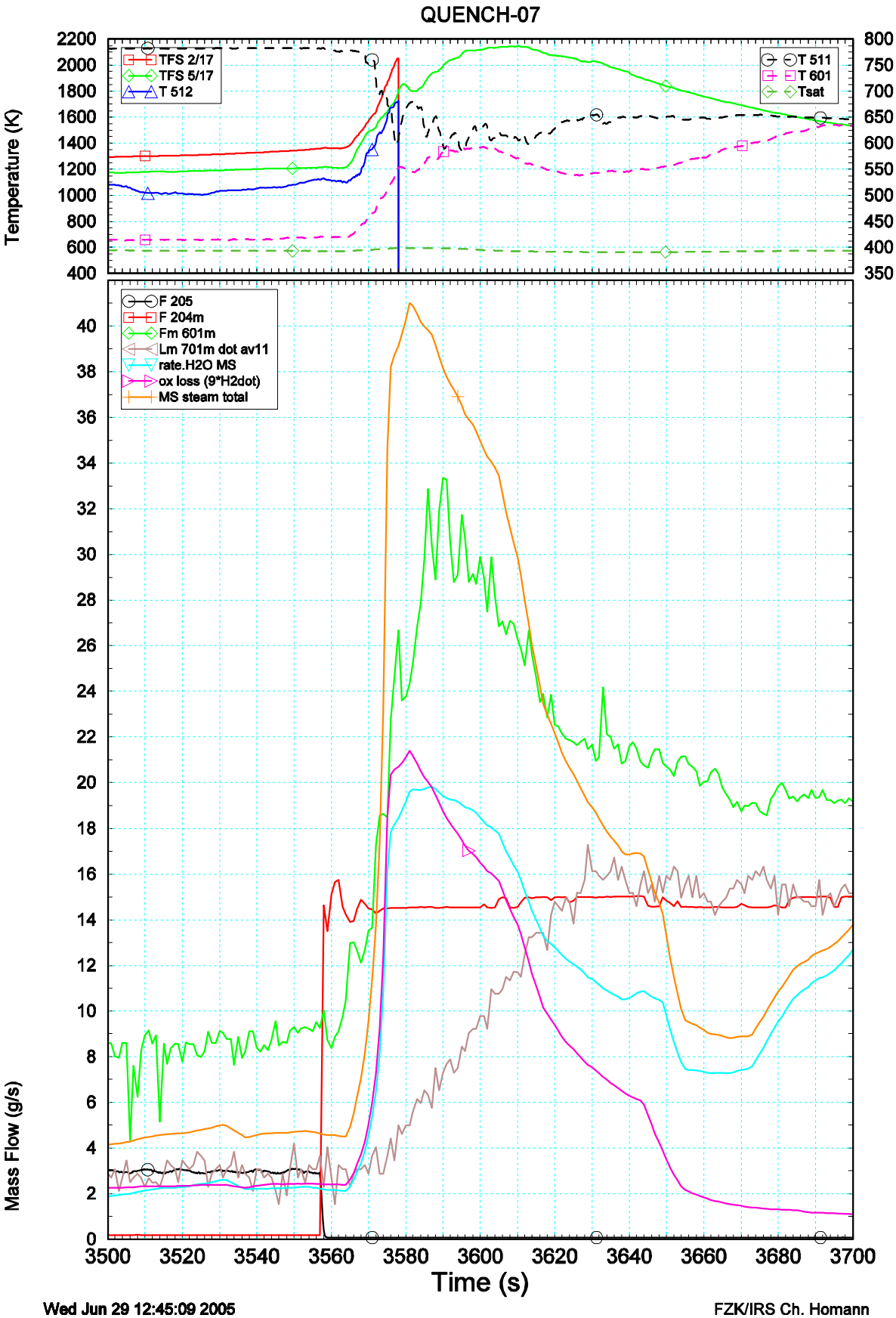

Fig. 7.4: Mass flow instrumentation in QUENCH-07 at start of the cool-down phase

The layout of this figure is the same as for Fig. 7.3.

”Prisma” mass spectrometer [17], although the peak should be smeared during the long transition time. Therefore, it seems that there is a common source for the observations.

For some further assessments for QUENCH-07, the large values of steam mass flow rates are assumed credible in spite of the objections outlined above. During the cool-down phase, the excess of total steam mass flow rate with respect to inlet value, i.e. between about 3570 s and 3650 s, sums up to about 1 kg. If it were totally due to evaporation in the off-gas pipe – in fact, evaporation in the steam feed pipe should occur after some time –, it would correspond to a film thickness of nearly 1 mm. Such a value seems reasonable.

The amount of condensed and evaporated water may be assessed from integrals of relevant variables in Fig. 7.4. An upper limit for condensation is the difference between consumed and injected steam in the interval from 3557 to 3575 s, namely 161 g. A lower limit for evaporation in the steam feed pipe is given by the excess of consumed steam between 3575 s and 3607 s, namely 120 g. Taking in mind that only bounds can be given, these two values are not too far away from one another. E.g. an additional 1.3 g/s of steam mass flow rate during steam excess interval, not consumed in the bundle, would increase evaporated steam from 120 to 162 g. However, a larger evaporation would be still more incredible.

Measured steam mass flow rate should consist of steam, not consumed in the bundle, and condensate in the off-gas pipe that is evaporated by the hot fluid. Unfortunately, experimental data are not sufficient to distinguish between these contributions, especially around the peak value. Not only is the steam mass flow rate at bundle outlet unknown, but also its temperature. T 512, measuring fluid temperature at bundle exit, is not representative for mean temperature, because that TC is outside the bundle and rather close to the water-cooling of the upper plenum, hence in a strong lateral temperature gradient.

With respect to consumed steam, some more conclusions can be drawn. T 204, steam temperature downstream of the steam generator, is about 437 K, 2 K above saturation value at the pressure at that location (~ 6.5 bar). Consequently, the energy, necessary for evaporation, cannot be transferred from steam to condensate. Argon that might enter into the feed pipe during condensation due to local pressure changes cannot evaporate the condensate due to its low heat capacity. Furthermore, if the excess of consumed steam is interpreted to come from evaporation in the steam feed pipe, its decrease after 3582 s suggests that the condensate in the steam feed pipe is mostly evaporated. T 303, however, stays continuously at saturation temperature up to 3666 s, and subsequently falls down to saturation temperature for several times, suggesting that in contrast to the assumption above, there should remain much condensate for a long time and evaporation should be limited. Finally, the situation is generally different to that in the off-gas pipe, when the steam mass flow rate is increased. Firstly, the off-gas pipe has been heated all the time before, whereas the steam feed pipe is cold up to cool-down initiation and secondly, the mass flow rate increases monotonously up to its final value, whereas in our case, there is a large overshooting. Pressure signals downstream of the steam generator, in the last vertical part of the inlet pipe, and at bundle inlet and outlet do not help for interpretation.

The same physical conditions probably also occur in previous QUENCH tests with steam cool-down, but normally, there are two differences with respect to QUENCH-07: the steam

inlet mass flow rate is higher in those tests, reducing the extent of condensation and giving a MS signal below inlet value, and oxidation just after cool-down initiation. Because of condensation and evaporation outside the bundle, the exact steam mass flow rate in the bundle during cool-down is unknown, at least during times that are relevant for hydrogen production. Since flow measurement is performed far away from bundle inlet for technical reasons, the respective readings are only relevant at their location, but not necessarily at bundle inlet.

Even after these considerations, the observations cannot be explained finally. Therefore, it cannot be excluded neither that MS signals not only for steam, but also for hydrogen generation rate are erroneous, at least during fast transients as after cool-down initiation. The excess steam in QUENCH-07 corresponds to a hydrogen production of 13.3 g; in the same time, hydrogen production is measured to increase by 65.5 g. In case of an error in the measurement, the total amount of hydrogen production would therefore probably be changed, at least by the value mentioned above. The scatter of the data in [8] is too large for more precise results or further conclusions. Besides, in [8] integral values for the whole test are given and makes interpretation for a single test phase impossible. Neither for production of CO and CO_2 nor for other QUENCH tests, can the consequences be assessed actually. A measurement error would also apply to ”Prisma” data. The comparison of the various methods to derive total hydrogen production in a test [8] suggests, however, MS data are not completely wrong during the whole test, but that errors are restricted, as supposed above.

Though the results in this report are based on experimental information only, it should be mentioned that in calculations for QUENCH-07 with ICARE/CATHARE the hydrogen production is underestimated even though temperatures in the cool-down phase are grossly overestimated [16]. This result supports the suspicion that the respective MS results are unreliable.
After the first peak of steam mass flow rates during cool-down in QUENCH-07, nonlinear damped oscillations start at about 3640 s, especially concerning steam mass flow rate, measured with MS (Fig. 7.5); their amplitudes vary by up to a factor of two. Such oscillations are not seen in the other measurement devices from which mass flow rates can be derived, they do not occur in the bundle temperatures, and they cannot be correlated to pressure oscillations. Time derivatives of TFS 5/16 and TFS 5/17, the only remaining TFS above level 10 at that time, show some oscillations, but different from MS steam mass flow signal. Hence, the oscillations of the MS signal for mass steam flow rate must be caused in the rear of the flow path.

In QUENCH-08, the total steam mass flow rate nearly reaches inlet value at about 2600 s and decreases to about 2 g/s just before cool-down initiation. The peak during cool-down amounts to about 18 g/s. Therefore, the effects are much more benign than in QUENCH-07.

In QUENCH-09, the total steam mass flow rate reaches input value just at the time of steam mass flow reduction and then decreases slowly. The same is true for both the measured steam mass flow rate and the hydrogen generation rate. The total mass flow rate seems to reach an equilibrium value of about 0.53 g/s. This value is above the inlet value of 0.4 g/s and may be an uncertainty of the measurement devices. If the value is correct, it can only be explained by evaporation of condensate from earlier test phases, but it means rather a high increase of the steam mass flow rate, namely of one third. The total steam mass flow rate

during cool-down reaches about 76 g/s for more than 10 s (Fig. 7.6). Due to the small argon concentration and due to the changed argon mass flow rate after failure of the inner cooling jacket at 3344 s, evaluation of MS data is difficult and the results less reliable. Apart from this drawback, the considerations are similar to those for QUENCH-07.

7.3 Condensation in the Test Section

In the second part of the cool-down phase of QUENCH-07, all relevant instruments for steam mass flow rate fall below steam inlet mass flow rate (Fig. 7.5). Inspection of shroud and inner cooling jacket TCs suggests that steam condenses in the annulus between shroud and inner cooling jacket. Consequently, the steam mass flow rate in the bundle changes with axial elevation during cool-down, and the value, measured in the off-gas pipe, can only refer to the value at bundle exit. Even this statement is only valid, if no condensation or evaporation in the off-gas pipe occurs.

In principle, steam can enter the annulus during the cool-down phase, because the shroud has failed before cool-down initiation. Fig. 7.7 shows that most TCs at the inner cooling jacket (TCI) finally decrease far quicker than before and suggested by convection and conduction, and TCI 15/0, not shown in that figure, always indicates temperatures below saturation value. Calculation of the difference between pressure in the bundle and the annulus between shroud and inner cooling jacket (P 406) cannot contribute to analysis. It is not clear whether bundle inlet (P 511) or bundle outlet (P 512) pressure is more representative for pressure at the axial elevations, where the shroud has failed, and the sign of this difference depends on that decision. In QUENCH-09, the situation is even worse.

The figure also shows that even if shroud TCs (TSH) show nearly the same temperature before cool-down initiation, strong asymmetries in the bundle may develop afterwards, leading to a difference of up to about 600 K. Even in the cooling jacket, temperatures at the same axial level differ by up to 300 K. The azimuthal position of maximum temperature in the inner cooling jacket changes with axial elevation. It is possible that details of shroud failure like azimuthal position and size at a given location determine steam flow paths and lead to such asymmetries.

The figure also shows that below axial level 13 temperatures in the shroud decrease faster than in the inner cooling jacket so that at those axial levels the radial heat flux is reversed during cool-down. Finally, it can be seen that the temperature in the inner cooling jacket reaches its maximum the later the lower the axial elevation.

In QUENCH-08, the GDA was switched off too early to draw conclusions to this aspect. In QUENCH-09, TCI at level 15 were not available during the test, but experience of all QUENCH tests suggests that in QUENCH-09, too, temperature of the inner cooling jacket is below saturation value at that level during the whole test. Therefore, condensation should occur similarly as stated for QUENCH-07 (Fig. 7.8). In contrast to that test, it is even at level 13 that temperature decrease in the shroud is faster than in the inner cooling jacket.

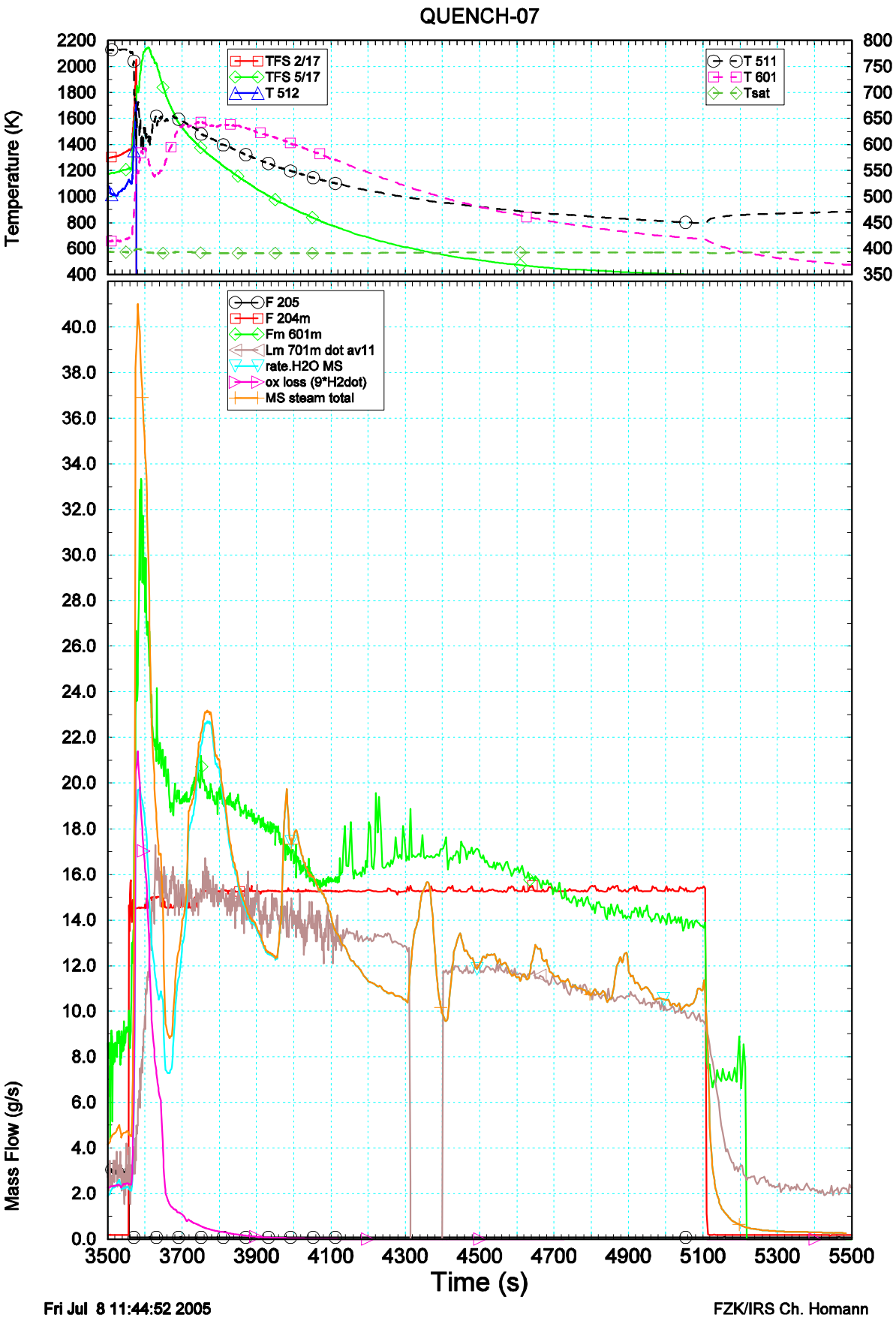

Fig. 7.5: Mass flow instrumentation in QUENCH-07 during the whole cool-down phase

The layout of this figure is the same as for Fig. 7.3.

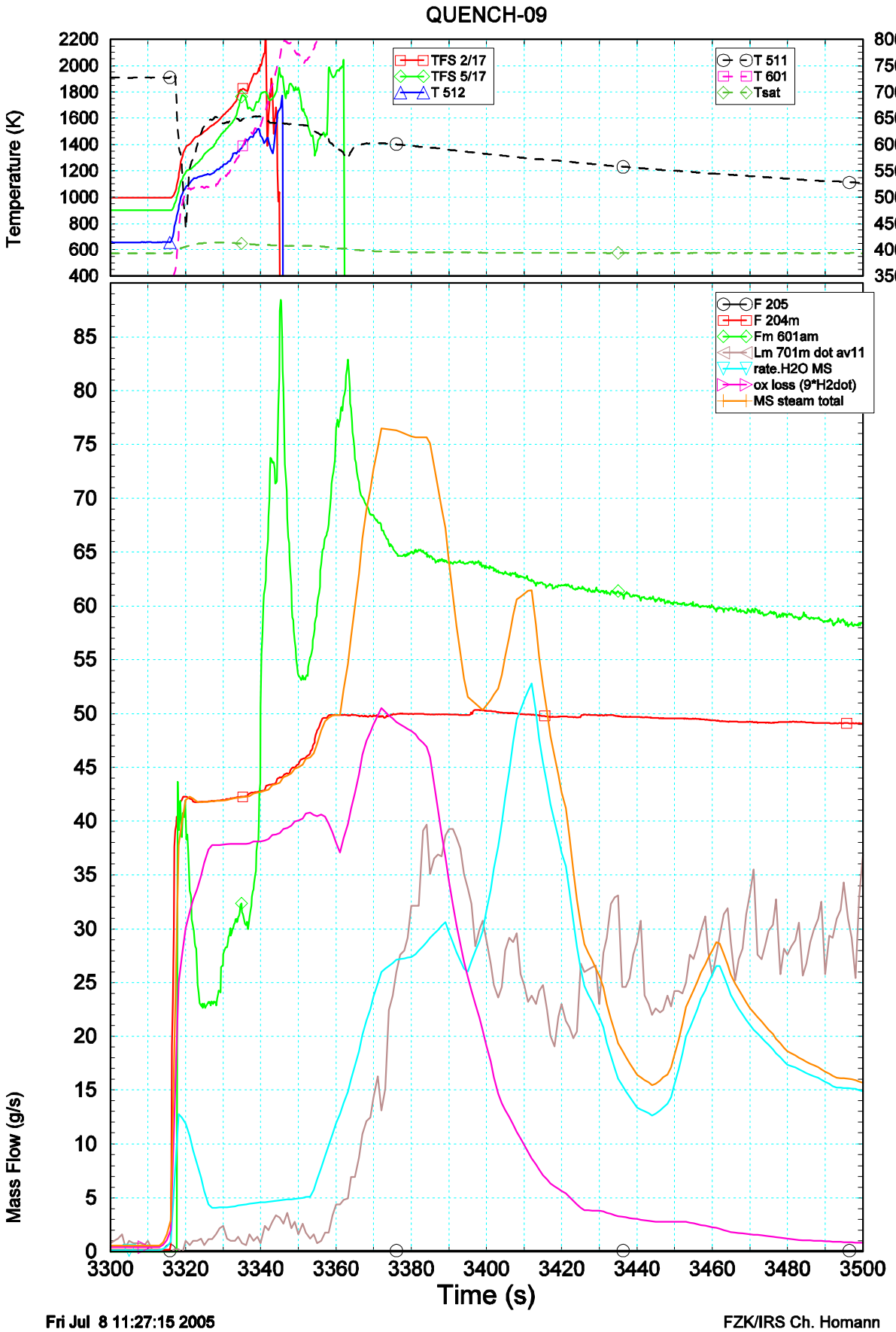

Fig. 7.6: Mass flow instrumentation in QUENCH-09 at start of the cool-down phase

The layout of this figure is the same as for Fig. 7.3.

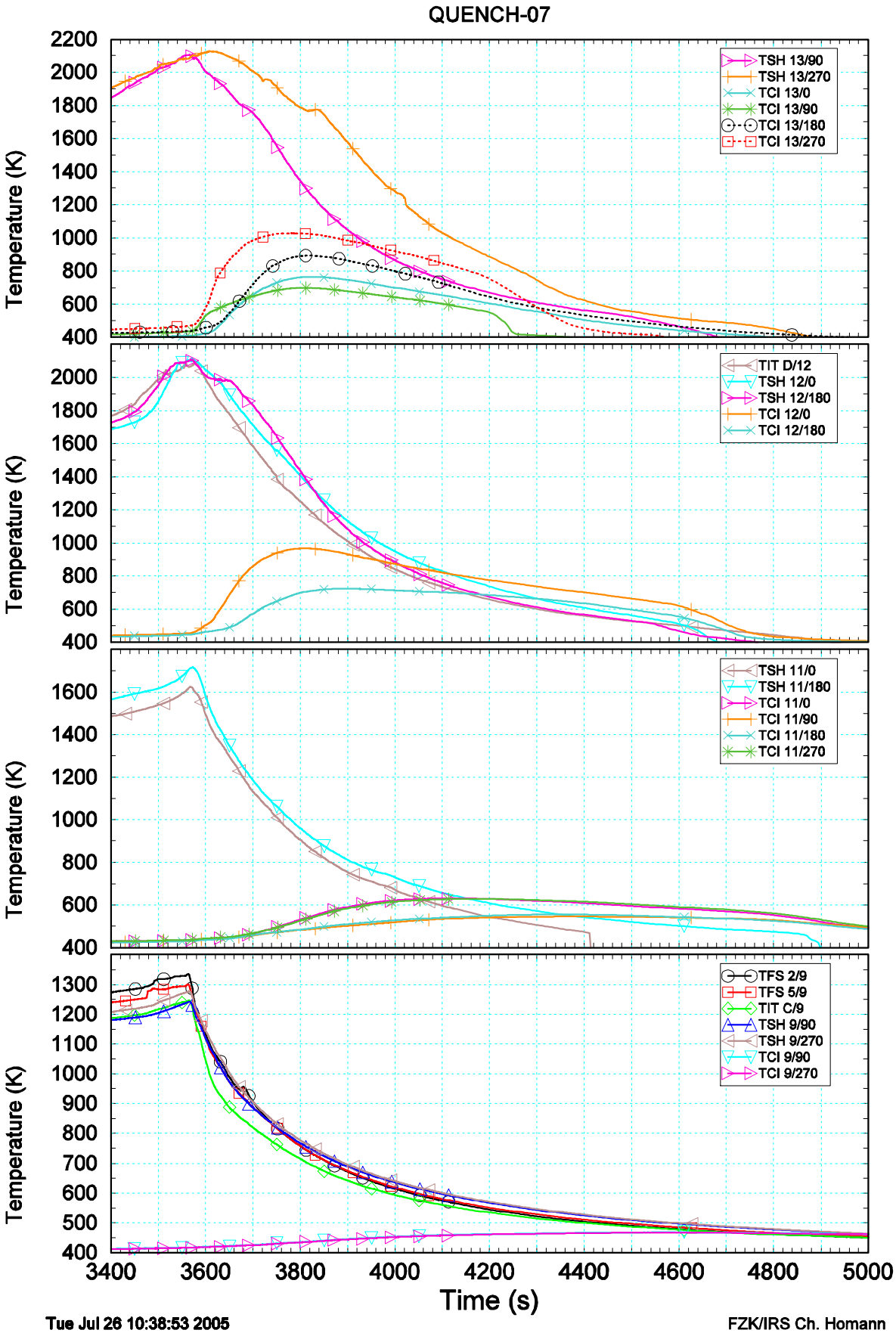

Fig. 7.7: Temperatures in the bundle, shroud, and inner cooling jacket in QUENCH-07

The figure shows TCs at axial levels in the upper half of the heated zone.

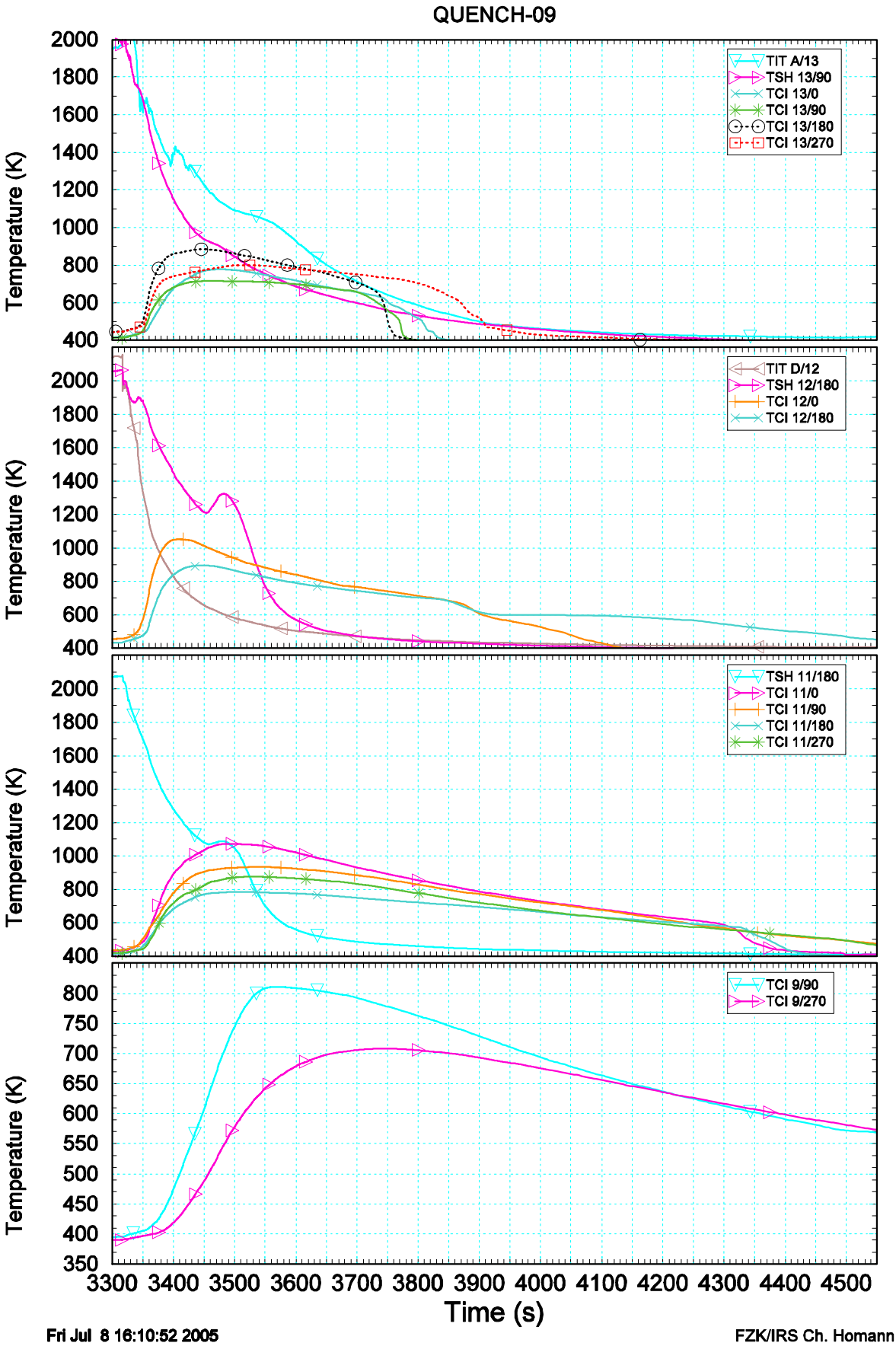

Fig. 7.8: Temperatures in the bundle, shroud, and inner cooling jacket in QUENCH-09

The figure shows TCs at axial levels in the upper half of the heated zone.

7.4 Hints for Material Relocation and Other Strange Temperature Signals

In QUENCH tests, material relocation is normally only deduced during PTE from examination of bundle cuts. Information from on-line data might be deduced from TC signals; other ways of detection are found difficult. A TC may give information about melt relocation for two reasons: The TCs may be hit directly by relocating melt on its way down or may detect a temperature increase due to radiative heat transfer from melt that passes the TC without direct contact. In both cases, temperature should increase at that location and that location only. In the first case, the TC signal should decrease more slowly than in the second case, because of the different thermal inertia, but for small amounts of melt, differences are expected to be small. Perhaps, SET may give some more insight about the width of temperature peaks for these two cases.

However, when melt is produced from fuel rod simulators, temperature at those positions is very high: at least about 2030 K for Zry, as received, 2200 K for β-Zry, 2250 K for α-Zr(O), and 2960 K for ZrO_2. In QUENCH tests, it is supposed that β-Zry is totally consumed at the location, where rod degradation starts. Melt of α-Zr(O) may be released in these tests, when the ZrO_2 scale has failed for one or another reason. Therefore, related TCs have already failed before melt release, or they fail at that time so that they cannot contribute to insight.

In QUENCH-07 and -09, there is also absorber melt, and it is formed far below temperatures, where the fuel rod simulators are degraded. Therefore, the GDA data are examined for hints that may be related to any melt relocation. It is emphasized that this is no more than a tentative interpretation of TC readings. It cannot be supported by other on-line data or PTE data, to get more confidence in this interpretation, and PTE, cited below, only indicates the bundle status after the test without any reference to the time, when the respective events occurred. If the interpretation is correct, it implies from the azimuthal position of some of the involved TCs that the relocation of the absorber melt is not always on a straight line. On the other hand, it seems difficult to find another reasonable explanation for some irregularities of a number of TCs.

Generally, TC information about absorber melt relocation may only be expected rather early after melt formation. Especially in the cool-down phase, a reliable interpretation is impossible due to the larger number of chemical and physical processes occurring and interacting in that phase. Besides, it should be kept in mind that TCs that have experienced very high temperatures do not give reliable signals as before or even form a junction at another location. So, they can no longer be used for quantitative evaluation. In QUENCH-08, no melt relocation is observed from TCs. This may be expected, because there is no control rod and the maximum temperature is only about 2350 K, measured with TFS 5/15 and TSH 14/270.

In QUENCH-07, a temperature double peak and a single peak are seen at quite low elevations, namely at 2560 s for TFS 2/1, and at 2620 s for TFS 5/4/0, i.e. at axial levels -250 mm and 50 mm, respectively (Fig. 7.9). They are local events. Here and in the following discussion, such peaks are interpreted as melt relocation. Indeed, some droplets of absorber melt have been found at axial level 73 mm in PTE. The low position of the respective TCs is a sign that viscosity of the melt is low as is also known from SET. The detection at TFS 5/4/0, i.e. close to the shroud, shows that radial spreading of the melt is large.

Since the maximum bundle temperature is even below 1750 K at that time, rod melting cannot yet have occurred. Therefore, the signal must be caused by absorber melt, if it is interpreted as coming from melt. As the second TC is located near the shroud, this implies a substantial radial transport of absorber melt. The time is more than 400 s after CR guide tube failure. There is a similar peak for TFS 3/8 at 3423 s (maximum bundle temperature 2040 K). Again, the material must be absorber melt.

Another shape and a smaller value of temperature change are seen at 3063 s for TFS 3/8. Before cool-down initiation, some other smaller local temperature changes can be detected with and without return to their previous value, but they are not discussed in detail, because other phenomena than material relocation might be their reason. So, withdrawal of corner rod B, beginning at 3090 s, causes slight local temperature changes.

In QUENCH-09, two peaks occur about 100 s after control rod guide tube has failed, namely at 2688 s at TFS 5/13 and at 2691 s at TFS 2/9 (Fig. 7.10). The maximum measured bundle temperature in the preceding temperature escalation is 2283 K (TFS 4/13). The TC may be installed at a different location than that of actual temperature maximum in the bundle, and bundle maximum temperature may be somewhat higher. Nevertheless, it seems reasonable to assume that the temperature peaks in Fig. 7.10 are caused by absorber melt, because maximum temperature is still below melting point of α-Zr according to the TC signal.

This interpretation leads, however, to some problems. The absorber melt should not come from elevations higher than level 13 because of the axial temperature profile and because the stack of B_4C pellets ends at 1008 mm. If absorber melt is transported across nearly the whole bundle cross section at level 13, a significant driving force is necessary. The control rod cladding failed about 100 s earlier so that helium overpressure cannot be the source. Steam mass flow rate has been reduced somewhat more than 50 s before the temperature peaks occur so that spreading of absorber melt, due to violent oxidation, should not be possible. The MS data show, however, that at that time the sum of consumed steam and measured steam mass flow rate is slightly above 1 g/s so that oxidation can indeed be possible. The driving force may also be due to hydrostatic pressure of the eutectic melt in the control rod. A pressure built-up may only occur, however, if locations of former failure of the guide tube are blocked for some time.

Another rather large peak occurs at 2846 s at TFS 2/13 (maximum temperature about 2060 K, measured with TFS 4/13 and TSH 12/180). In contrast to the other ones, it is much broader. For this reason, one may think of a direct contact between melt and TC, but SET are necessary for clarification, as stated before. From the available data, one may only derive that the effects are local ones, because the other TCs are not affected.

Some other strange temperature signals occur during the cool-down phase, but are probably not related to possible relocation of absorber melt as discussed above. In QUENCH-07, several deviations from normal cool-down can be detected, at 3580 s and 3720 s for TSH 13/270, at 3618 s for TSH 11/0, at 3600 s TSH 12/180, at 3600 s and 3668 s for TSH 13/90, and at 3676 s for TFS 2/9. They occur possibly after a temperature escalation at cool-down initiation. These events can hardly be correlated to hydrogen generation rate, firstly because these effects are evidently local and hence limited (TSH 13/90 and TSH 13/270 show these

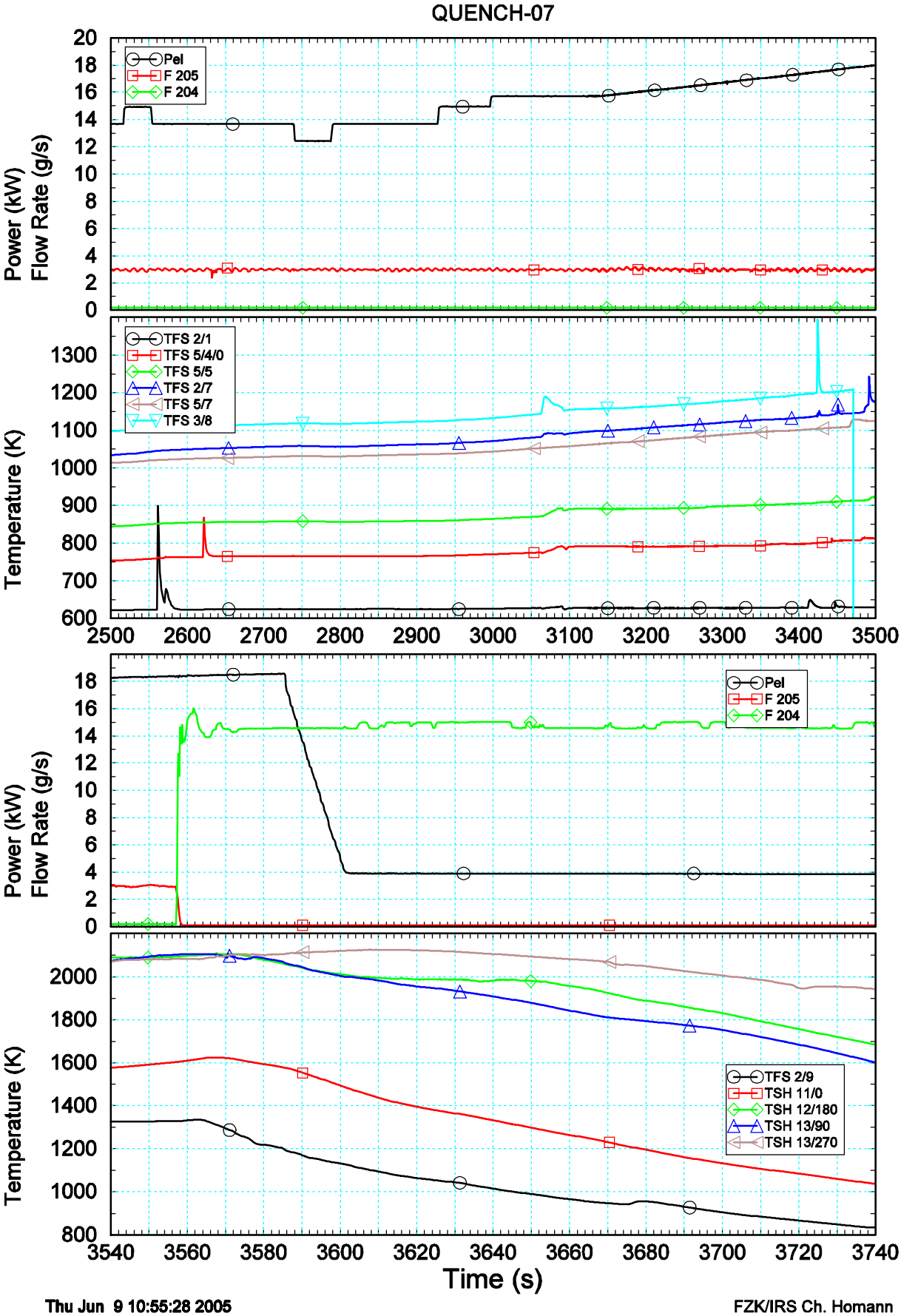

Fig. 7.9: Unexpected temperature signals in QUENCH-07

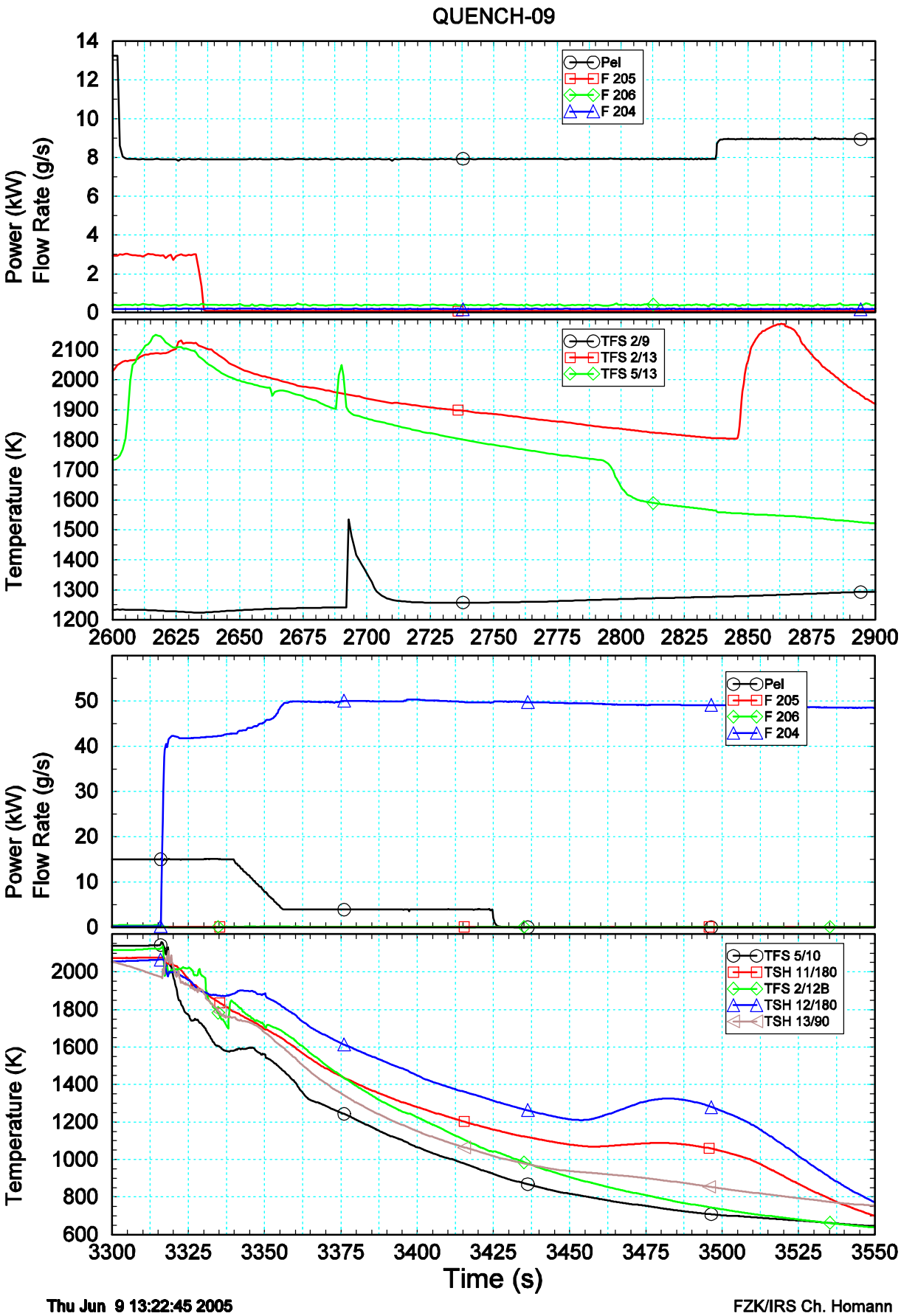

Fig. 7.10: Unexpected temperature signals in QUENCH-09

effects at distinctly different times) and secondly because signals of shroud TCs are delayed and distorted because of thermal inertia of the surrounding structures. For TSH 13/270, events as pointed out above also occur later, namely at 3813 s and 4000 s. Only for this event, some small increase of hydrogen generation rate at about 3970 s might be correlated to that event. Local temperature has already dropped below 1300 K at this time; out of the remaining TCs, this is the highest measured value at that time.

It is reminded that the temperature readings may be unreliable at that time, e.g. because a new junction has formed during high temperature phase (see section 2.1), and PTE shows that TCs in the hot region have disappeared. For this reason, not even the axial level of the events is known. PTE cannot give further insight, because it only reveals the bundle status after the test. In sum, an unambiguous attribution of the effects during cool-down phase to material relocation is impossible.

During cool-down in QUENCH-09, temperature increases occur at 3337 s simultaneously at TFS 5/10, TSH 12/180, and TSH 13/90 and, less clearly at TFS 12/B. Further similar events are at 3453 s for TSH 11/180 and TSH 12/180 at a maximum temperature of about 1350 K (maximum measured temperature 2050 K according to TSH 16/0), and at about 3500 s at TIT A/13. Hydrogen generation rate is already rather low and still decreases at the time of temperature increase. Such temperature increases are known from SET and may be due to effects like freezing of melt, phase transitions or hydrogen uptake, but as for QUENCH-07, interpretation of the temperature readings and hence conclusions are as difficult as for QUENCH-07.

The rod surface, the corner rod and the shroud TCs at level 9 (550 mm) are low temperature TCs. All of them fail between 3122 s and 3142 s at temperatures between 1740 K and 1770 K, probably due to material interaction, leading to eutectic melt. In fact, post-test bundle cuts [3] show substantial damage at all of these locations.

At least for the time intervals, shown in the upper parts of Fig. 7.9 and Fig. 7.10, the respective TCs behave normally in comparison to surrounding ones and continue to do so after the spikes. Therefore, they are supposed to be intact. If at least the sharp peaks in temperature readings are interpreted as a sign of melt relocation in both tests, inspection of the experimental data shows that the amount of events is small. Probably the number of TCs is too small to get representative results. Furthermore, the available TCs might be on the more distant side of the respective rods to detect an effect in the neighbourhood. Finally, the amount of melt relocation is perhaps rather small. As far as absorber melt is concerned, this is quite clear because of the limited amount of control rod material that may melt. During cool-down, the situation and hence the interpretation is still more difficult, because a number of TCs fail at about the time of cool-down initiation.

8 Global Analysis

Up to now, rather detailed analyses of the three QUENCH tests were made. For global analyses, another presentation of the results, the test sequence diagram (TSD), explained in this section, may be more appropriate, because it gives a condensed overview of a test on a single page and because other data sources can be included more easily. However, knowledge of the facility and experience are required to build such TSDs. In addition, some time is needed, and the respective diagrams for this report were available rather late because of restricted work force. They would also have helped for the discussions in the previous chapters, but they would not have changed any conclusion. Since they can be used for a wide range of problems to be solved and insight to be gained, they are included nevertheless in this report, but only some short examples for application are given. Since this report is restricted deliberately on experimental results, mainly on-line data, computational results are not included at all. As a first step, the data that may be used for such analyses of QUENCH tests are listed and their significance is assessed in a table.

8.1 Available Data Sources

Available data that may be used to derive a consistent interpretation of the processes and phenomena in a test and their influence on the direct vicinity may come from a number of sources, even from outside the test itself. For QUENCH tests, they are listed in Tab. 8.1 and rated for global analyses.

With respect to computational basis, a comparison between pre-test and post-test calculations gives insights in lacking understanding of either the bundle or facility behaviour. The reasons for such drawbacks may be on the experimental or the analytical side. The clear

Tab. 8.1: Overview of available data sources and their importance for integral analyses

Data Source	Derived Data	Remarks
Final test protocol, Test conduct	Intended test sequence	Low importance
GDA	Fluid and structure temperatures, mass flow rates, electrical power	High importance
Mass spectrometer data	Fluid composition	High importance
Removable corner rods	Intermediate state of oxidation	Medium importance
Non-destructive PTE	Optical inspection Extension of damage	Reveals final bundle state
Destructive PTE	Radial extension of damage Local material composition	Support
Separate effects tests	Material behaviour under idealized conditions	Support
Post-test analyses with best estimate codes	Bundle status as a function of time and axial elevation	Separation of facility effects and reactor conditions

identification of such drawbacks on the influence of damage and degradation is a prerequisite for profound understanding of the physical, thermal-hydraulic, and chemical processes and their interactions promoting bundle damage. Calculations with best estimate codes can also resolve problems that cannot be derived from experimental data. An example is the evolution of the axial power profile during the test. In electrically heated bundles, it changes substantially with local temperature; furthermore, it is not reactor typical.

8.2 Test Sequence Diagrams

The TSD was developed [21], [22] to allow for a more detailed interpretation of CORA experiments [23]. It integrates all available on-line data as well as the PTE results; other data sources like computational results may be added. The purpose of a TSD is to identify the temporal sequences during the experiment and their spatial or at least their axial location and to do so in a form as condensed as possible. It does not only give an overview of the whole test, but also facilitates its interpretation and helps to solve a number of detailed problems without any further change. It can also be used for comparisons of several tests, as will be shown in this section.

While traditional methods are restricted either on results versus time or on axial temperature profiles, a TSD combines both in its central part, using isotherms in a t-z diagram that indicate the time and space when a given temperature is reached (Fig. 8.1 will be seen as an example). By this means, it allows extracting immediately the temperature history in each elevation as well as the axial temperature profile at each time. The detailing of the presentation depends on the number of isotherms, chosen for that case. Typically, temperatures are selected that are representative for important events like material interactions or melting points. The time scale can be varied to address short-term phases such as the reflood or steam cool-down phase [23].

For the construction of isotherms, only bundle surface TCs (TFS) are used, because their heat capacity is smaller than for protected TCs like corner rod TCs (TIT) or shroud TCs (TSH). Since not only the accuracy of measurements is limited, but also the radial temperature gradient is small compared to the axial one, only one temperature is considered for a given axial elevation. Consequently, the deduction of the isotherms cannot be done by a simple algorithm alone; instead, each temperature history has to be analyzed for qualification to identify irregularities like spikes or damaged TCs that would falsify the result. This procedure implies that neither effects that are restricted to very small regions nor radial or azimuthal asymmetries can be resolved.

To facilitate and to extend interpretation, the inlet mass flow rates as well as the electrical power as a function of time are added below the isotherms. Other time dependent results as failure of components or mass spectrometer data of hydrogen, steam, and tracer gases can be given in further windows. Right of the part with the isotherms, the TSD contains a window about the bundle damage state as a function of the axial position (Fig. 8.2). From the detected sequence of material layers a temporal identification can be given. Further results depending on the axial elevation may be added. This feature may help to localize the axial position of events detected by mass spectrometer or other global detection methods.

8.3 Test Sequence of QUENCH-07

In Fig. 8.1, a typical example of a TSD without post-test data is given for QUENCH-07. For this test, a temperature range between 800 K and the maximum measured temperature of 2273 K was used. Mainly those temperature values were used that correspond to smooth values either in K or in °C. The value of 1620 K is representative for steel melting, useful for questions about degradation without material interaction, that of 1750 K as a rough measure for the start of temperature escalations. Interrupted isotherms in later times indicate damaged or unreliable thermocouples. For the removal of the corner rod, start and end times are indicated by a triangle instead of a stroke as for other events, because the time for removal was rather long.

As an advantage of TSD, the extension and evolution of the hot zone can be seen from the TSD at a glance, howsoever the limiting value of “hot zone” may be defined in a special case. In the following, some examples of more detailed information that can be gained from TSD are outlined. Up to 2100 s, all isotherms show similar behaviour, dominated by the axial power profile of the electric bundle heating and the convective heat losses. They are approximately symmetric to the elevation of about 800 mm. CR cladding failure at 2022 s, indicated by helium release, can be localized in the TSD between 850 mm and 950 mm. The curvature of the 1500 K isotherm suggests that this region is probably not much larger. First release of CO and CO_2, hence of reaction products of B_4C oxidation, detected app. 100 s later, should also stem from that axial region.

Quasi-stationary temperatures in the subsequent temperature plateau phase can be identified by the nearly horizontal slopes of the isotherms between 2200 s and 3140 s, but a slight axial extension of the hot zone in that test phase can also be detected in Fig. 8.1. The symmetry of isotherms is destroyed by enhanced oxidation in the upper part of the bundle. At app. 3400 s, i.e. during the second transient, a fast temperature increase can be seen in the upper electrode zone. Its extension can be identified much easier than with conventional data presentation. During the cool-down phase, the hot zone extends from app. 900 to 1350 mm; the lower elevation is estimated from results of post-test investigations.

The two highest temperatures in Fig. 8.1 were only measured in the upper electrode zone, between 1100 mm and 1200 mm. At lower elevations in the supposed hot zone, TCs failed so that the TSD cannot be complete for those elevations. There remains only the qualitative assessment from PTE, given above, that the high temperature region goes down to about 900 mm. Melt relocation goes down to about 750 mm, but SEM/EDX analyses [2] indicate that at that elevation the melt consists mainly of molybdenum of the upper electrode and is hence a facility effect. These analyses also show that molybdenum melt also plays a role at 850 mm. The contribution of melt oxidation to hydrogen production, favoured by the experimental team to explain the high hydrogen production during the quench or cool-down phase of a number of QUENCH tests, can therefore be limited from TSD considerations as far as Zr melt is concerned; the lacking TC information inhibits, however, to assess the contribution of melt oxidation better. The increase of absorber melt should also be generated mainly in the hot zone as defined above: temperatures essentially decrease directly after cool-down initiation below 850 mm and are below 1350 K at 550 mm, and below the hot zone, steam should

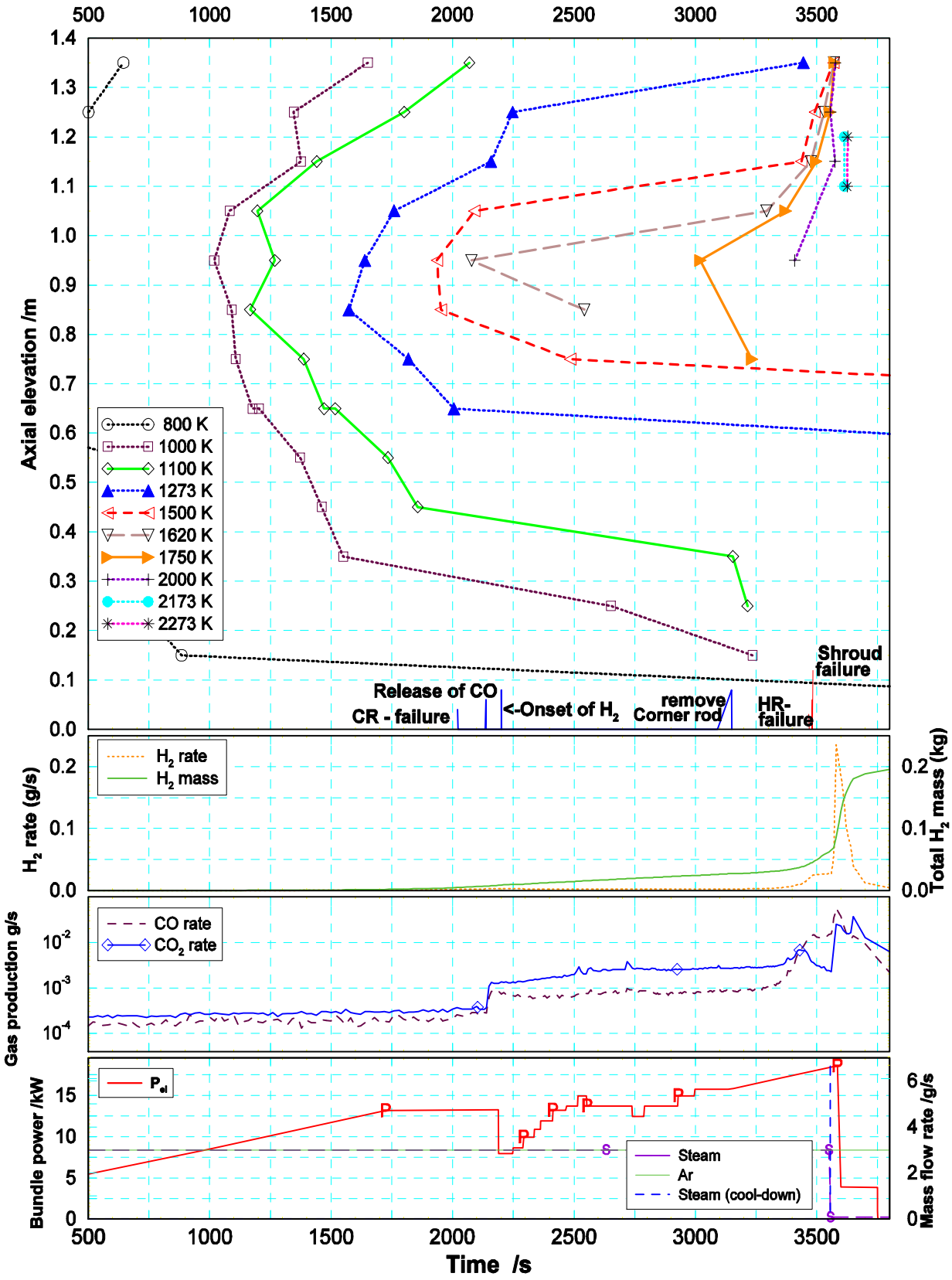

Fig. 8.1: Test sequence diagram for QUENCH-07

The figure shows from top to bottom isotherms and detected events, hydrogen generation rate and total mass, CO and CO_2 generation rates, inlet mass flow rates, and electrical power.

always be available so that conditions for oxidation should not change with cool-down initiation.

The axial temperature distribution of QUENCH-07 is similar to other QUENCH or CORA tests with negligible material relocations. No direct influence of the CR on bundle damage and degradation is seen in the isotherms. Since conduct of test QUENCH-08 was largely similar to that of QUENCH-07 up to cool-down initiation in QUENCH-08, no TSD is established for that test.

8.4 Test Sequence of QUENCH-09

Similar to QUENCH-07, a TSD was constructed for QUENCH-09 (Fig. 8.2) and extended by an overview of the post-test bundle state, derived from post-test analyses [3]. A comparison of isotherms for both tests is included in Fig. 8.3. In the latter figure, the time window for QUENCH-09 is shifted by -225 s, because in QUENCH-09 the first transient starts later by that time (Tab. 2.1). The development of the temperature field is similar to QUENCH-07 during the first transient: Isotherms up to 1100 K are close together, as stated earlier, but the slightly larger downwards extension for QUENCH-09 can better be seen in Fig. 8.3 than in time histories as shown in Fig. 4.3. The first bundle damage, the failure of the CR cladding at 2280 s, can be localized at app. 950 mm (Fig. 8.2) as for QUENCH-07. After subsequent reduction of electrical power, temperatures between 750 mm and 1050 mm are above Zry melting point, evidently because of strong local release of chemical power due to oxidation.

After steam mass flow rate has been reduced, convective heat removal is reduced in the whole bundle. This effect alone leads to an upstream and downstream extension of the hot zone. In addition, increased temperatures in the lower part of the bundle imply an increase of oxidation in that region, further increasing local temperatures. As an example, the axial elevation of 450 mm is heated up to 1500 K at 3250 s. Therefore fluid temperature increases likewise. In the upper part of the bundle, no more steam is available to continue oxidation as before steam mass flow reduction so that temperatures should decrease in that region, but evidently, decrease of convective heat removal has a larger effect. As an example, after about 2600 s the 1750 K isotherm extends from 750 mm to 1150 mm, hence into the upper electrode zone, indicating a very flat axial temperature profile.

Zr melt, produced after reduction of electrical power, may relocate between about 2700 s and 3400 s, as indicated in Fig. 8.2, and increase temperature locally. Temperature may further increase due to appreciable melt oxidation, assumed by the experimental team to contribute significantly to hydrogen production. However, these effects cannot be quantified.

After cool-down initiation, there should be steam excess in the whole bundle. Since the preceding steam starvation phase is long enough so that ZrO_2 is dissolved markedly [10], Zry oxidation in the upper part of the bundle is rather violent, driving those regions to temperatures above α-Zr(O) melting point.

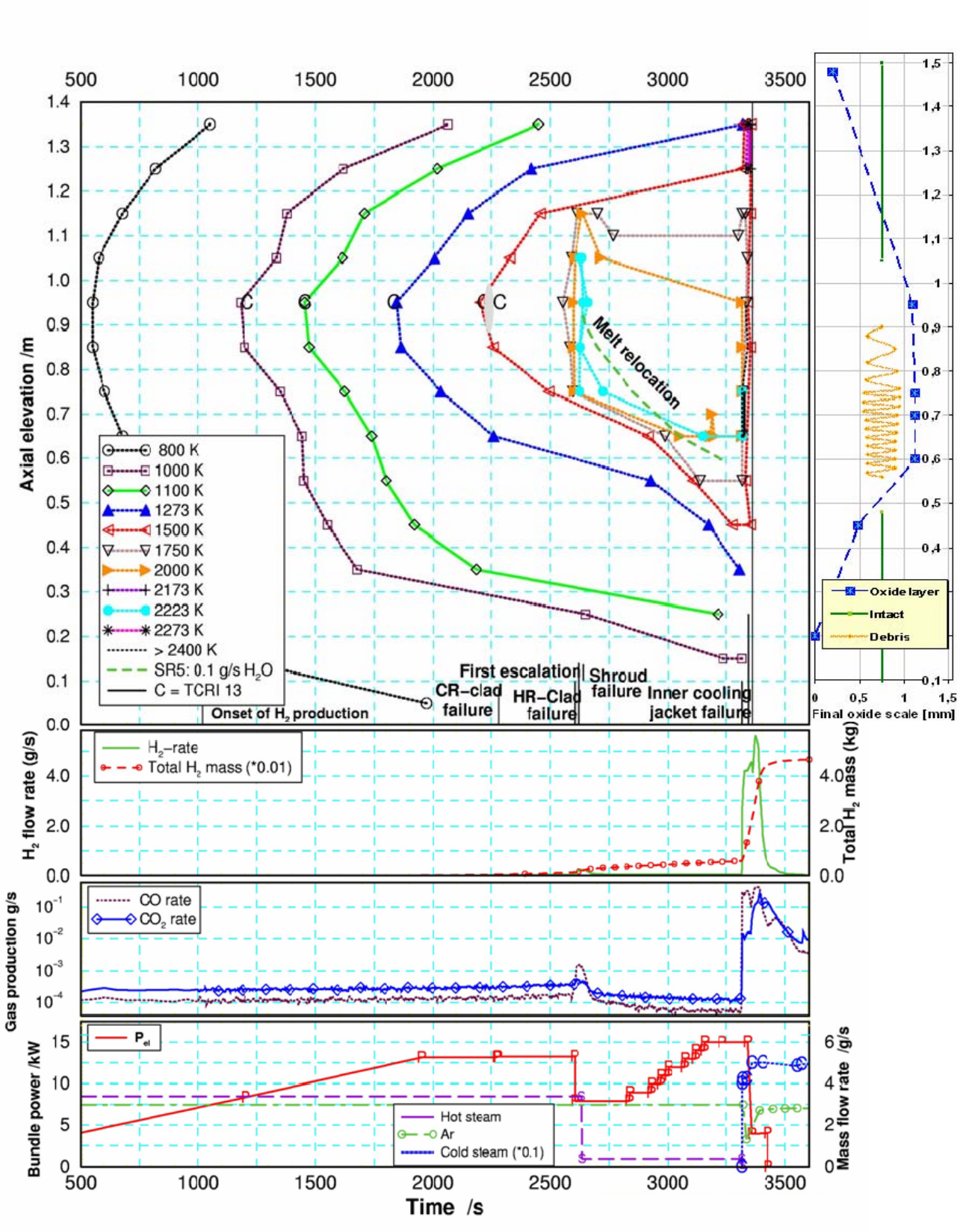

Fig. 8.2: Test sequence diagram for QUENCH-09

The layout of this figure is similar to Fig. 8.1.

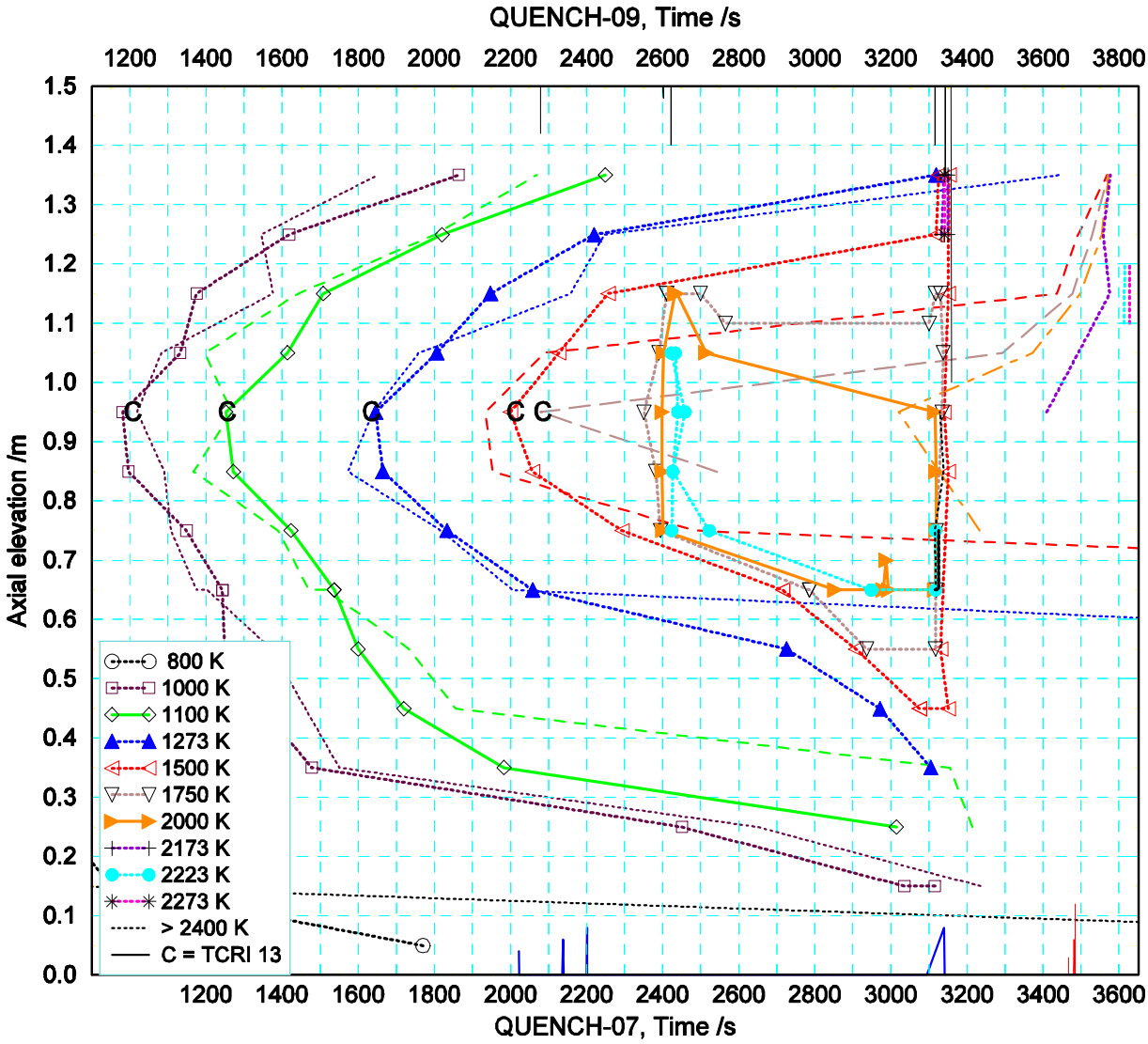

Fig. 8.3: Comparison of QUENCH-07 and -09 isotherms

Isotherms for QUENCH-07 are given as thin lines and those for QUENCH-09 as bold lines.

Similarly to QUENCH-03, electrode material was liquefied and traces were found in relocated materials during PTE. Such events, too, can be included in a TSD. In Fig. 8.2, this is done for such an event at 3344 s, i.e. at the time of the inner cooling jacket failure. A red arrow indicates the start and a probable end of the relocation; the latter is seen to be at a temperature above 2400 K. This effect is initiated by facility specific conditions and has to be separated from the supposed behaviour of a nuclear reactor.

In sum, the comparison of QUENCH-07 and -09 shows that the main differences exist at 1273 K and above (Fig. 8.3). In contrast to QUENCH-07, a number of isotherms for QUENCH-09 extend downwards to a bundle elevation of 350 mm because of the different steam mass flow rates at that time. The 2000 K isotherm, bordering the hot zone of the bundle in later times, is at a significantly lower elevation for QUENCH-09, compared to QUENCH-07. In addition to the consequences of the small steam mass flow rate, relocated

melt may play an important role. The damage of the shroud above 1250 mm at 3480 s in QUENCH-09 is neglected in the figure.

The course of the 1273 K and 1500 K isotherms in Fig. 8.3 suggest that the lowest locations of 650 mm and 503 mm, where absorber melt is found in the gap between CR cladding and guide tube should not be far from the elevation where this absorber melt freezes due to low ambient temperature. Comparison of these two isotherms also suggests that in QUENCH-09 this elevation should be somewhat below that for QUENCH-07 as it has been supposed in section 6, based on the knowledge, outlined in that context.

9 Conclusions

Out-of-pile tests QUENCH-07 to QUENCH-09 aim at studying the behaviour of B_4C control rods and their influence on fuel rod degradation during an accident scenario under low system pressure in a Western type light water reactor. The tests cover a wide range of accident conditions, QUENCH-08 being intended as a reference test with an unheated fuel rod simulator instead of a control rod. Apart from computational work, a detailed analysis of the experimental data and a thorough comparison of the test results are indispensable to get an adequate benefit that justifies the large expense, time, and effort, related to such integral tests. The work also gave insight into other issues than control rod behaviour. Results of post-test examination complement and extend the evaluation of the data recorded during the test ("on-line data"). As far as there is an overlap, the findings of these two different data sources are compatible with one another.

As a first step, a general comparison of the three test conducts is necessary for understanding and for any other work, described in this report. Its outcome demonstrates that the experimental conditions of the early test phases were reproduced to a high degree. The bandwidth for heat-up time to about 1700 K in the first transient, e.g., is ±5 %; and the difference depends on several reasons, not all of them clearly known and some of them with opposite effects. Experimental data for the end of the first transient in QUENCH-07 and -09 proved to be a good basis to derive safety margins for such test conditions.

At high temperatures during the second transient, when hydrogen production is large, the test conduct of QUENCH-07 and -08 was essentially different, insofar as in QUENCH-07 the high temperature regime before cool-down initiation was about 80 s longer than in QUENCH-08, resulting in a different status of the bundle at cool-down initiation. A direct comparison of experimental data of these two tests that includes the whole second transient of both tests or the subsequent cool-down phase, e.g. to derive the influence of control rod on bundle degradation, is therefore unreasonable and may lead to wrong conclusions. Up to the time of high temperature in the second transient, however, hydrogen production is close together in both tests, and a comparison can give valuable insight, as demonstrated in this report.

During the preparation of QUENCH-08, the importance of this issue was not realized clearly enough. In future tests, however, some effort should be spent for improvements, but such differences can hardly be avoided completely, because the time for immediate data evaluation during that test phase and subsequent operator reactions is rather short.

In QUENCH tests QUENCH-07 and -09, the control rod failed near the upper end of the heated zone during the first transient and in two steps; both of them due to the formation of eutectic melt. At first, the steel clad failed at temperatures of about 1550 K. 114 s (QUENCH-07) and 310 s (QUENCH-09) later, the metallic parts, if still existing, as well as the oxide scale of the guide tube failed. The marked difference in this time interval indicates some variation of control rod degradation and absorber melt release in detail, but it is sure that the former assumption, in QUENCH-09 the oxide scale of the guide tube has been intact until the start of cool-down, cannot be maintained. Since in QUENCH-09 the guide tube failure oc-

curred shortly before steam mass flow reduction, identification of control rod failure was facilitated in that test.

The final distribution of absorber melt, released after the rather early guide tube failure in QUENCH-07 and seen in PTE, indicates lateral spreading in form of melt lumps as well as axial spreading as falling droplets. Whereas the droplets are non-oxidized, the continuing oxidation of the lumps should have limited their mobility and contributed to chemical interactions with the surrounding rods. In contrast, the delayed guide tube failure in QUENCH-09 should have caused some melt superheating and viscosity decrease until release. Furthermore, the reduction of steam mass flow rate shortly after melt release enables intensive chemical interactions at contact with surrounding rods, but limits or even inhibits their oxidation. According to PTE, highly porous melt has been formed that blocks the damaged bundle and embeds the rod residues, the cladding of which is completely dissolved. Finally, all interaction products are ceramic, but the morphology allows distinguishing closed porosity from open porosity and steam flow channels. It is clear that the oxidation took place mainly during the cool-down phase in steam, accompanied by melt formation at and relocation from higher levels. Unfortunately, the complex mechanism of bundle degradation during the steam starvation phase cannot be identified from the final state.

Mechanistic models about rod degradation in the steam starvation phase have to consider a number of phenomena. Some of them are the partial dissolution of their thick oxide scale, clad failure by axial splitting, split opening (“flowering”), collection of some absorber melt in thus formed funnels and internal downward relocation, as identified in PTE, dissolution of metallic and ceramic rod components by absorber melt, and subsequent formation of “diluted” products.

With some caution, the contribution of B_4C oxidation to total hydrogen production can be quantified for all test phases from original mass spectrometer data for CO, CO_2, CH_4, and H_2. This contribution is limited to generally less than 10 % for hydrogen generation rate, total hydrogen production, as well as total chemical energy release. Late in the cool-down phase, where higher contributions are assessed for some time, the results are questionable because of the complex processes at that time, but generation rates are so small that this uncertainty does not play a role.

The oxidation of degradation products of the control rod may also have indirect impacts on hydrogen production. In any case, it increases temperature locally and in this way increases rates for oxidation of zirconium. At the time, when in QUENCH-07 the control rod guide tube fails, a limited increase of Zry oxidation can be derived from a small stepwise increase of hydrogen generation rate. Afterwards, such impacts on Zry oxidation can only be derived from a comparison of QUENCH-07 and -08. Up to cool-down initiation in QUENCH-08, hydrogen productions are close together in both tests; the difference comes also from small differences in the conduct of the two tests. Therefore, also the indirect influence of B_4C oxidation on Zry oxidation must be rather limited at least up to that time. For the subsequent time, no conclusion can be drawn, because the conduct of the two tests was too different.

The on-line data, as analysed in the scope of this report, suggest that control rod damage is imbedded in normal bundle damage and degradation. PTE indicates that control rod behaviour has consequences on fuel rods and enhances their damage or degradation.

Conclusions can also be drawn about limits and restrictions of the test data evaluation. At the start of the cool-down phase, the steam mass flow rate in the bundle is to some extent uncertain due to consecutive condensation and evaporation in the steam feed pipe. This effect was very pronounced in QUENCH-07, leading to a sensible delay of hydrogen production after cool-down initiation. Another source of uncertainties is steam condensation in the annulus between shroud and inner cooling jacket after shroud failure, leading to a loss of steam flow in the bundle downstream of the failure position, its extent being unknown. Steam condensation and evaporation in the off-gas pipe are additional reasons of uncertainties of mass spectrometer signals for the steam mass flow rate. Hydrogen generation rate and cumulated hydrogen mass are overestimated at least in the cool-down phase of QUENCH-07, but actually, no conclusion is possible. For model development, these experimental restrictions should be kept in mind.

Analysis of the on-line data, gave some additional insight about the tests. In collaboration with the experimental group, inconsistencies of the data sources in QUENCH-07 were attributed to insufficient synchronisation of computers. For that test, the error could be corrected largely; for subsequent tests, synchronisation is changed so that the problem should not occur any more.

Technically, the condensation of the whole of necessary or useful information on a single page as it is done for the many time dependent results is very useful. Test sequence diagrams, condensing important data for the whole test in a single page, can do this work for a large variety of questions. As an example, the larger downward extension of the damage zone in QUENCH-09 with respect to QUENCH-07, found in PTE, has its counterpart in the different form of the high temperature isotherms. In a number of cases, time derivatives of experimental data proved to be a sensible indicator in spite of the noise for the detailed analysis of important events during the test.

The analysis of the experimental data confirms that material behaviour is not an isolated topic, but an interaction with thermal-hydraulic environment that must therefore be analysed carefully. It also confirms that the QUENCH tests are integral tests and hence represent a whole system. Changes, e.g. by operator actions, effect the whole system. For reliable interpretations, the whole system must therefore be considered to understand the tests and, in particular, to derive reliable conclusions on the interplay of processes. For reliable interpretations, it is also indispensable to use the whole amount of data and to verify that conclusions are compatible with the whole amount of knowledge.

The present work demonstrates that much insight, including a large amount of quantitative results, can be gained from such analyses of on-line data without any further source of information, especially without computational support. A wide spectrum of issues can be covered, not only about control rod behaviour, the main subject of this report. In this way, it also demonstrates the value of the experimental data alone, if analysed adequately. However, much work is necessary for this purpose, and limits concerning the amount of data or their

reliability are reached in some cases, so that open questions may remain. The work also demonstrates the value of PTE, relying on a different approach to learn from test results. The various topics in this report reveal clearly that both methods have their advantages and their limitations. Both methods complement one another, and in a number of cases, they overlap insofar as each of them leads to the same conclusions. For further analyses than dealt in this report, not only the on-line data and those derived during post-test analysis are necessary for this purpose, but also any other knowledge, including computational analyses. Such additional work is also necessary to identify effects that are merely due to peculiarities of the facility and test conduct and that are hence irrelevant for reactor conditions.

10 Acknowledgments

This work was funded by Program NUKLEAR at Forschungszentrum Karlsruhe. Tests QUENCH-07 and QUENCH-09 were co-financed by the European Commission under the Euratom Fifth Framework Programme on Nuclear Fission Safety 1998 – 2002 (COLOSS Project). Our thanks are to all members of the experimental group, above all to Alex Miassoedov, Leo Sepold, Martin Steinbrück, and Juri Stuckert.

11 References

[1] Hózer, Z., Nagy, I., Windberg, P., Balasko, M., Matus, L., Prokopiev, O., Czitrovszky, A., Nagy, A., Jani, P.: CODEX-B4C Experimental Data Report, SAM-COLOSS-P020, D17, Budapest, October 2001.

[2] Steinbrück, M., Homann, C., Miassoedov, A., Schanz, G., Sepold, L., Stegmaier, U., Steiner, H., Stuckert, J.: Results of the B_4C Control Rod Test QUENCH-07, Forschungszentrum Karlsruhe, FZKA 6746, May 2004.

[3] Steinbrück, M., Miassoedov, A., Schanz, G., Sepold, L., Stegmaier, U., Steiner, H., Stuckert, J.: Results of the QUENCH-09 Experiment with a B_4C Control Rod, Forschungszentrum Karlsruhe, FZKA 6829, December 2004.

[4] Phebus FP programme Semi-Annual Progress Report October 2004 - March 2005, editor R. Zeyen, CPF-320, IRSN, France, May 2005.

[5] Stuckert, J., Boldyrev, A. V., Miassoedov, A., Palagin, A. V., Schanz, G., Sepold, L., Shestak, V. E., Stegmaier, U., Steinbock, L., Steinbrück, M., Steiner, H., Veshchunov, M. S.: Experimental and Computational Results of the QUENCH-08 Experiment (Reference to QUENCH-07), Forschungszentrum Karlsruhe, FZKA 6970, August 2005.

[6] Homann, Ch., Hering, W., Birchley, J., Fernandez Benitez, J.A., Ortega Bernardo, M.: Analytical Support for the B_4C Control Rod Test QUENCH-07, Forschungszentrum Karlsruhe, FZKA 6822, SAM-COLOSS-P055, April 2003.

[7] Homann, Ch., Hering, W.: Analytical Support for the B_4C Control Rod Test QUENCH-09, Forschungszentrum Karlsruhe, FZKA 6853, SAM-COLOSS-P057, April 2003.

[8] Steinbrück, M.: Analysis of Hydrogen Production in QUENCH Bundle Tests, Forschungszentrum Karlsruhe, FZKA 6968, May 2004.

[9] Homann, Ch., Hering, W., Miassoedov, A., Sepold, L.: Detailed Investigation of Thermal-Hydraulic Aspects during the Reflood Phase in QUENCH Experiments, Proc. of the 12th Internat. Conf. on Nuclear Engineering (ICONE-12), Arlington, Va., April 25-29, 2004, New York, N.Y.: ASME, 2004, CD-ROM ICONE12-49517, ISBN 0-7918-3734-3.

[10] Stuckert, J., Stegmaier, U.: Behavior of the cladding oxide layer under steam starvation conditions, 9th Internat. QUENCH Workshop, Karlsruhe, October 13 - 15, 2003. Proc. on CD-ROM.

[11] Homann, Ch., Hering, W.: Strategy for the Conduct of Test QUENCH-08, 9th International QUENCH Workshop, Forschungszentrum Karlsruhe, 13 - 15 October 2003.

[12] Stuckert, J., Homann, C., Miassoedov, A., Sepold, L., Steinbrück, M.: Results of the QUENCH-08 Experiment as a Reference to QUENCH-07 (with B_4C Absorber), Annual Meeting on Nuclear Technology, Düsseldorf, Germany, 25. - 27. May 2004, Berlin : INFORUM GmbH, 2004, p. 131 – 134, Proceedings on cd-rom.

[13] Descartes, R.: Discours de la méthode pour bien conduire sa raison, & chercher la vérité dans les sciences. Plus la dioptrique, les Météores, et la Géometrie, qui sont les essais de cette méthode (Discourse on rightly conducting one's reason and searching for truth in the sciences. Including Dioptics, Météores and Geometry which are examples of this method), Ian Maire, Leyden, Netherlands, 1637.

[14] Steinbrück, M.; Meier, A.; Nold, E.; Stegmaier, U.: Degradation and oxidation of B_4C control rod segments at high temperatures., Forschungszentrum Karlsruhe, FZKA 6980, Mai 2004.

[15] Steinbrück, M., Meier, A., Stegmaier, U., Steinbock, L.: Experiments on the Oxidation of Boron Carbide at High Temperatures, Forschungszentrum Karlsruhe, FZKA 6979, May 2004.

[16] Seiler, N., Bertrand, F.: Analysis of QUENCH Tests Including a B_4C Control Rod with the ICARE/CATHARE Code and B_4C Oxidation Modelling Assessment, Proc.of the 11th Internat.Topical Meeting on Nuclear Reactor Thermal-Hydraulics (NURETH-11), Avignon, France, October 2-6, 2005, CD-ROM Paper 086.

[17] Sepold, L., Krauss, W., Miassoedov, A., Piel, D., Stegmaier, U., Steinbrück, M., Homann, C.: QUENCH-07 Test Data Report, Forschungszentrum Karlsruhe, internal report PSF 3360, SAM-COLOSS-P024, January 2002.

[18] Sepold, L., Krauss, W., Miassoedov, A., Steinbrück, M., Stuckert, J., Homann, C., Horn, S.: QUENCH-09 Quick Look Report, Forschungszentrum Karlsruhe, internal report PSF 3378, SAM-COLOSS-P041, November 2002.

[19] Boldyrev, A. V., Palagin, A. V., Shestak, V. E.: Application of the SVECHA/QUENCH code to the simulation of the QUENCH bundle test Q-07, Final Report, NSI–SARR–184–04, December 2004.

[20] Sepold, L., Hering, W., Homann, C., Miassoedov, A., Schanz, G., Stegmaier, U., Steinbrück, M., Steiner, H., Stuckert, J.: Experimental and Computational Results of the QUENCH-06 Test (OECD ISP-45), Forschungszentrum Karlsruhe, FZKA 6664, Feb. 2004.

[21] Hering, W.: Interpretation und Modellierung des Experimentes CORA mit dem erweiterten Kernschmelz-Code SCDAP/MOD1, Thesis, IKE 2-100, 1993.

[22] Hering, W., Minato, K., Nagase, F.: Behaviour of the Zircaloy Cladding in PWR-Specific CORA Experiments, Nuclear Technology, Vol. 102, S. 100-115, April 1993.

[23] Hering, W., Hofmann, P.: Material Interactions during Severe LWR Accidents; Summary of Separate Effects Results, Forschungszentrum Karlsruhe, KfK 5125, February 1994.